The Role of the Atmosphere in Marine Heatwaves

Lauren Nicole Schmeisser

A dissertation

submitted in partial fulfillment of the

requirements for the degree of

Doctor of Philosophy

University of Washington

2020

Reading Committee:

Thomas P. Ackerman, Chair

Nicholas Bond

Robert Wood

Program Authorized to Offer Degree:

Atmospheric Sciences

University of Washington

Abstract

The Role of the Atmosphere in Marine Heatwaves

Lauren Nicole Schmeisser

Chair of the Supervisory Committee:
Professor Emeritus Thomas P. Ackerman, Chair
Department of Atmospheric Sciences

Marine heatwaves (MHWs) are events of abnormally warm sea surface temperatures (SSTs) that last for an extended period of time. MHWs have devastating impacts on marine ecosystems and coastal economies, and thus there is motivation to better understand these extreme events and forecast their evolution in order to improve the adaptive capacity of communities experiencing these impacts. Although MHWs are extreme oceanic events, both the atmosphere and the ocean affect the buildup, maintenance, and decay of MHWs. This dissertation focuses on the role of the atmosphere during MHWs. While it is well documented that the atmosphere can trigger MHWs through a stalled ridge of high pressure and/or a decrease in winds, not much is known about the role of the atmosphere after SST anomalies emerge. This dissertation documents atmospheric behavior *during* MHWs.

Chapter 2 surveys the data needed for MHW analysis. I outline the variety of atmospheric and oceanic data products that are available for studying the physics of MHWs and provide an evaluation of which products are best suited for certain research questions. For individual MHW

events where regionally well-validated reanalysis products are available, reanalysis data provide a large suite of atmospheric and oceanic variables over a longer time period than the newer generation of satellite observations. However, reanalysis products are not recommended for global MHW analyses, as most reanalysis products are not well-validated over the entire globe and errors are regionally variable. For global MHW analyses, satellite data are preferred, as they provide the best available global estimates of SSTs, radiative fluxes, and clouds.

Chapter 3 expands on the survey of data products by providing an in-depth evaluation of reanalysis products compared to satellite observations over the Northeast Pacific Ocean, with the goal of finding the best reanalysis dataset for examining the 2013-2016 Northeast Pacific MHW. There is large variability in performance between reanalyses, including how well they capture variables within the datasets and sub-regional variability within the Northeast Pacific. However, for radiative fluxes and cloud fractions, the Climate Forecast System Reanalysis (CFSR) product generally has the smallest errors compared to NASA's Clouds and the Earth's Radiant Energy System (CERES) satellite observations, and thus CFSR is selected as the best dataset to analyze MHWs within the Northeast Pacific region.

Chapter 4 analyzes the role of clouds and radiative fluxes during the unprecedented 2013-2016 Northeast Pacific MHW, known as the Blob. The warm waters observed during the Blob altered the surface energy balance and disrupted ocean–atmosphere interactions in the region. In principle, ocean–atmosphere interactions following the formation of the MHW could have perpetuated warm SSTs through a positive SST-cloud feedback. The actual situation was more complicated. While CFSR reanalysis data show a decrease in boundary layer cloud fraction and an increase in downward shortwave radiative flux at the surface coincident with warm SSTs, this

was accompanied by an increase in longwave radiative fluxes at the surface, as well as an increase in sensible and latent heat fluxes out of the ocean mixed layer. The result is a small negative net heat flux anomaly (compared to the anomalies of the individual terms contributing to the net heat flux). This provides new information about the midlatitude ocean–atmosphere system while it was in a perturbed state. More specifically, a mixed layer heat budget reveals that anomalies in both the atmospheric and oceanic processes offset each other such that the anomalously warm SSTs persisted for multiple years. The results show how the atmosphere–ocean system in the Northeast Pacific is able to maintain itself in an anomalous state for an extended period of time.

Chapter 5 zooms out and takes a broader perspective on the role of the atmosphere during MHWs all across the globe. Here I use satellite data from 2001-2019 to identify MHWs and anomalous atmospheric variables, including radiative heat fluxes, turbulent heat fluxes, and cloud cover, associated with these events. CERES satellite data are used instead of reanalysis data, despite the shorter time series, because satellite data are well-validated worldwide. We find robust patterns in SST-cloud and SST-heat flux relationships that show important geographical differences in atmosphere-ocean interactions during MHWs. Because of these regional differences, we don't expect MHWs to evolve the same way in all regions. We also find that the cloud response observed during MHWs globally corresponds well with the cloud response to future warming, as identified in the Cloud Feedback Model Intercomparison Project (CFMIP) ensemble of global climate models. This suggests that MHWs can provide valuable insight to anomalous atmosphere-ocean interactions under future warming.

Chapter 6 employs a surface heat flux feedback framework in order to quantify the response of surface heat fluxes to underlying SST anomalies during MHWs. Physically, the net surface heat flux feedback is expected to be strongly negative over the world's oceans (the atmosphere strongly damps underlying SST anomalies) due primarily to enhanced upward turbulent and longwave radiative heat fluxes over warm SST anomalies. However, the atmospheric response can modulate the negative feedback. It is useful to understand regional and seasonal variability in climatological net heat flux feedbacks, as this sheds light on the nature of regional ocean-atmosphere interactions. Climatologically, there is large spatial and seasonal variability in net heat flux feedbacks. This is driven primarily by variability in the shortwave and latent heat flux feedbacks. Although computed feedbacks show that the global net surface heat flux is largely negative as expected, certain regions- including the Northeast Pacific, central and eastern subtropical and tropical Pacific, Northwest Atlantic, and west tropical Atlantic- have positive feedbacks during certain seasons. A statistical analysis shows that net heat flux feedback parameters and MHW length are negatively correlated. This is an important finding, as it indicates that regions with near zero or positive feedbacks are more prone to persistent MHWs.

This dissertation lays out multiple lines of evidence showing that the atmosphere plays an important role during the evolution of MHWs. After warm SST anomalies form during MHWs, anomalies in clouds, radiative heat fluxes, and turbulent heat fluxes are observed. These atmospheric anomalies feed back onto SSTs and affect the progression of MHWs. There is large spatial and seasonal variability in the atmospheric patterns during MHWs, therefore, we do not expect MHWs to evolve the same in all regions and all seasons. Furthermore, some areas are more prone to persistent MHWs due to near zero or positive climatological net surface heat flux feedbacks in that region. These new insights into the role of the atmosphere during MHWs are

key for helping develop our understanding and get closer to properly modelling and forecasting these extreme events. Using results from the dissertation, we know that coupled atmosphere-ocean models will be needed to capture MHWs. Furthermore, models will need to adequately represent the spatial variability in atmosphere-ocean interactions in order to capture the heterogeneity in the evolution of MHWs around the globe.

TABLE OF CONTENTS

List of Figures

List of Tables

GLOSSARY

CERES: Clouds and the Earth's Radiant Energy System satellite data

CFSR: Climate Forecast System Reanalysis

ERA-Interim: European Center for Medium-Range Weather Forecasts (ECMWF) Reanalysis

JRA-55: Japanese 55-year Reanalysis

LW: Longwave radiative flux

MERRA2: The Modern-Era Retrospective analysis for Research and Applications, version 2

MHW: Marine heat wave

NCEP2: National Center for Environmental Protection Reanalysis 2

OAFlux: Objectively Analyzed Air-Sea Fluxes

SW: Shortwave radiative flux

ACKNOWLEDGEMENTS

I would like to thank my advisor, Dr. Tom Ackerman, for his excellent mentorship and unending support for the past five years. I am immensely grateful for all I have learned from Tom about science, academia, and life. I extend my sincere gratitude to Dr. Terrie Klinger, one of my greatest academic role models, for her authentic encouragement and for providing me so many unforgettable interdisciplinary experiences during my time as a graduate student. Thank you to Dr. Nick Bond, for sharing his immense knowledge of the atmosphere-ocean system and for always bringing a positive attitude and sense of humor to the world of science. I would like to thank Dr. David Battisti for his guidance and for many excellent conversations about topics ranging from big picture research direction to detailed research methods to teaching undergraduate climate courses. I extend gratitude to Rob Wood for very helpful discussions and direction, especially related to the cloud analyses in this dissertation.

I also wish to thank my office mates and fellow graduate students for providing a supportive and vibrant community in which I was able to thrive for five years. Finally, I would like to thank Erica Coleman, former graduate student advisor in the Department of Atmospheric Sciences, for her amazing and selfless service to the students of this department.

DEDICATION

This dissertation is dedicated to my family- Mom, Dad, Jack, Kate, and Sean. Thank you for being my biggest cheerleaders. Home is where the heart is, and my heart is with you all!

Chapter 1 Introduction & Background

Temperature extremes are an inevitable aspect of the natural climate system; however, these extremes are changing due to anthropogenic climate change (IPCC SREX, 2012). Warm temperature extremes negatively impact ecosystems, human health, and the economy, so the scientific information needed to predict and monitor progression of such events is essential for risk management (IPCC SREX, 2012). With mean global temperatures rising, an increase in the frequency of warm temperature extremes is of growing concern. Atmospheric heatwaves on land are generally well documented and well understood, and it is common practice in many places to have early warning systems to help society prepare. Marine heatwaves (MHWs), on the other hand, are only recently being documented and our scientific understanding of the events is currently inadequate. Developing a thorough understanding of the processes during the buildup, maintenance, and decay of MHWs is a key step in helping society plan for and adapt to the negative impacts associated with these extreme oceanic events (Frölicher & Laufkötter, 2018; Holbrook et al., 2019).

There are many ecological and economic impacts of MHWs that often scale with the intensity and duration of the event. MHWs can cause shifts in species ranges to cooler waters (Cavole et al., 2016; Oliver et al., 2017; Wernberg et al., 2017; Smale et al., 2019; Sanford et al., 2019) and in severe cases, local extinctions (Garribou et al., 2009; Jones et al., 2017; Oliver et al., 2017; Smale et al., 2019). Shifts in or disappearance of species can devastate fisheries and coastal communities during MHWs. Anomalously warm sea surface temperatures (SSTs) during these events can also cause coral bleaching, damaging reefs that are already distressed due to ocean acidification (Le Nohaïc et al., 2017; Hughes et al., 2017; Fordyce et al., 2019; Smale et al., 2019). During the particularly persistent and severe 2013-2016 Northeast Pacific MHW, anomalous SSTs and ocean processes were coincident with the largest harmful algal bloom ever recorded (McCabe et al., 2016; Trainer et al., 2019). This harmful algal bloom caused high levels of the neurotoxin domoic acid to build up in marine animals, leading to closures of profitable fisheries along the west coast of the United States and harming the economies of coastal towns (McCabe et al., 2016; Cavole et al., 2016; Ritzman et al., 2018). The consequences of the harmful algal bloom led the state of California to ask the U.S. Department of Commerce for a federal fishery disaster declaration. A better understanding of MHWs and the ability to forecast

these events could lead to improved adaptive capacity of communities experiencing these impacts.

MHWs are generally defined as an extended period of time during which SSTs exceed an upper threshold. Specifically, MHWs are commonly identified as a region where SSTs surpass the 90th percentile of climatological SSTs for at least five consecutive days (Hobday et al., 2016). Other thresholds such as the 98th percentile of the climatological mean SST have also been used (Holbrook et al., 2019). Defining the threshold for MHWs should depend on the research goals of a specific study. MHWs can be categorized based on their intensity, duration, and frequency, which helps compare events in space and time (Hobday et al., 2018). MHWs have become more frequent and more severe throughout the last century (Oliver et al., 2018; Frölicher et al., 2018). This trend is mainly attributed to an increase in global mean SSTs due to anthropogenic climate change (Oliver, 2018; Frölicher et al., 2018). It has also been shown that the duration of MHWs has increased over the past few decades (Oliver et al., 2018). Many portions of this dissertation focus specifically on understanding persistent MHWs, in part because these events are more likely to have greater impacts and more robust atmospheric responses.

Not only have global MHW statistics shifted due to anthropogenic climate change, attribution studies have confirmed that climate change has played a key role in the severity of many individual MHW events. In fact, MHWs are some of the first events for which the fraction of attributable risk (FAR) was computed as equal to one (FAR = 1 indicates that the event would not have occurred without climate change). For the 2015/2016 Tasman Sea MHW, Oliver et al. (2017) show that it was likely (FAR > 0.9) that climate change increased intensity of the event, and virtually impossible for the duration of the event to occur without climate change (FAR = 1). Jacox et al. (2018) find that the 2016 SST anomalies observed in the California Current Large Marine Ecosystem were remarkable both in terms of anomaly magnitude and duration, and anomalies observed that year were never before reached in the historical record. This extreme warming event, as confirmed with models, has a FAR =1. The SST anomalies associated with MHWs in the Gulf of Alaska and Bering Sea in 2016 had FARs of 0.88 to 1 and 1, respectively, indicating that most, if not all, models have no instances of anomalies like this in the pre-industrial climate runs (Walsh et al., 2018).

As MHWs become more common due to climate change, a priority for the scientific community studying MHWs is to understand the processes driving the evolution of these

extreme events (Frölicher & Laufkötter, 2018; Holbrook et al., 2019). While large scale climate models and teleconnection processes play a role in determining the likelihood of MHW occurrence, local processes dominate the progression and persistence of MHWs (Holbrook et al., 2019). The local processes controlling the evolution of MHWs can be split into two categories- atmospheric processes (consisting of the net heat flux at the ocean surface) and ocean processes (consisting of horizontal ocean advection, entrainment and diffusion at the bottom of the mixed layer). This dissertation focuses on atmospheric processes during MHWs.

It is well established that atmospheric processes can trigger MHWs through, for example, a stalled high pressure ridge and/or a reduction in winds that reduces latent heat fluxes from the ocean (e.g., Bond et al., 2015). The focus of the research here will be on the role of atmospheric processes *during* MHWs, after the SST anomalies have been established. Our understanding of the atmosphere's role in the evolution of MHW SST anomalies is still underdeveloped, so filling this knowledge gap will be essential in understanding the physics of the coupled atmosphere-ocean system throughout the duration of a MHW.

Though analyses of atmosphere-ocean interactions during MHWs are still limited in number, analyses of atmosphere-ocean interactions in general are plentiful. We can use the existing knowledge of the atmosphere-ocean system to hypothesize different ways in which the atmosphere may change during anomalously warm SSTs. There is continuous heat exchange between the atmosphere and the ocean, and thus all of the ways in which the atmosphere could change during anomalous SSTs can be considered through changes in the surface net heat flux (consisting of longwave radiation, shortwave radiation, latent, and sensible heat fluxes). For example, changes in atmospheric temperature, humidity, or clouds can alter the downward longwave radiative flux at the ocean surface. Changes in clouds modify the downward shortwave radiative flux reaching the ocean. Changes in winds, as well as changes in temperature or humidity in the overlying atmospheric column, affect the energy transfer via turbulent heat fluxes. The literature suggests that all of these atmosphere-ocean interactions vary with geographic region of interest.

One useful way of framing the interaction between warm SSTs and the atmosphere is via net surface heat flux feedbacks. The net surface heat flux feedback over the global oceans is generally negative (Frankignoul et al., 1998; Frankignoul & Kestenare, 2002; Park et al., 2005). This feedback damps warm SST anomalies via an increase in longwave radiative and turbulent

fluxes from the ocean surface. However, atmospheric responses to SST anomalies can modulate the feedback (Park et al., 2005). For example, in response to warm SST anomalies the negative surface heat flux feedback weakens if atmospheric moisture and/or temperature increases, wind speed decreases, or low cloud cover decreases over warm SST anomalies. Understanding the dominant heat flux components (i.e., latent, sensible, longwave or shortwave radiative fluxes) in the feedback further elucidates features of the local coupled atmosphere-ocean system. For example, where shortwave radiative response plays a large role in the net surface heat flux feedback during MHWs, regional cloud response to underlying SST anomalies is likely important. Understanding how those cloud changes feed back onto SST anomalies provides valuable information on regional cloud feedbacks, which in turn helps constrain our uncertainty of net global cloud feedbacks. Past studies analyzing global surface heat flux feedbacks using many decades of observational data show substantial seasonal and spatial variability in feedbacks (Frankignoul & Kestenare, 2002; Park et al., 2005). This implies that *when* and *where* warm SST anomalies build to MHW levels can influence the persistence of the event.

Physics dictates that a net negative heat flux feedback will drive MHW SST anomalies to relax back to climatology in a given e-folding time, but the persistence of a MHW can be strongly modulated by the atmospheric response that controls the individual components of the net surface heat flux feedback. A few studies have shown that an ocean mixed layer heat budget analysis during MHWs is a good tool for analyzing processes, including net heat flux, controlling MHW evolution (e.g., Bond et al. (2015); Oliver et al. (2017); Myers et al. (2018); Schmeisser et al. (2019)). Although these studies are essential steppingstones on the path to understanding MHWs, they only analyze a slice of one event in time or a portion of the event in space. What is missing is a systematic analysis of the role of mechanisms, surface heat flux feedbacks in particular, in the evolution of MHWs worldwide, paying particular attention to regional patterns and differences. Holbrook et al. (2019) is the first paper to perform a unifying assessment of global MHWs and their drivers. They found strong correlations between some climate modes and MHWs in certain ocean basins; furthermore, they showed which local processes are important in driving each MHW. However, there is still considerable work to be done to systematically understand the details of the atmospheric processes and feedbacks at play during MHWs worldwide. Chapters 4, 5 and 6 of this dissertation focus on anomalous atmospheric processes and the role of surface heat flux feedbacks in the evolution of past MHWs.

Future climate change is expected to lead to changes in frequency, duration, spatial extent and intensity of climate extreme events (IPCC SREX, 2012), including MHWs (Frölicher et al., 2019). MHWs will likely become more frequent in the future simply due to an increase in mean SSTs (see Figure 1.1; Frölicher & Laufkötter, 2018). Although future climate change is expected to increase land temperatures faster than ocean temperatures due to enhanced heat capacity of the ocean, the increase in marine heat waves is expected to far exceed the increases in land heat waves. This is because SSTs have less variability than air temperatures and thus a shift in the mean of the narrow distribution of ocean temperatures means a much higher likelihood of exceeding a MHW temperature threshold (see Figure 1.1; Frölicher & Laufkötter, 2018). Preliminary work has been done to analyze future MHW statistics in global climate models. Frölicher et al. (2018) find the probability of MHW days increases in nearly all regions of the globe for many different global warming levels, ranging from 1 °C to 3.5 °C warming. For 3.5 °C warming, there is expected to be an increase in MHWs by a factor of 41, an increase in the average spatial extent of MHWs by a factor of 21, and an increase in duration of MHWs by 112 days (Frölicher et al., 2018). If climate model predictions are correct and MHWs continue to increase in frequency and severity as they did in the last century (Oliver et al., 2019) and continue to devastate local ecosystems, it will be more pressing than ever to improve our scientific understanding of the mechanisms like surface heat flux feedbacks that drive the evolution of these events worldwide. The research presented in this dissertation provides essential new developments in our understanding of the role of the atmosphere in MHWs.

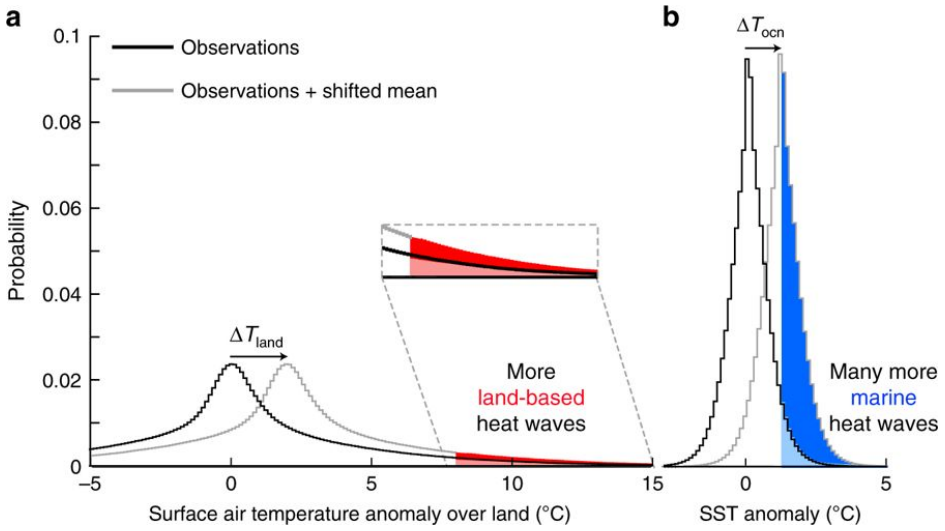

Figure 1.1 From Frölicher & Laufkötter (2018): A theoretical framework outlining why MHWs are expected to increase in severity and frequency in the future, to an even greater extent than land-based heatwaves. The left side of the plot shows temperature distribution of land temperatures (black line) with current land-based heatwaves in light red shading, along with a projected theoretical increase in mean land temperature (grey line) and increased future land-based heatwaves in dark red shading. The right side of the plot shows sea surface temperature distribution (black line) with current marine heatwaves in light blue shading, along with a projected theoretical increase in mean SSTs (grey line) and increased future marine heatwaves in dark blue shading. Change in land temperatures (ΔT_{land}) is assumed to be approximately 1.5x larger than change in ocean temperatures (ΔT_{ocn}).

This dissertation is guided by two broad, over-arching inquiries:

(1) What atmospheric anomalies are observed during MHWs?

(2) How do atmospheric anomalies observed during MHWs in turn affect the evolution of SST anomalies?

The analyses presented here tackle these research questions using a variety of data and methods. Chapter 2 explores different datasets available for study of the coupled atmosphere-ocean system during MHWs. Challenges and opportunities associated with in-situ data, reanalysis products, and satellite observations are discussed, and recommendations are made for selecting the appropriate dataset to address research questions related to MHWs. Chapter 3 dives deeper into data over the ocean with an evaluation of five reanalysis data products over the Northeast Pacific, with the aim of finding a reanalysis product that is most comparable to the best-available satellite observations and is suitable for an analysis of MHWs in that region. Chapter 4 presents a case study analysis of clouds and radiative fluxes during the most persistent

MHW ever observed – the 2013-2016 Northeast Pacific MHW, using 40-years of reanalysis data validated in Chapter 3. Reanalysis data are used in this chapter to provide more context for anomalies observed during this particular marine heatwave, which lasted many years. Chapter 5 provides a global perspective on how the atmosphere changes during MHWs, which highlights the global spatial variability in atmospheric response to SST anomalies. This chapter also provides a comparison between cloud changes observed during MHWs to cloud response to warming in global climate models. 18 years of satellite estimates are utilized in Chapters 5 & 6, since these data provide the best available temporal and spatial resolution of the variables of interest. The research culminates in Chapter 6 where the application of a net heat flux feedback framework proves a useful context for understanding the effects of SST anomalies on the atmosphere and the effects of the atmosphere on those SST anomalies. A net heat flux feedback climatology is presented, as well as a comparison between net heat flux feedbacks during MHWs and climatological conditions. Chapter 7 summarizes the most important findings of the research, presents implications of these analyses, and suggests promising research paths for future work.

Chapter 2 Data Over the Oceans

2.1 Introduction

Analysis of coupled atmosphere-ocean processes during MHWs requires concurrent and spatially synchronous information about the atmosphere and ocean and choosing appropriate data for analysis of these events is not always straightforward. While different types of data offer their own unique advantages, each also has important shortcomings. For example, much of the ocean and overlying atmosphere are sparsely sampled in situ. Remotely sensed data has key limitations when observing the surface. Reanalyses and model output are imperfect. Here we investigate the advantages and disadvantages of four data types that can be used for MHW analysis – in-situ data, satellite observations, reanalysis products, and combination products. We will examine available datasets in each category, as well as discuss which types of research questions are best suited to different data types. This chapter provides a rich context for Chapter 3, in which an in-depth evaluation of reanalysis products in the northeast Pacific Ocean is presented.

This section is tailored to exploring datasets that are useful for the research questions proposed in this dissertation – specifically datasets that include concurrent measurements of sea surface temperature, ocean currents, air temperature, humidity, surface radiative fluxes, turbulent fluxes, and cloud cover over the global oceans. Other coupled atmosphere-ocean datasets may be available (e.g., biological datasets) that are not discussed here since they do not provide variables necessary for this research.

2.2 In-situ measurements of the atmosphere and ocean

Direct in-situ measurements of the atmosphere and ocean are highly desirable, as they have the potential to provide well-validated, quality controlled, and accurate representations of the state of the atmosphere-ocean system. In-situ measurements are invaluable because they provide ground truthing to validate remotely sensed or modeled data. The available options for concurrent in-situ observations of both the atmosphere and ocean at a given location are generally measurements made on buoys, coastal platforms, and ships.

The National Oceanic and Atmospheric Administration (NOAA) operates and maintains a network of buoys through the National Data Buoy Center (NDBC). As of March 2020, the NDBC has 1422 buoy stations deployed at locations all across the globe. These buoys provide a variety of atmospheric and oceanic information – measuring and transmitting some combination of variables including sea surface temperature, wave height, wave period, salinity, water currents, visibility, water quality, wind speed, wind direction, air pressure, humidity, air temperature, precipitation, and surface radiative fluxes. Surface latent and sensible heat fluxes can be computed from the measured meteorological variables using bulk flux algorithms.

In the case of the 2013-16 Northeast Pacific MHW, NOAA's Papa Buoy (also referred to as Ocean Station Papa; Freeland, 2007), located at approximately 50 °N 145 °W, was situated in the middle of the largest (in area) and longest MHW ever recorded. The buoy data afforded valuable insight into the physics of the MHW at that one location- it was used as a ground validation of what was happening to air temperature, SST, specific humidity, and fluxes at the ocean surface. Figure 2.1a shows a time series from 2010-2016 of Papa Buoy measurements of some variables of interest during the 2013-2016 NE Pacific MHW- skin temperature (Figure 2.1a), specific humidity adjusted to 2 m (Figure 2.1b), and total net heat flux (Figure 2.1c), which suggest anomalous processes during the 2013-2016 MHW duration. Figures 2.1d-2.1f show time series of the anomalies of the same variables measured at the buoy; Figures 2.1g-2.1i show monthly climatologies of the variables during the MHW (red bars) and before the MHW (blue bars). The buoy data show an increase in sea surface temperature and specific humidity associated with the MHW. Additionally, total net heat flux out of the ocean was reduced during summer months of the MHW. This buoy data provided an essential near-real-time first look at how atmospheric and oceanic variables behaved during the start of the large MHW. The information from the buoy helped form research questions about the evolution of the MHW. But, when the warmest waters of the MHW moved closer to shore and away from the buoy, observations from Papa Buoy were less useful for tracking the event, and a spatially gridded dataset was needed.

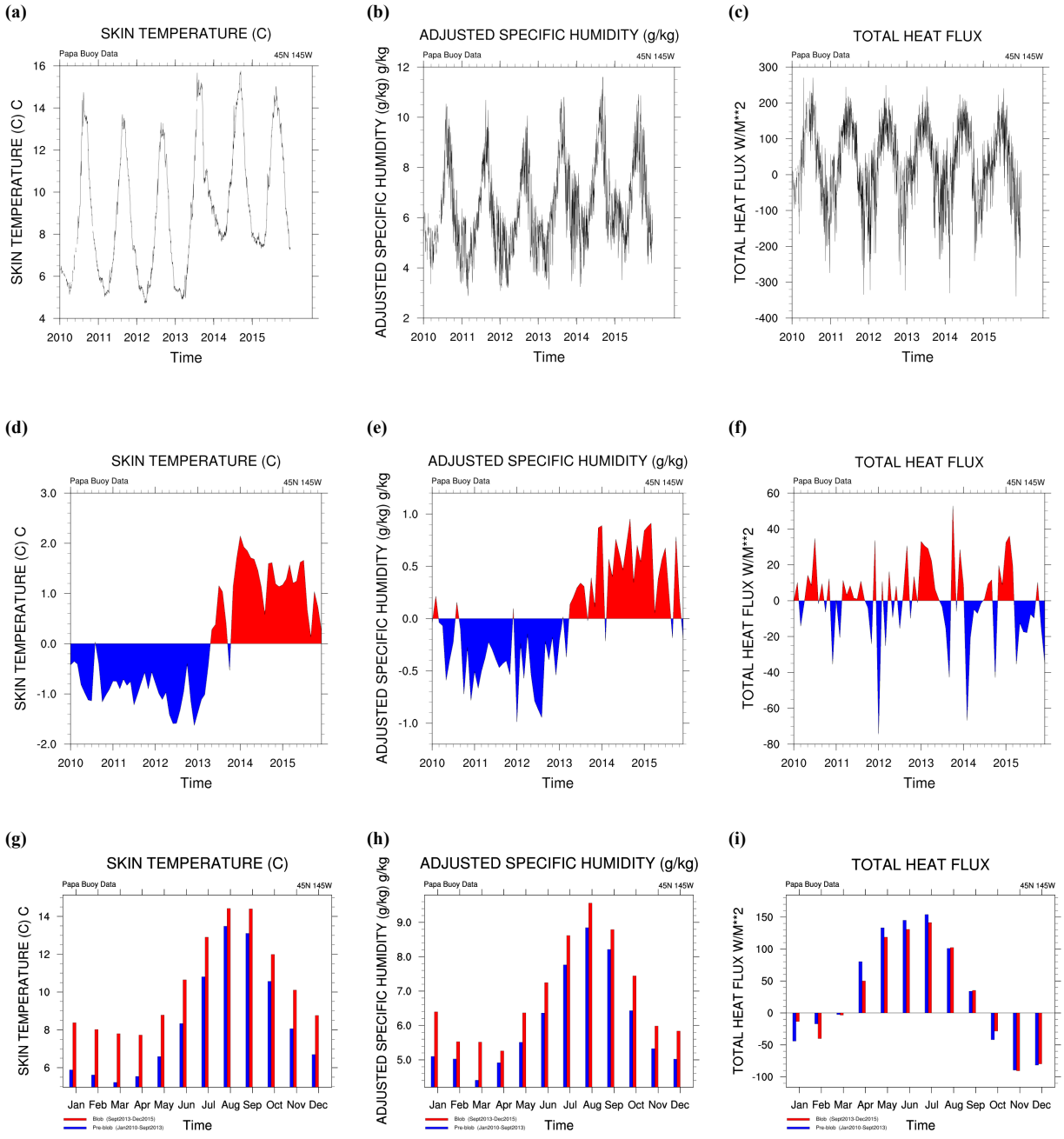

Figure 2.1 Time series of measurements from the buoy at Ocean Station Papa from 2010-2016 for (a) sea surface temperature (°C), (b) adjusted specific humidity (g/kg), (c) total net heat flux (W/m^2); time series of anomalies from Papa Buoy measurements for (d) sea surface temperature (°C), (e) adjusted specific humidity (g/kg), and (f) total net heat flux (W/m^2); climatology of Papa Buoy measurements for the time period before the MHW in blue, and climatology of buoy measurements for the time period during the 2013-2016 NE Pacific MHW (aka 'the Blob') for (g) sea surface temperature (°C), adjusted specific humidity (g/kg), and total net heat flux (W/m^2).

Ship measurements are useful as they can provide ocean transects, offering a spatial slice of the atmosphere-ocean system. However, there is typically no time series information available from ship measurements, as the ship is in motion and thus only sampling a particular place for one moment in time. Over time, ship measurements can help build a climatology for well-measured areas of the ocean. Examples of available ship measurements include the Voluntary Observing Ship Climate (VOSClim) Fleet, which is a collection of data measured from ships available through NOAA. Additionally, NOAA supports research cruises that traverse the same route multiple times a year, taking measurements along the way. Line P is one such program, that takes measurements on a route from the coast to the aforementioned Papa Buoy (hence line 'P') three times a year (Freeland, 2007). Many scientific collaborators manage instrumentation on these line routes, and a diverse array of data are available from the cruises. Ship measurements can provide good ground truthing, but for tracking rare and extreme events like MHWs, ship measurements barely provide enough of a snapshot. A ship equipped with both atmospheric and oceanic instrumentation and deployed intentionally to a region experiencing a MHW could provide strategic insight into these events; however, to the author's knowledge, this has not yet been done.

There are other in-situ data products worth considering for MHW analysis, including the International Comprehensive Ocean Atmosphere Data Set (ICOADS). ICOADS is the largest collection of freely available, verified atmosphere-ocean data. The dataset includes a combination of hundreds of millions of observations from ships, buoys, coastal platforms, and oceanographic instruments, available in a gridded format with variables including SST, air-sea fluxes and meteorological variables (Freeman et al., 2017). ICOADS has a very long time record, extending back to the 17th century, with sparse measurements at the beginning of the record becoming more frequent and widespread approaching present day. The ICOADS dataset is not corrected beyond initial quality control, and most importantly, coverage is sparse and comprehensive maps of certain variables can be difficult or impossible to create (Deser & NCAR Staff, 2019).

An advantage of in-situ data from buoys, ships, and platforms is that the instruments are generally well-calibrated, taking direct measurements and reporting in near-real time. In-situ observations like this are essential for helping validate other data sources like satellite observations and model output. Disadvantages of in-situ data include the cost of deployment and

maintenance of instrumentation, particularly since platforms and buoys are subject to harsh open ocean conditions and can be targets of vandalism (Teng, 2009). In-situ instruments left unattended for long periods of time can have maintenance issues, as they are left unmanned for much of the year in harsh maritime environments with large beating waves and rusting sea spray. If an instrument breaks, it might be weeks before a ship can be deployed with the scientists and technicians needed to fix it. This can impact availability of data for a continuous time period of interest. In addition, in-situ data by definition only offer measurements at one point in space (in the case of buoys and coastal platforms) and/or time (in the case of ship transects). Since MHWs are widespread events, measurements from one location do not provide a comprehensive perspective on the event.

In-situ data can provide a valuable first look at MHWs. In the case of the 2013-2016 Northeast Pacific MHW, buoy data proved useful in getting near-real-time information on the event as it developed, then eventually helping validate other datasets, like those from satellites or reanalysis, to continue further analyses. In-situ data from buoys and ships can also give a detailed picture of what is happening simultaneously with the atmosphere and ocean at one location as a MHW develops, provided the necessary instrumentation to monitor variables of interest is all available and operational at the location of interest. However, buoy datasets are generally not sufficient for complete MHW analyses, including those presented here. Atmosphere-ocean datasets with more comprehensive spatial coverage will be explored next.

2.3 Satellite data

The advantage of satellite data is its near complete global spatial coverage and relatively frequent temporal sampling. Satellite data can be an invaluable tool for analyses over remote areas, like the oceanic regions studied here. In addition, many atmospheric parameters are available in satellite datasets, including air temperature, radiative fluxes, and cloud cover. One weakness of satellite data is that the products do not provide direct observations- instead, complex algorithms convert raw radiance data into atmospheric variables of interest. While the algorithms are advanced and perform well, there is always uncertainty in satellite data. In addition, satellites only pass over a given location once or twice a day; consequently, care needs to be taken with temporal interpolation of variables that have high temporal variability or a large

diurnal cycle. Many of the most useful satellite products are only available over the last 20 years or so, so time series are relatively short compared to the length of other data records. While some satellite products are available back through the 1970s, the earlier satellite datasets are not as reliable as more recent satellite products. An additional weakness of satellite data in the context of MHW analyses is that satellites cannot easily 'see' through cloudy areas down to the surface; furthermore, satellites cannot 'see' beneath the ocean surface. Therefore, surface data beneath cloudy regions are less certain, and the non-satellite data products are needed to provide subsurface ocean parameters like ocean currents.

Despite some unavoidable weaknesses of satellite data, they generally provide highly desirable information for global analyses of climate events like MHWs. A variety of satellite datasets are available for the atmospheric and sea surface variables of interest for MHW analyses. Some of these products, including CERES and MODIS products, which will be examined briefly here.

NASA's Clouds and the Earth's Radiant Energy System (CERES) satellite product provides the best available radiative flux estimates globally (Kato et al., 2012a; Kato et al., 2012b; Kato et al., 2018). Since the response of the surface radiative fluxes to SST anomalies is key to understanding the development of MHWs, a satellite dataset like CERES that provides well-validated radiative flux data is valuable for many MHW analyses. In this dissertation, the CERES data product was used to evaluate reanalysis products in the NE Pacific (Chapter 3), and for direct use on an analysis of global marine heat waves (Chapters 5 & 6). More information about the CERES product is available in Section 3.3.1.

NASA's Moderate Resolution Imaging Spectroradiometer (MODIS) provides a wide variety of measurements, most notably cloud cover and cloud optical properties. Cloud change in response to SST anomalies is important in dictating the net heat flux response to MHWs, and thus global MODIS cloud data are particularly useful for MHW analyses. Some CERES products utilize MODIS cloud data in their radiative transfer schemes to compute surface radiative fluxes, and thus package MODIS cloud data in with CERES datasets, making a convenient singular dataset of radiative fluxes and cloud data on the same spatial grid with the same temporal resolution. MODIS data (via CERES EBAF data) is used for analyses presented in Chapters 4 and 5.

Satellite observations provide an excellent opportunity for global analyses of MHWs. Satellite datasets are best for analyzing MHWs through an atmospheric lens, examining how the atmosphere changes during anomalously warm SSTs. Satellite products are less ideal for very cloudy regions which may impede the satellite's ability to accurately detect surface parameters. However, even in most cloudy remote regions, satellites are arguably still the best available data for MHW analyses.

2.4 Reanalysis data

Reanalysis products use observations of the ocean and/or atmosphere in combination with a numerical model to provide best estimates of the state of the global climate over time. One advantage of reanalysis products is that they provide global coverage of a wide variety of variables, all with a complete time series without missing data. In addition, variables are forced to be physically consistent due to the numerical model. A disadvantage of reanalysis products is that they are generally not well-validated regionally. While there are some studies that evaluate how reanalysis products capture global climatology of some atmospheric or ocean variables, there are few studies that evaluate a large range of reanalysis products and variables against observations in specific regions.

A variety of atmospheric reanalysis products exist, as do oceanic reanalysis products; however, coupled atmosphere-ocean reanalysis products are few. Ideally, a MHW analysis utilizes a coupled product that can capture the interaction between atmosphere and ocean during times of extreme ocean temperatures. It is possible, however, to pair an atmospheric reanalysis product to a separate ocean reanalysis product with the understanding that the different reanalysis products may not be physically consistent, and residuals may be introduced in some computations. For the case of MHW study in particular, surface heat fluxes are especially important, and any selected atmospheric reanalysis product may have a net surface heat flux determined using a different representation of the ocean than the ocean reanalysis product selected, thus introducing potential residual heat exchange when using the two products together.

Reanalysis products can be very useful for MHW analyses since they can provide a large suite of variables with a longer time series than the newer generation of satellite products.

However, careful validation of a reanalysis product against in-situ or satellite observations is recommended before use. Sometimes reanalysis products agree well with observations on an annually averaged global scale, but do not agree well with observations on a local scale or on short time scales. Therefore, thorough evaluation is needed to understand reanalysis uncertainty and fit to proposed research questions. Chapter 3 goes into detail evaluating the performance of five atmospheric reanalysis products and one coupled atmospheric-ocean reanalysis product in the Northeast Pacific Ocean. This reanalysis evaluation from Chapter 3 informed the use of the Climate Forecast System Reanalysis (CFSR) product for analysis of the 2013-2016 Northeast Pacific MHW in Chapter 4. Using a reanalysis product for *global* analysis of MHWs is not recommended, since the proper global validation of reanalyses at regional spatial scales and monthly time scales is not currently available.

2.5 Combination products

There are some data products that do not fall neatly into the above categories, and are not easily tagged as in-situ, satellite, or reanalysis. Often a data product is a combination of some or all of these categories.

Many SST datasets are combination products, utilizing all available measurements of ocean temperatures to provide best estimates of SSTs throughout space and time. Three global SST datasets were considered for use in the MHW analyses presented in this dissertation- the NOAA Extended Reconstructed Sea Surface Temperature version 5 (ERSSTv5), the NOAA Optimum Interpolation Sea Surface Temperature (OISST), and the Hadley Centre Sea Ice and Sea Surface Temperature dataset (HadISST). The NOAA ERSSTv5 reconstructs SSTs from 1854 to present, providing monthly data on a 2° x 2° grid. ERSSTv5 uses ICOADS ship and buoy data, ARGO float information, and HadISST sea ice concentrations to produce the final SST product. The NOAA OISST dataset provides weekly SSTs from 1981-present on a 1° x 1° grid, formed using a combination of satellite measurements, buoy data, and ship observations. The HadISST dataset provides monthly SSTs from 1870 to present day at 1° x 1° spatial resolution. SSTs are constructed using the Met Office marine data bank, ship data, buoy measurements, and satellite observations. The ERSSTv5 dataset is especially useful if a very long record of sea surface temperatures is needed; however, it is less desirable for MHW analysis

given the coarser spatial resolution. OISST and HadISST datasets offer the same finer spatial resolution, and generally agree quite well when compared (though OISST slightly underestimates global SSTs compared to HadISST). Since HadISST does offer a longer time record from which to compute recent MHW anomalies, it gives a better sense of MHWs in a historical context. Furthermore, HadISST data are highly regarded in the scientific community as one of the best available SST datasets. For these reasons, HadISST provides SST data for the MHW analyses presented in Chapters 4, 5, and 6.

2.6 Conclusions

There are many available datasets over the ocean that include both atmospheric and oceanic variables to analyze MHWs. Ultimately, the selection of data choice is a balance between the advantages and disadvantages of the product, as well as fit of the dataset to answer the proposed research questions. There is not one 'best fit' dataset that suits all MHW analyses. In-situ data might be the right fit for an in-depth analysis of a MHW event at one location in space. A satellite dataset might be the right fit for MHW analyses that aim to compare atmospheric and oceanic processes in different MHWs around the globe. Reanalyses products might be the right fit for a regional analysis of a single MHW event. Often, combination data products, particularly those that provide SST and turbulent heat fluxes, may be needed in addition to any of the categories of datasets mentioned above.

Though data collection over the world's oceans is a challenging endeavor, an impressive variety of datasets exist. It is important to choose a dataset that is the best tool for a proposed analysis. Careful selection of a dataset, in addition to an understanding of the dataset's uncertainties and limitations, is best practice for any MHW analysis.

Chapter 3 Evaluation of Radiation and Clouds from Five Reanalysis Products in the Northeast Pacific Ocean

3.1 Introduction

Atmospheric reanalysis products are valuable tools for climate scientists because they provide long time series of most atmospheric variables with complete global spatial coverage. Reanalysis data can be useful for studying a variety of atmospheric and climate processes. Reanalysis makes use of both observations and models to produce an optimized global set of atmospheric variables. This global dataset is created using a single version of a forecast model and a series of atmospheric observations at high time resolution (sub-daily). The data are assimilated into the model resulting in a model-generated dataset that is global, uniformly produced, and as consistent with observations as possible (Betts et al., 2006). Even though observations of the atmosphere are not consistent in space or time, an assimilation model provides a forward interpolation that 'fills in' these gaps and maintains dynamically and energetically consistent fields. Forecast models are imperfect representations of the atmosphere due to a combination of finite grid resolution, uncertainty in the parameterization of sub-grid scale processes, and imprecision in initial conditions. However, the assimilation of observations continually adjusts the model fields to be more consistent with the observations (Betts et al., 2006). The resulting long-term datasets are the best available representation of long-term and large-scale atmospheric fields.

Despite the utility of reanalysis, past studies illustrate the potential for biases in reanalysis products (e.g., Betts et al., 2006; Bosilovich et al., 2008; Dee et al, 2011). Some atmospheric variables are better represented by reanalysis models than others. For example, variables for which we have large observational datasets, are smooth at all scales, and are well understood in terms of model physics (e.g., temperature) are generally reproduced well by reanalysis (e.g., Betts et al., 1998; Betts et al., 2006; Dulière et al., 2011; Bao & Zhang, 2013; Donat et al., 2014). There are exceptions to this, as some studies show moisture is not well reproduced by reanalysis products (e.g., Jiang et al., 2015)). On the other hand, variables for which we have fewer or less accurate observational data, are more variable at small scales, and depend on model parameterizations have much larger biases in reanalysis products (e.g., clouds and precipitation;

Zib et al., 2012; Walsh et al., 2009; Bosilovich et al., 2008; Vey et al., 2010; Pfeifroth et al., 2013; Lindsay et al., 2014). In addition, the quality of a reanalysis dataset at a particular location and time depends on both the numerical model and the number and quality of observations input to the assimilation framework (Arakawa and Kitoh, 2004; Fujiwara et al., 2017), so biases may have a regional structure.

Numerous studies have specifically evaluated radiative fluxes and cloud fraction from reanalyses using observations, most found substantial biases in the reanalyses, many found a pattern of consistent overestimation of downward shortwave radiative flux and underestimation of cloud fraction. Zib et al. (2012) used surface radiative flux measurements to assess radiative fluxes and total clouds fraction at two locations in the Arctic region and found that all reanalyses had substantial biases in cloud fraction, especially during the winter. Radiative flux biases varied widely depending on the reanalysis- ERA-Interim and CFSR generally had the smallest biases and NCEP2 had the largest biases. Decker et al. (2012) used flux tower observations from all over the world to evaluate incoming shortwave radiation and found that although the reanalyses captured the annual cycle very well, all reanalyses overestimated the incident shortwave radiative flux. NCEP had the largest biases, exceeding 25 Wm^{-2} at many of the sites analyzed, while ERA-Interim showed the smallest shortwave biases. Similarly, Zhang et al. (2016) found all reanalyses products overestimated incoming shortwave radiative fluxes, with the exception of ERA-Interim which had a small positive bias of -2.98 Wm^{-2} compared to CERES EBAF satellite data.

Most evaluations of reanalysis datasets have been performed on a global scale and tend to focus on investigating long-term annual averages (e.g., Dee et al., 2011). These analyses provide important assessments of reanalysis quality and usefulness. However, many atmospheric phenomena happen on smaller regional and temporal scales, and long-term global reanalysis evaluations do not provide information on the value of these datasets at smaller spatio-temporal scales. Regional evaluations give more detailed insight into reanalysis performance at finer resolutions, which is particularly important for ‘data-sparse’ regions with limited surface and in-situ observations. Surface and in-situ observations provide quality-controlled data with excellent temporal coverage that can help constrain both satellite and reanalysis data. While reanalysis products are arguably the best available atmospheric information for regions lacking surface and in-situ measurements (Jakobson et al., 2012; Screen and Simmonds, 2011) due to their complete

spatio-temporal coverage and comprehensive output of atmospheric variables, it is precisely in these data-sparse regions where reanalysis datasets are most susceptible to large uncertainties because there are less data to assimilate. The Arctic is an exemplar region exhibiting this discrepancy. While reanalysis data are essential tools for studying the Arctic atmosphere, reanalysis products perform poorly in this region, particularly with modeling temperature, radiative fluxes, precipitation, relative humidity, wind speed, and ice thickness (Bromwich et al., 2007; Walsh et al., 2009; Lüpkes et al., 2010; Porter et al., 2011; Jakobson et al., 2012; Lindsay et al., 2014). These case studies in the Arctic suggest that other data-sparse regions require reanalysis evaluations as well.

We are specifically interested in the performance of reanalysis products in the Northeast (NE) Pacific. There are a number of reasons to study climate and climate variability in the NE Pacific; for example, its atmosphere-ocean interactions affect weather downstream in North America and it is a sensitive and productive region for fisheries, including shellfish. Our attention was drawn specifically to this region by a recent large and persistent marine heatwave that occurred in this area from 2013-2016, colloquially referred to as 'the Blob' (Bond et al., 2015). The NE Pacific region, however, has very few in-situ observations (e.g., Ocean Station Papa at 50°N, 145°W; an array of National Data Buoy Center buoys near the coast (Meindl and Hamilton, 1992); a ship making observations between the coast and Papa Buoy along a route called line-P; and only select variables available from satellite estimates (e.g., satisfactory turbulent heat fluxes are not available from satellite measurements). Thus, reanalysis products are an indispensable tool for studying the region. However, given potential uncertainty in reanalysis products, it is prudent to exercise caution when using them as a means to examine physical processes on small scales. In this study, we compare radiative fluxes and cloud fraction from reanalyses in the NE Pacific to satellite estimates in order to evaluate usefulness of these reanalysis quantities for regional studies.

We use NASA's Clouds and the Earth's Radiant Energy System (CERES) Energy Balanced and Filled (EBAF) satellite estimates to evaluate the surface radiative fluxes and total cloud fraction from five reanalysis products. The reanalyses include the European Center for Medium-Range Weather Forecasts reanalysis (ERA-Interim), NASA's Modern-Era Retrospective analysis for Research and Applications version 2 (MERRA2), the Japanese Meteorological Agency 55-year reanalysis (JRA-55), the National Center for Environmental Prediction and Department of

Energy reanalysis 2 (NCEP2), and NCEP Climate Forecast System Reanalysis (CFSR). Three approaches are used to evaluate the reanalysis datasets, as summarized in the following research questions:

1. How well do reanalysis products replicate the seasonality of surface radiative fluxes and total cloud fraction in the NE Pacific?
2. Do reanalysis products adequately capture the spatial distribution of surface radiative fluxes and total cloud fraction in the NE Pacific?
3. How well do reanalysis products reproduce anomalies in surface radiative fluxes and total cloud fraction in the NE Pacific?

3.2 Background

The five reanalysis products assessed here have been evaluated in various capacities throughout many regions of the globe. Results show biases that vary widely by location, variable of interest, and reanalysis product (e.g., Bosilovich et al., 2008; Dee et al., 2011). Consequently, the choice of reanalysis product to use for climate analysis in a given region can yield very different results for the same diagnostic (Fujiwara et al., 2017).

We are aware of only one previous study that evaluates reanalysis data in the NE Pacific. Ladd and Bond (2002) compare NCEP1 (also referred to as NCEP/NCAR) reanalysis output with measurements from multiple moored buoys in the Bering Sea and one moored buoy (the aforementioned Ocean Station Papa) in the NE Pacific from 1995 to 2000. Wind, radiation, cloud cover, and sea level pressure were evaluated. The direction of 10 m winds and sea level pressure from the reanalysis product were satisfactory compared to buoy observations. Speed of 10 m winds, on the other hand, was biased high by about 5%. The shortwave radiative flux from NCEP1 showed a 70 Wm^{-2} bias in the Bering Sea and a 20 Wm^{-2} bias in the NE Pacific. The positive bias in shortwave radiative flux in the NE Pacific was present in both the summer and winter. Further analysis in Ladd and Bond (2002) suggests radiative flux biases are likely due to the NCEP1 biases in clouds. In particular, they found the reanalysis model has the largest biases during fair weather events when low clouds are prevalent. Here we expand on this previous

analysis by considering different meteorological quantities and five newer reanalysis datasets, all for a longer time period.

It should be noted that there are emerging efforts within the scientific community to systematically evaluate reanalysis products to provide comparisons of reanalysis data for all variables and regions of the globe. One such effort is the SPARC Reanalysis Intercomparison Project (S-RIP), which was formed to diagnose biases in reanalysis products, with a focus on the upper troposphere, stratosphere, and lower mesosphere (Fujiwara et al., 2017). Consequently, the S-RIP will be less useful for those interested in the performance of reanalysis products at the surface, making assessments such as ours still necessary.

3.3 Data and Methods

3.3.1 NASA satellite estimates

We use the CERES Edition 4 EBAF satellite estimates (Wielicki et al., 1996; Kato et al., 2013; Kato et al., 2018) as our baseline for comparison with surface radiative fluxes from the five reanalyses. The CERES EBAF-Surface (Kato et al, 2013; Kato et al., 2018) product is based on the Edition 4 CERES synoptic 1° monthly averaged data (SYN1deg-Month) (Rutan et al., 2015) radiative flux dataset. The underlying SYN1deg-Hour fluxes are obtained by applying a radiative transfer model to atmospheric profiles of temperature and water vapor from GEOS5, cloud parameters from MODIS and geostationary satellite observations. The monthly averaged SYN1deg-Month data is then constrained to match the top of atmosphere (TOA) radiative fluxes from the CERES Ed. 4. EBAF-TOA (Loeb et al., 2009), which itself has been constrained to the ocean heat storage. The basic approach in this process is to vary the SYN1deg input values within their uncertainty bounds until a good match with the TOA fluxes is achieved. Adjustment of the cloud parameters takes advantage of the higher quality active cloud measurements from CALIPSO and CloudSat (Kato et al., 2013; Kato et al., 2018). The final EBAF-surface monthly mean downward and upward shortwave and longwave radiative fluxes at the surface are provided on a 1°x1° global grid. Total cloud fraction data for comparison to the reanalyses is provided by SYN1deg-Month satellite estimates.

The satellite estimates are not without uncertainty. Since surface irradiance values are only available through a radiative transfer model that requires input of atmospheric variable measurements (e.g., aerosol and cloud), the accuracy of the satellite retrievals depends on the accuracy of these inputs (Kato et al., 2012a). Estimates suggest CERES EBAF monthly gridded estimates of surface upward shortwave radiative flux over the ocean are accurate within 8.3 Wm^{-2}, downward shortwave radiative flux within 6.9 Wm^{-2}, downward longwave radiative flux within 4.3 Wm^{-2}, and upward longwave radiative flux within 11.5 Wm^{-2} (scaled from Kato et al., 2018; see also Kato et al., 2012a; Kato et al., 2012b; Kato et al., 2013). Cloud fraction uncertainty is estimated at 5%, per the CERES EBAF Surface Data Quality Summary (https://ceres.larc.nasa.gov/documents/DQ_summaries/CERES_EBAF-Surface_Ed4.0_DQS.pdf) We expect these uncertainties are further reduced when spatially averaging over the region of the NE Pacific, so the uncertainty estimates here are conservative. The satellite uncertainty estimates are used here as thresholds for acceptance of agreement between satellite and reanalysis data. If the bias between reanalysis and satellite observations is less than the cited satellite uncertainty, the reanalysis and satellite observations are considered to be in adequate agreement. If the bias is larger than the satellite estimate uncertainty, the bias is significant, and the reanalysis product is not in agreement with satellite estimates.

CERES EBAF is one of the only long-term satellite datasets available for the entirety of the NE Pacific region. Other available satellite datasets include the International Satellite Cloud Climatology Project (ISCCP) Flux product (Zhang et al., 1995) and the NASA/GEWEX Surface Radiation Budget product (Zhang et al., 2013). ISCCP is produced at 2.5 ° resolution, which is much lower than that of CERES EBAF. Furthermore, both ISCCP and NASA/GEWEX estimates have similar or larger uncertainties than those for CERES EBAF, which is why CERES EBAF is used here for evaluation of reanalysis products.

CERES satellite estimates of radiative fluxes have not been assimilated into ERA-Interim, MERRA2, JRA-55, NCEP2 or CFSR. Therefore, comparison to the CERES EBAF radiative fluxes can be considered an independent measure of the quality of the reanalysis radiative fluxes. However, CERES utilizes data from geostationary satellites, MODIS and CALIPSO to derive cloud variables and radiative fluxes, and some aspects of these products are

assimilated into the reanalyses. For example, MODIS aerosol estimates are assimilated into MERRA2 and ERA-INTERIM.

3.3.2 Reanalysis products

Monthly averages of radiative fluxes and total cloud fraction from five reanalysis products (ERA-Interim, MERRA2, JRA-55, NCEP2 and CFSR) are evaluated here. Although other reanalysis products do exist for this region, the five investigated here are: (a) the most up to date versions of older available reanalysis models, and (b) commonly used and highly cited in the literature. Table 3.1 outlines technical information about each of the reanalysis datasets. The rest of Section 3.3.2 provides descriptions of each reanalysis product.

Table 3.1 Reanalysis products evaluated

Product	Model grid resolution	Availability	Reference
ECMWF ERA-Interim	T255, 60 vertical levels	01/1979-present	Dee et al. (2011)
NASA MERRA2	0.5ºx0.625º, 72 vertical levels	01/1980-present	Gelaro et al. (2017)
JRA-55	T319, 60 vertical levels	12/1957-present	Kobayashi et al. (2015)
NCEP2	T62, 28 vertical levels	01/1979-present	Kanamitsu et al. (2002)
CFSR	T382, 64 vertical levels	01/1979-present	Saha et al. (2010) Saha et al. (2014)

3.3.2.1 ECMWF ERA-Interim

ERA-Interim is a long term reanalysis product from ECMWF and is well documented in Dee et al. (2011). ERA-Interim data are available from January 1979 to December 2017 at sub-daily, daily and monthly time steps. The model uses a T255 grid with 60 vertical levels, and data is available at 0.75ºx0.75º at 60 vertical levels. The ERA-Interim product improves upon the ERA-40 system (described in Uppala et al., 2005) by using a 4D-Var data assimilation system that more fully integrates observations from the satellite era and more completely incorporates

measurements made between analysis times. ERA-Interim has an improved hydrologic cycle and stratospheric circulation compared to ERA-40 (Fujiwara et al., 2017).

3.3.2.2 NASA MERRA2

MERRA2 is the most recent version of the reanalysis product from NASA's Global Modeling and Assimilation Office. Detailed information about MERRA2 can be found in Gelaro et al. (2017) and Bosilovich et al. (2015). MERRA2 has data available from January 1980 to November 2017 at sub-daily, daily and monthly time steps. The MERRA2 data are available at a resolution of 0.5ºx0.625º with 72 vertical levels. MERRA2 improves upon the former NASA MERRA reanalysis product by ingesting new data types and implementing improvements to the model, including closed balance between surface water fluxes and total atmospheric water, a modified gravity wave scheme, improved treatment of the upper atmosphere, and assimilation of aerosol optical depth measurements (Fujiwara et al., 2017; Bosilovich et al., 2015; Randles et al., 2017).

3.3.2.3 JMA JRA-55

JRA-55 is the most recent version of the JMA reanalysis effort and is documented in Kobayashi et al. (2015). JRA-55 is available from December 1957 to July 2017 at sub-daily and monthly time steps. The native and available model resolution is T319 with 60 levels. JRA-55 is an update of its predecessor, JRA-25 (Onogi et al., 2007) and assimilates satellite data as well as upper air data using a 4D-Var assimilation scheme (Kobayashi et al., 2015; Fujiwara et al., 2017).

3.3.2.4 NCEP/DOE Reanalysis 2

NCEP/DOE Reanalysis 2 (NCEP2) has data available from January 1979 to January 2018 at sub-daily, daily and monthly time steps. The native resolution of the NCEP2 reanalysis model is T62 with 28 levels, which is the lowest resolution of all the reanalysis products evaluated here. The available data resolution is 2.5ºx2.5º with 28 vertical levels. Detailed description of the

NCEP2 and the corrections and updates implemented since its previous version NCEP/National Center for Atmosphere Research (NCAR) Reanalysis 1 (NCEP1) (Kalnay et al., 1996) are found in Kanamitsu et al. (2002).

3.3.2.5 NCEP CFSR

The Climate Forecast System Reanalysis (CFSR) product is the most advanced reanalysis product produced by NOAA NCEP. CFSR is available from January 1979 to February 2011, and the operational model on which this reanalysis product is based was upgraded in March 2011 to the Climate Forecast System Reanalysis version 2 (CFSv2). Since the time period of interest in this study spans both the CFSR and CFSv2, the two reanalysis products were merged to get a continuous reanalysis dataset, which is referred to throughout as CFSR. Detailed information on CFSR is found in Saha et al. (2010), while details on CFSv2 and how the model was improved compared to the previous version are found in Saha et al. (2014). Although there are small differences between the CFSR and CFSv2 reanalysis products that could affect working across the two datasets (Saha et al., 2014), we expect no problems with merging the two datasets here given the variables of interest, as many previous studies have done so without issue (Betts et al., 2006; Fujiwara et al., 2017).

The CFSR is unique from the other reanalyses studied here because it is a coupled atmosphere-ocean-land-sea ice system model. The model assimilates measurements of carbon dioxide, trace gases, and aerosols, and should reflect changes in climate due to these variables. The CFSR is improved from the NCEP/DOE reanalysis in that it is a coupled model and assimilates more observations with a more sophisticated assimilation scheme. However, fewer evaluations of CFSR have been conducted compared to other reanalysis products, so its performance globally is not yet well established.

3.3.3 Methods

For our purposes, the NE Pacific region is defined from 40°-60° N and 180°-120° W. In order to compare reanalysis and satellite products, all datasets were re-gridded to match the

dataset with the lowest resolution- in this case, the NCEP2 2.5°x2.5° grid. Re-gridding was performed using bilinear interpolation. The time period from 2001 to 2015 was used in order to maximize overlap of reanalysis products with currently available satellite data. (The processing of CERES data to produce surface fluxes lags a half year or more behind acquisition of the satellite data).

Surface all-sky radiative fluxes, including downward shortwave, upward shortwave, downward longwave, and upward longwave, are evaluated here. Not all of the reanalysis datasets provide clear-sky radiative fluxes, and thus analysis of clear-sky variables is not included here. For the entirety of this manuscript, reference to radiative fluxes assumes surface, all-sky values unless otherwise indicated. Total cloud fraction is analyzed instead of cloud fraction at different levels, because the satellite and reanalysis products do not provide cloud fraction information at the same vertical levels.

We examine how reanalysis products reproduce seasonality, spatial distribution, and anomalies of radiative fluxes and total cloud fraction in the NE Pacific compared to satellite observations, which we treat as the objective standard. Monthly means of variables are utilized throughout. Most of the evaluation presented here, particularly the statistics and plots presented in Sections 4.1 and 4.3, are spatially averaged over a box from 40-60°N and 180-120°W, unless indicated otherwise.

Monthly climatologies of the variables are computed by averaging the monthly mean values for each month of each year of the time series from 2001-2015 to yield a mean annual cycle. Five measures are utilized throughout to quantify reanalysis performance: bias, mean absolute deviation, relative bias (as percent of the mean), root mean square deviation (RMSD) and correlation coefficient. All differences are computed as model minus satellite values. The mean absolute deviation is computed by averaging the absolute value of the difference at every point in a time series, which avoids underreporting of the magnitude of differences due to averaging out of positive and negative biases. Relative bias reports the bias as a percentage of the multi-year annual mean of that variable.

Mean spatial distributions (as in Fig. 3.3,3.4) were computed by averaging the variable annual means from 2001-2015 in each grid box. Contour plots show the smoothed long-term annual means at each point in the domain. Spatial distributions of reanalysis bias were computed

by subtracting annual averaged satellite estimates from annual averaged reanalysis data, then plotted at each point in the domain.

Anomalies were computed as monthly values minus long-term monthly climatology. Standardized anomalies were computed by dividing the anomaly by the standard deviation of the time series. Standardized anomalies take into account differences in the reanalysis time series and help visually compare magnitudes of anomalies between reanalyses and satellite estimates. To evaluate more intense anomalous events for each variable, all time steps where the CERES estimates exceeded one standard deviation of the mean were considered. At each of those time steps, anomalies were computed as reanalysis value minus satellite value at that time step.

3.4 Results

3.4.1 Monthly climatology and seasonality of radiative fluxes and total cloud fraction

Monthly mean values of the radiative fluxes and total cloud fraction are computed for reanalysis products and CERES EBAF for the period from 2001 to 2015 and are summarized in Table 3.2. The table also provides statistical comparison of the reanalyses to observations of radiative fluxes and total cloud fraction over the entire NE Pacific domain. In the left column in Figure 3.1 are plots of the monthly climatology of radiative fluxes from satellite observations in black and the reanalyses in the colors. In the right column are reanalysis biases compared to CERES EBAF radiative fluxes.

Annual average downward shortwave radiative flux at the surface is overestimated by every reanalysis dataset for most months of the year. Annual average positive biases range from 0.7 Wm^{-2} (CFSR) to 21.2 Wm^{-2} (NCEP2). The annual average of the absolute values of the differences range from 3.8 Wm^{-2} (CFSR) to 21.2 Wm^{-2} (NCEP2), though JRA-55 and NCEP2 are the only products with biases that exceed the uncertainty of the satellite estimate and are thus considered significant. The average NCEP2 shortwave bias is similar to the NCEP1 bias of 20 Wm^{-2} in the NE Pacific reported by Ladd and Bond (2002). The high bias in the NCEP2 reanalysis constitutes 15% of the average downward shortwave radiative flux from that product; but the summer bias (47 Wm^{-2}) is much greater than the winter bias and constitutes closer to

20% of the average downward shortwave radiative flux in the summer. Reanalyses have the largest biases in the summer, which is expected since summer also has the largest magnitude of shortwave radiative flux at the surface. However, every reanalysis product, with the exception of MERRA2, gets the seasonal cycle of downward shortwave radiative flux correct. This finding is not surprising given the pronounced annual cycle of solar radiation in the north Pacific region; it serves, however, as a zero-order evaluation of radiative fluxes in the reanalyses. Zhang et al. (2016) found that globally MERRA, JRA-55, NCEP2 and CFSR overestimated downward shortwave radiative flux at the surface, while ERA-Interim underestimated downward shortwave radiative flux. They found that global mean biases ranged from -3 Wm^{-2} to 22 Wm^{-2}, which is similar to biases found here, with the exception of ERA-Interim, which showed biases of the opposite sign. CFSR also had the smallest global biases in downward shortwave radiative flux according to Zhang et al. (2016).

Table 3.2 Statistical comparison of monthly radiative fluxes and total cloud fraction from reanalysis data and CERES EBAF satellite estimates, spatially averaged over the domain from 40°-60° N and 180°-120° W. Statistics are provided for the mean, bias, mean absolute deviation (MAD), relative bias, root mean square deviation (RMSD) and correlation coefficient in annual cycles between CERES satellite data and reanalyses. Biases and MADs are bolded if they are larger than the uncertainty in satellite estimates, meaning bias is significant.

Data Product	Measures	Downward shortwave radiative flux (Wm^{-2})	Upward shortwave radiative flux (Wm^{-2})	Downward longwave radiative flux (Wm^{-2})	Upward longwave radiative flux (Wm^{-2})	Total cloud fraction (%)
CERES EBAF	Mean	119.4	9.09	313.5	356.2	88.4
	Uncertainty	6.9	8.3	4.3	11.5	5.0
ERA-Interim	Mean	124.9	10.1	313.9	356.9	78.9
	Bias (MAD)	5.5 **(7.7)**	1.0 (1.0)	0.41 (2.1)	0.71 (0.72)	**-9.5 (9.5)**
	Relative Bias (%)	4.4	10.0	0.13	0.20	12.0
	RMSD	10.5	1.4	2.6	0.86	9.6
	Correlation coeff.	0.99	0.99	0.99	0.99	0.67
MERRA2	Mean	122.4	10.7	304.6	353.5	70.8
	Bias (MAD)	3.0 **(7.1)**	1.7 (1.7)	**-8.9 (8.9)**	-2.7 (2.7)	**-17.5 (17.5)**
	Relative Bias (%)	2.4	15.5	2.9	0.78	24.7
	RMSD	10.1	1.7	9.2	2.8	17.7
	Correlation coeff.	0.99	0.99	0.99	0.99	0.74
JRA-55	Mean	131.7	11.2	309.6	358.7	66.7
	Bias (MAD)	**12.3 (12.3)**	2.1 (2.1)	-3.8 (3.9)	2.5 (2.5)	**-21.6 (21.6)**
	Relative Bias (%)	9.4	18.6	1.3	0.69	32.4
	RMSD	15.1	2.1	4.7	2.5	21.7
	Correlation coeff.	0.99	0.99	0.99	0.99	0.41
NCEP2	Mean	140.6	12.7	307.6	357.4	66.7
	Bias (MAD)	**21.2 (21.2)**	3.6 (3.6)	**-5.8 (5.9)**	1.2 (2.1)	**-21.7 (21.7)**
	Relative Bias (%)	15.1	28.6	1.9	0.35	32.6
	RMSD	26.0	4.0	7.7	2.4	22.3
	Correlation coeff.	0.99	0.99	0.96	0.99	0.43
CFSR	Mean	120.3	11.1	317.1	357.4	80.4
	Bias (MAD)	0.86 (3.8)	2.0 (2.0)	3.6 (3.6)	1.3 (1.3)	**-8.0 (8.0)**
	Relative Bias (%)	0.7	18.0	1.1	0.36	9.9
	RMSD	4.6	2.2	3.9	1.4	8.1
	Correlation coeff.	0.99	0.99	0.99	0.99	0.79

Annual average upward shortwave radiative flux at the surface is overestimated by all reanalysis products, with biases ranging from 1.0 Wm^{-2} (ERA-Interim) to 3.6 Wm^{-2} (NCEP2), corresponding to 10 to 28.6% of average upward shortwave radiative flux values (see Table 3.2). These biases are not significant, however, because they are all within the bounds of uncertainty of the satellite estimates. Biases in upward shortwave radiative flux in the reanalysis dataset over the NE Pacific are largely attributable to the biases in downward shortwave radiative flux, since the domain of interest is mostly ocean surface (little to no change in surface albedo). Despite biases, correlation coefficients for both upward and downward shortwave radiative fluxes are 0.97 or higher for all reanalysis datasets. This is not surprising given that the seasonal cycle of

these variables in each dataset is adequate and dominates the correlation (Zhang et al., 2016). Yang et al. (1999) evaluated the older versions of the ECMWF and NCEP reanalysis products, ERA-40 and NCEP1, respectively, and found consistent overestimation of reflected shortwave radiative flux throughout the globe compared to Earth Radiation Budget Experiment (ERBE). Though the Yang et al. (1999) study is not directly comparable to results shown here, due to the difference in observations used, reanalysis products, time periods (Yang et al. (1999) used years 1985 and 1986), and analysis location (they looked at the top of the atmosphere), this does highlight a consistent problem in overestimation of upward shortwave radiative flux across reanalyses.

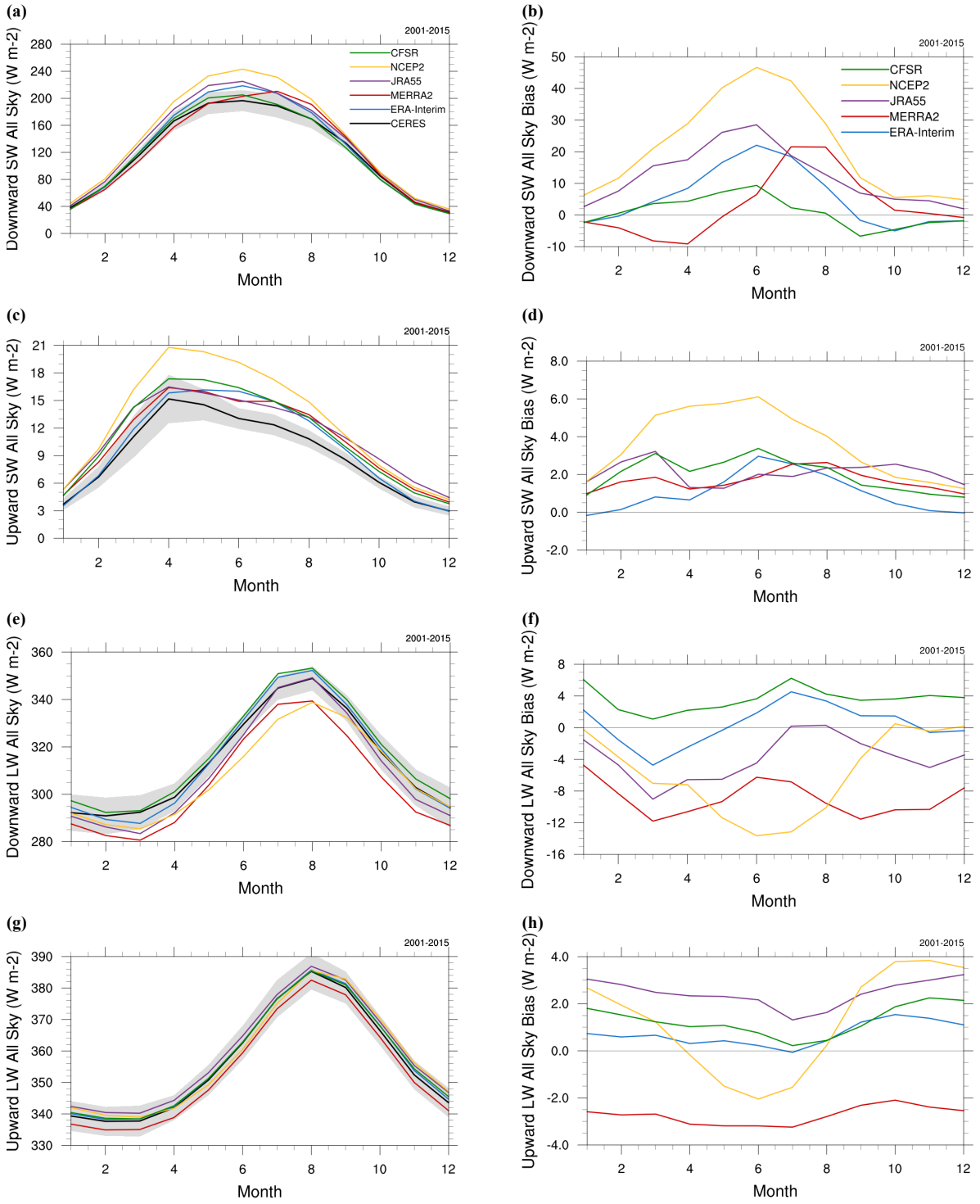

Figure 3.1 Monthly climatology (left column) and bias (right column) of radiative fluxes. The black line in plots (a), (c), (e), and (g) represents CERES EBAF climatology, and gray shading is standard deviation of CERES EBAF variables. Green line is CFSR, yellow line is NCEP/DOE R2, purple line is JRA55, red line is MERRA2 and blue line is ERA-Interim in all plots. Subplots (a) and (b) show downward shortwave, subplots (c) and (d) show upward shortwave, subplots (e) and (f) show downward longwave and subplots (g) and (h) show upward longwave radiative flux.

The reanalysis datasets have annual average biases in downward longwave radiative flux ranging from -8.9 (MERRA2) to 3.6 Wm^{-2} (CFSR) (Figure 3.1e,f & Table 3.2). Downward longwave flux biases from ERA-Interim, JRA-55, and CFSR are in reasonable agreement with the satellite estimates, while biases in MERRA2 and NCEP2 are significant. Few studies have investigated reanalysis bias of downward longwave radiative flux, and we are not aware of any studies that provide a detailed analysis of downward longwave radiative flux in the NE Pacific specifically. Wang and Dickinson (2013) evaluated downward longwave radiative flux from reanalysis against in-situ measurements and found high correlation coefficients (0.96-0.98), and globally averaged negative biases of -0.19 Wm^{-2} (CFSR), -2.31 (ERA-Interim), and -14.51 (MERRA). The biases in MERRA2 in the NE Pacific reported here are similar to those Wang and Dickinson (2013) report for MERRA globally. The contour maps in Figure 16 in Wang and Dickinson (2013) show biases between CERES SYN satellite estimates and reanalysis in the NE Pacific region that are very similar to those reported here. Biases in longwave radiative flux are most likely attributable to difficulty in accurately modeling clouds (Yang et al., 1999; Wang and Dickinson, 2013), but could also be attributed to differences in temperature and water vapor profiles.

Reanalysis biases in upward longwave radiative flux are shown in Figure 3.1g,h. ERA-Interim, JRA55, and CFSR all show positive biases throughout the year, with slightly smaller biases in summer compared to winter. MERRA2 shows consistently negative biases in upward longwave radiative flux throughout the year. NCEP2 has positive biases in the winter and negative biases in the summer. However, since all biases are smaller than uncertainties in the satellite estimates, the biases are not significant. Since the reanalysis products (with the exception of CFSR) do not interactively assimilate sea surface temperatures (in other words, reanalysis products read in SST observations which stay fixed and do not change based on radiation and cloud changes in the reanalysis model), the biases in upward longwave radiative flux are likely a combination of differences in SST and differences in downward longwave radiative flux reaching the surface. Differences in upward longwave radiative flux in CFSR could be due in part to differences in sea surface temperatures compared to CERES (CFSR has a SST bias of 0.22 K, not shown).

Figure 3.2a shows monthly climatologies of total cloud cover from satellite estimates and reanalysis data, with the corresponding biases in Figure 3.2b. All reanalysis products underestimate total cloud cover, with multiyear mean negative biases ranging from -8% (CFSR) to -21.7% (NCEP2) total cloud fraction. Cloud biases in all reanalysis products are significant. NCEP2 most grossly underestimates total cloud cover, sometimes by ~30%, particularly in the summer months, which is likely part of the reason for the large positive biases in downward shortwave radiative flux in NCEP2. While cloud fraction bias and shortwave bias tend to be negatively correlated in the reanalyses, sometimes the relationship is weaker than expected, suggesting other factors like different in cloud optical thickness, cloud height, or, possibly, aerosols also contribute (see Appendix A).

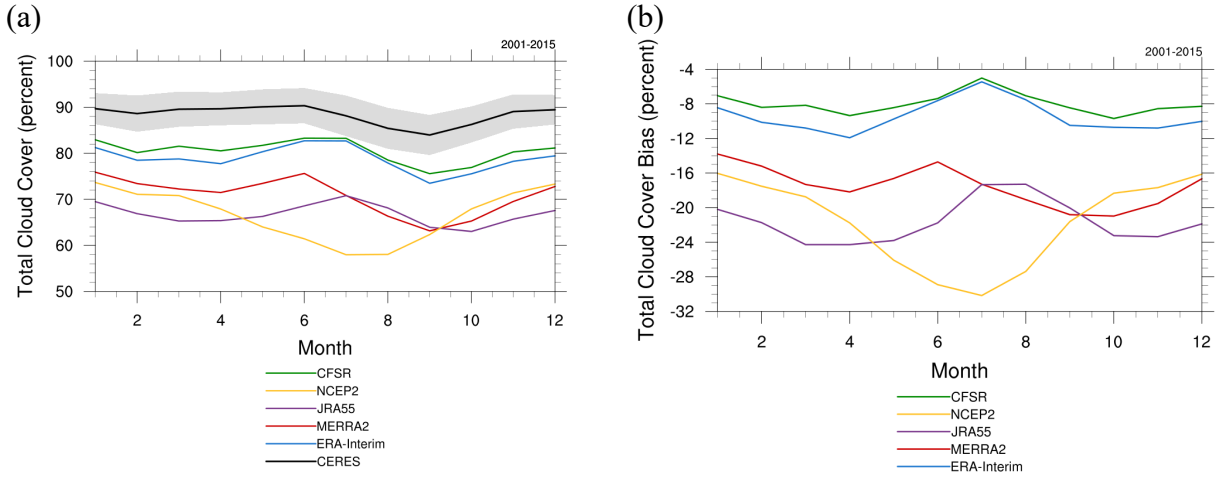

Figure 3.2 Monthly climatology (left column) and bias (right column) of total cloud cover. The black line in plot (a) represents CERES EBAF climatology, and gray shading is standard deviation of CERES EBAF variables. Green line is CFSR, yellow line is NCEP/DOE R2, purple line is JRA55, red line is MERRA2 and blue line is ERA-Interim in all plots.

There are no studies that evaluate total cloud fraction in the NE Pacific in particular; however, many other studies point out discrepancies in cloud fraction estimates by reanalysis products. Arguably the most comparable studies to our region of interest analyze the Arctic. Walsh et al. (2009) find that NCEP1 and JRA25 consistently underestimate cloud fraction at the Barrow, Alaska site, while ERA-40 represents cloud fraction better; furthermore, they note that radiative flues are well represented in reanalysis datasets if/when the cloud fraction is also well represented.

3.4.2 Spatial distribution of radiative fluxes and total cloud fraction

Evaluation of the domain-averaged parameter climatologies in Section 4.1 obscures spatial variations in the satellite measurements and reanalyses, which we explore in this section. For brevity, we discuss only spatial distribution of biases in net shortwave and net longwave radiative fluxes at the surface. It is useful to keep in mind that the climatological biases discussed in Section 4.1 show that net shortwave biases are dominated by biases in downward shortwave radiative flux and net longwave biases are generally dominated by biases in downward longwave radiative flux. There is very little spatial variation in total cloud cover biases so we do not discuss them further.

Most of the reanalysis products analyzed here exhibit an east-west gradient in radiative flux biases. The top panel of Figure 3.3 shows the annual mean climatological distribution of CERES EBAF net shortwave radiative flux, while the following panels of Figure 3.3 show the long-term mean annual differences between the satellite estimates and the reanalysis products. ERA-Interim, JRA55, NCEP2 and CFSR all show larger positive net shortwave biases in the west portion of the domain, with smaller positive or even negative (CFSR) net shortwave biases in the eastern portion of the domain nearer to the coast. MERRA2 is the only reanalysis product that has a north-south gradient in net shortwave radiative flux bias, with positive biases in the south, corresponding to larger average climatological net shortwave fluxes at the surface. Betts et al. (2006) compared NCEP2 and ERA-40 reanalysis data to ISLSCP-II data from 1986-1995 and present spatial maps of biases in their Figures 10 & 11 for downward shortwave radiative flux. Not much spatial variation is apparent in the NE Pacific in winter, though summer shows higher downward shortwave biases nearest the coast for ERA-40 reanalysis (which is different than what is found here for ERA-Interim), and highest biases off the coast of Washington and Oregon and then south of the Gulf of Alaska for NCEP2. Large biases are also apparent in NCEP2 near the coast here, though Betts et al. (2006) do not report the large biases also seen here in the western part of the NE Pacific domain. Lack of agreement in Betts et al. (2006) results and those shown here could be due to a variety of factors, including the different time periods analyzed, the different observations used for comparison, or the different versions of the ECMWF reanalysis products evaluated.

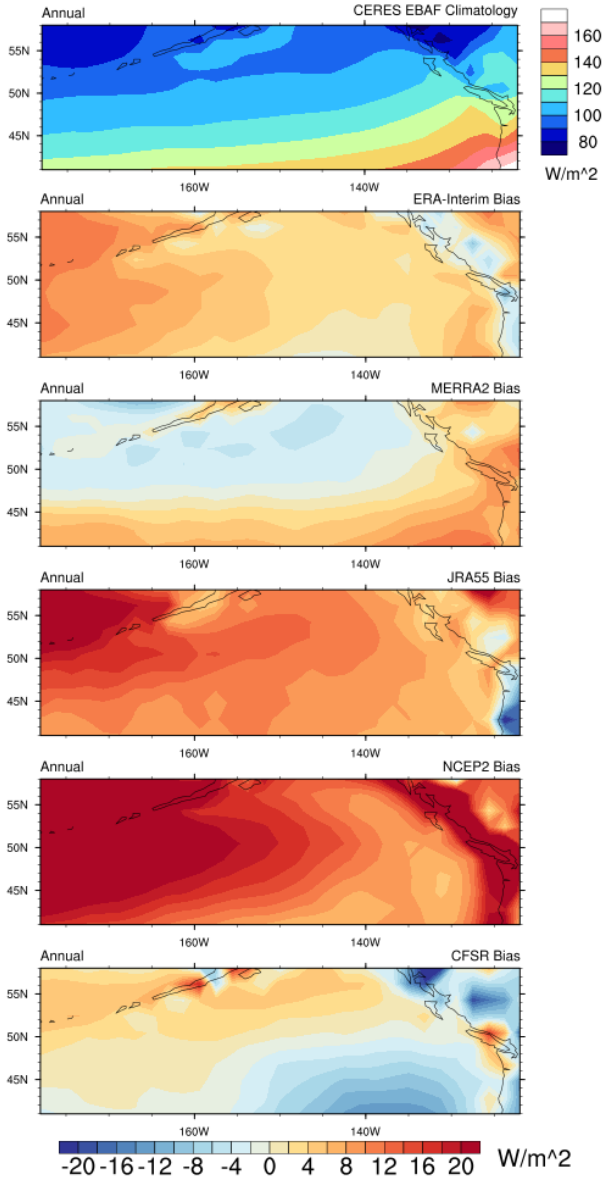

Figure 3.3 Annual mean climatology of net shortwave radiative flux from CERES EBAF satellite estimates in the NE Pacific (top panel). Subsequent panels show spatial distribution of biases in reanalysis dataset net shortwave radiative flux for ERA-Interim, MERRA2, JRA55, NCEP2 and CFSR, respectively.

Patterns in the spatial distribution of net longwave radiative flux biases in reanalysis datasets are less consistent (Figure 3.4). ERA-Interim has positive biases in the open ocean in the south of the domain and negative biases in the north and along the coast. MERRA2 has negative biases throughout the domain, with largest biases in the zone of coastal upwelling. JRA55 has little spatial variation, although largest negative biases occur to the north. NCEP2 also has large

negative biases in the north and along the coast. Finally, CFSR biases vary from west to east, with larger positive biases for the ocean in the west and negative biases occurring along the coast. Figure 14 in Betts et al. (2006) show that the largest biases in summertime downward longwave radiative flux in the NE Pacific occur near the coast for both NCEP2 and ERA-40. These results are not consistent with those presented here, likely for similar reasons mentioned previously.

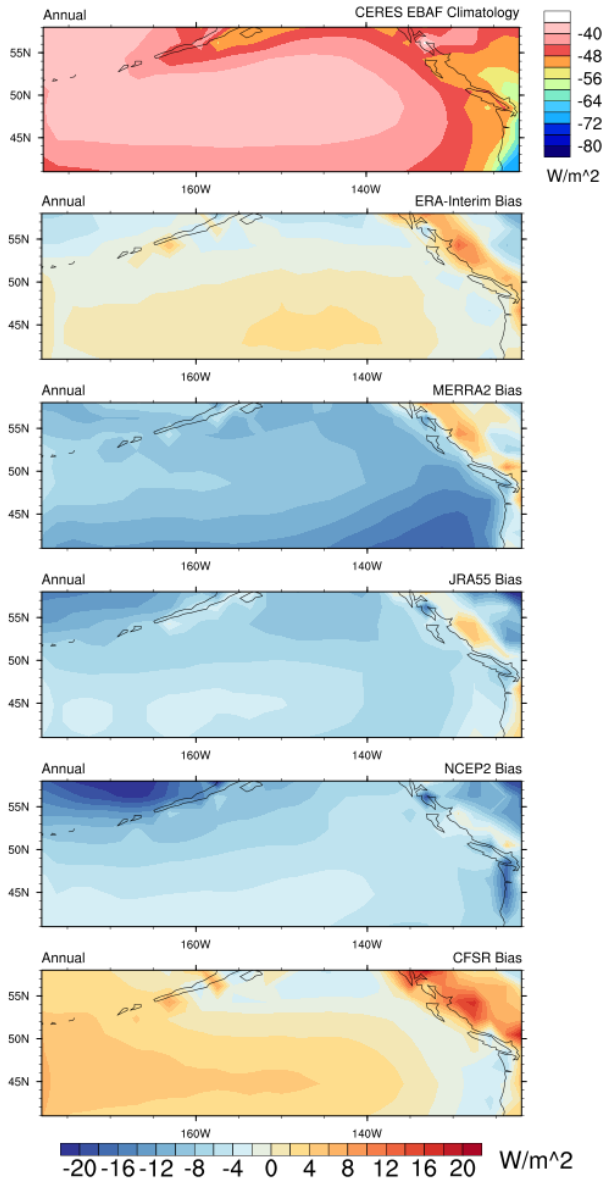

Figure 3.4 Annual mean climatology of net longwave radiative flux from CERES EBAF satellite estimates in the NE Pacific (top panel). Subsequent panels show spatial distribution of biases in reanalysis dataset net longwave radiative flux for ERA-Interim, MERRA2, JRA55, NCEP2 and CFSR, respectively.

Another sub-region of interest within the domain is the mountain chain along the coast, ranging from Oregon and Washington up into British Columbia. There are clearly larger biases along these mountain ranges compared to surrounding areas. Biases in reanalyses at higher altitudes is documented in other studies (e.g., Dulière et al., 2011) so will not be discussed in detail here.

3.4.3 Anomalies in radiative fluxes and total cloud fraction

Just as global reanalysis evaluations do not supply detail of reanalysis performance at small spatial scales, annual climatological reanalysis evaluations do not supply detail of reanalysis performance on short temporal scales. Anomalous events are of particular interest to climate scientists as they provide insight into the climate and interactive processes when the system is pushed towards extremes. For the reasons mentioned in the introduction, reanalysis products can be important tools for studying anomalous climatic events, but it is essential to understand the performance of reanalysis models during the anomalous periods. Some studies have evaluated representation of temperature and precipitation extremes in reanalysis products (Dulière et al., 2011; Donat et al., 2014), though we are unaware of studies that evaluate anomalies in radiative fluxes and cloud fraction.

Time series of anomalies of radiative parameters and total cloud fraction from CERES EBAF satellite estimates are compared to those from the reanalysis data, spatially averaged over 40°-60° N and 180°-120° W. Table 3.3 presents statistics both for comparison of all anomalies, as well as comparison of just anomalous events that exceed 1 standard deviation (σ) of the mean.

Table 3.3 Statistical comparisons of radiative flux and total cloud fraction monthly mean anomalies from reanalysis data and CERES EBAF satellite estimates, spatially averaged over the domain from 40-60 N and 180-240 E. Statistics include mean absolute deviation (MAD), root mean square deviation (RMSD), and correlation coefficient comparing all anomalies in CERES data and reanalysis data, as well as bias, mean absolute deviation (MAD), RMSD and correlation coefficient for anomalous events exceeding 1 standard deviation (≥1σ). Biases and MADs are bolded if they are larger than the uncertainty in satellite estimates, meaning bias is significant.

Data Product	Measures	Downward shortwave radiative flux (Wm^{-2})	Upward shortwave radiative flux (Wm^{-2})	Downward longwave radiative flux (Wm^{-2})	Upward longwave radiative flux (Wm^{-2})	Total Cloud Fraction (%)
ERA-Interim	MAD	2.6	0.28	1.8	0.51	1.4
	RMSD	3.5	0.39	2.5	0.71	1.7
	Correlation coeff.	0.62	0.76	0.83	0.97	0.56
	Bias (≥1σ (MAD)	**12.9 (13.5)**	1.0 (1.1)	-0.86 (2.8)	0.46 (0.94)	**-9.6 (9.6)**
	RMSD (≥1σ)	15.6	1.4	3.6	1.1	9.9
	Correlation coeff. (≥1σ)	0.99	0.97	0.99	0.99	0.73
MERRA2	MAD	3.5	0.27	1.9	0.48	1.8
	RMSD	4.9	0.36	2.5	0.62	2.2
	Correlation coeff.	0.48	0.82	0.80	0.98	0.37
	Bias (≥1σ) (MAD)	2.4 (9.4)	**1.5 (1.5)**	**-9.3 (9.3)**	-2.9 (2.9)	**-17.4**
	RMSD (≥1σ)	11.6	1.6	9.8	3.1	**(17.4)**
	Correlation coeff. (≥1σ)	0.96	0.98	0.98	0.99	17.6
						0.75
JRA-55	MAD	2.4	0.26	1.8	0.27	1.5
	RMSD	3.2	0.36	2.5	0.36	2.0
	Correlation coeff.	0.67	0.81	0.82	0.99	0.47
	Bias (≥1σ) (MAD)	**20.3 (20.3)**	**2.0 (2.0)**	**-5.1 (5.2)**	2.4 (2.4)	**-22.1**
	RMSD (≥1σ)	21.8	2.2	6.1	2.4	**(22.1)**
	Correlation coeff. (≥1σ)	0.99	0.95	0.99	0.99	22.3
						0.56
NCEP2	MAD	3.1	0.51	2.1	0.37	1.7
	RMSD	4.4	0.81	2.8	0.49	2.2
	Correlation coeff.	0.40	0.83	0.75	0.99	0.45
	Bias (≥1σ) (MAD)	**34.1 (34.1)**	**5.1 (5.1)**	-4.4 **(5.4)**	1.0 (2.1)	**-21.6**
	RMSD (≥1σ)	36.4	5.4	7.3	2.4	**(21.6)**
	Correlation coeff. (≥1σ)	0.98	0.96	0.95	0.99	22.3
						0.43
CFSR	MAD	2.2	0.38	2.8	0.36	1.4
	RMSD	2.9	0.52	3.4	0.46	1.8
	Correlation coeff.	0.82	0.78	0.60	0.99	0.75
	Bias (≥1σ) (MAD)	5.1 (6.3)	**2.5 (2.5)**	1.5 (3.5)	1.2 (1.3)	**-8.2 (8.2)**
	RMSD (≥1σ)	7.2	2.7	4.2	1.5	8.5
	Correlation coeff. (≥1σ)	0.99	0.97	0.98	0.99	0.89

Figure 3.5a shows the time series of standardized anomalies of downward shortwave radiative flux from 2001-2015 for CERES EBAF and the five reanalysis datasets. On average, the mean absolute deviations of the anomalies range from 2.2 Wm^{-2} (CFSR) to 3.5 Wm^{-2} (MERRA2) (Table 3.3), which are all small enough to be in acceptable agreement with the

satellite estimates. For anomalous events that exceed 1 σ, those mean absolute deviations are much larger, ranging from 6.3 Wm^{-2} (CFSR) to 34.1Wm^{-2} (NCEP2). The deviations from ERA-Interim, JRA-55, and NCEP2 are significant. The time series in Figure 3.5a make it apparent that CFSR best captures the anomalous changes in downward shortwave radiative flux that are documented in the CERES EBAF datasets, particularly in the last few years of the time period. The anomaly comparison statistics indicate that on the whole, the reanalysis products are not reproducing extreme anomalous events (≥1σ) well, even when they are adequately reproducing the climatology of downward shortwave radiative flux in the NE Pacific.

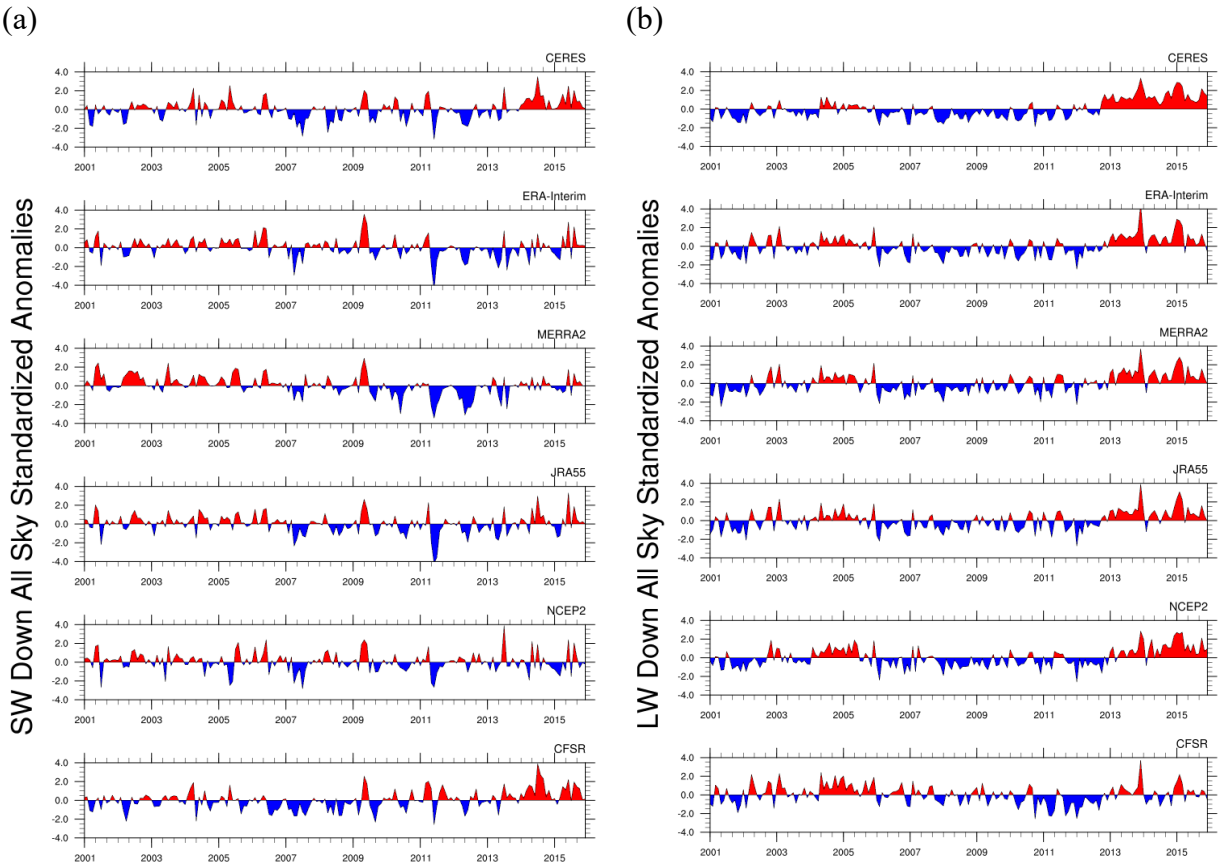

Figure 3.5 Time series from 2001-2015 of monthly standardized anomalies of all sky downward (a) shortwave radiative flux and (b) longwave radiative flux from CERES, ERA-Interim, MERRA2, JRA55, NCEP2, and CFSR. Positive anomalies are shaded red and negative anomalies are shaded blue.

Figure 3.5b shows the time series of standardized anomalies of downward longwave radiative flux from 2001-2015 for CERES EBAF and the five reanalysis datasets. On average the mean absolute deviations of anomalies range from 1.8 Wm^{-2} (ERA-Interim) to 2.8 Wm^{-2}

(CFSR). These deviations are not significant. For anomalous events that exceed 1 σ, those mean absolute deviations are larger, ranging from 2.8 Wm^{-2} (ERA-Interim) to 9.3 Wm^{-2} (MERRA2), again suggesting reanalyses do less well in capturing the magnitudes of large anomalies compared to smaller anomalies. The deviations in MERRA2, JRA-55, and NCEP2 are significant. The larger deviations for larger anomalies are likely at least in part due to the larger magnitudes associated with more extreme anomalous events.

For brevity, anomaly biases for total cloud fraction are not discussed here, though comparison statistics are presented in Table 3.2. All cloud fraction biases and MADs for anomalous events exceeding 1 σ are significant. These biases in radiative fluxes and cloud fraction have implications for the use of reanalysis products when studying anomalous events. For example, reanalysis products are not informative tools to use to study a climate extreme event in which the signal falls within the biases presented here.

3.5 Discussion

Our analysis evaluates radiative fluxes and total cloud fraction from reanalysis models relative to CERES EBAF satellite estimates. One interpretation of these biases is that they provide bounds of uncertainty for parameters in reanalysis datasets. In this case, the uncertainty in regional mean downward shortwave radiative flux can be interpreted as ±7.7 Wm^{-2} (ERA-Interim), ±7.1 Wm^{-2} (MERRA2), ±12.3 Wm^{-2} (JRA-55), ±21.2 Wm^{-2} (NCEP2), and ±3.8 Wm^{-2} (CFSR). Uncertainties for the remaining variables can be specified from the mean absolute deviations presented in Table 3.2. These uncertainties are similar or greater for anomalous events greater than 1 σ (see Table 3.2). This means that extra caution should be taken when using reanalyses to analyze anomalous events in the climate system in the NE Pacific.

For most of the fields evaluated here, CFSR has the smallest differences compared to satellite estimates. The low biases, particularly in total cloud fraction, found in CFSR suggest the importance of air-ocean-sea ice interactions, specifically how SSTs are important for determination of clouds and radiative fluxes and vice versa, at least in the region of the NE Pacific. Studies have shown that SSTs and low cloud are negatively correlated in the subtropical and midlatitude North Pacific (e.g., Klein et al., 1994; Norris & Leovy, 1994); therefore, it

makes sense that using a coupled ocean-atmosphere model in this region could be important for replicating observed cloud cover. NCEP2 often has the largest biases in radiative fluxes and total cloud fraction compared to satellite estimates, which suggests very large uncertainties in the reanalysis data. Though CFSR and NCEP2 both come from the same modeling center, the models and resolutions used in each are quite different. Furthermore, the difference in performance between the coupled reanalysis product (CFSR) and non-coupled reanalysis product (NCEP2) is stark. The evidence that the coupled CFSR outperforms NCEP2 and the other non-coupled reanalyses in most variables suggests that the ocean-atmosphere coupling could be partially responsible for improved reproduction of atmospheric variables. This could be especially pertinent in the NE Pacific midlatitudes where atmosphere-ocean interactions are important, and coupled models should be utilized when possible.

Disregarding dataset biases when using reanalysis products can produce substantial problems. Consider an analysis of the ocean surface radiative budget in the NE Pacific using data from the poorest performing reanalysis product, NCEP2, in the summer months, when NCEP2 typically has its largest biases. With summer downward shortwave biases on the order of 40 Wm^{-2}, upward shortwave biases on the order of 6 Wm^{-2}, downward longwave biases on the order of -12 Wm^{-2}, and upward longwave biases on the order of -2 Wm^{-2}, the net radiative flux biases would be on the order of 32 Wm^{-2}. Assuming a mixed layer ocean depth of 10 m (a reasonable summer mixed layer depth in this region), these net radiation biases would mean that estimations of temperature for 1 m^2 of the ocean mixed layer would be off by ~2.1 °C (~3.8 °F) over 1 month. This 'the worst case scenario' of SST error is well outside of typical standard deviation of SSTs in this region.

Our analysis also highlights the need for more in-depth evaluation of reanalysis products before their application to climate studies. A thorough understanding of reanalysis performance is necessary in order to (a) choose the reanalysis product most appropriate for the region and variables of interest, and (b) quantify uncertainties in results reached by using these reanalyses. Though there are some in-depth, observationally-based, regional evaluations of reanalyses (e.g., Jin-Huan et al., 2014 (Eastern Himalayas); Josey, 2001, & Josey et al., 2002 (North Atlantic); Newman et al., 2000 and Kumar & Hu, 2012 (tropical Pacific); Ma et al., 2008 (China); Yu et al., 2010 and Ming et al., 2013 (Antarctica)), more projects that systematically evaluate and compare reanalysis products for many regions around the globe would help address this need.

Our study suggests that there is no one 'gold standard' reanalysis that is best for all climate studies. The most appropriate reanalysis product depends on the atmospheric variables of interest, the sub-region of the NE Pacific domain that is being studied, the time period of interest, and whether the reanalysis products are needed to represent climatology or anomalies. Generally, reanalysis products perform best at large spatial and temporal scales, whereas the biases are much larger when looking at smaller spatial scales and sub-annual time scales. This study, for example, shows that for the region of the NE Pacific, CFSR may be the most appropriate reanalysis product to use if studying downward shortwave radiative flux at the surface, since this dataset has the smallest biases (Table 3.2). On the other hand, ERA-Interim has the smallest biases for downward longwave radiative flux at the surface, which means the ECMWF product may be best for studies that are particularly sensitive to longwave radiative flux accuracy (Table 3.2). A study of the coastal NE Pacific might avoid using NCEP2 and MERRA2, which show particularly large biases in shortwave and longwave radiative fluxes near the coast compared to the open ocean (Figs. 3.3, 3.4). Furthermore, studies focused on anomalous events might choose to use CFSR data, which has the smallest biases during anomalous events defined to be outside 1 σ of climatology (Fig. 3.5).

3.6 Conclusions

This study evaluates the quality of radiative fluxes and total cloud fraction from five reanalysis products compared to CERES EBAF satellite estimates in the NE Pacific (40°-60°N, 180°-120°W). The analysis quantifies uncertainties in the variables that can help guide appropriate use of reanalyses in this region. Biases in climatological annual cycles of downward shortwave radiation ranged from 0.86 Wm^{-2} (CFSR) to 21.2 Wm^{-2} (NCEP2) while biases in climatological mean of upward shortwave radiative flux ranged from 1.0 Wm^{-2} (ERA-Interim) to 3.6 Wm^{-2}. Biases in climatological annual cycles of downward longwave radiation ranged from -8.9 Wm^{-2} (MERRA2) to 3.6 Wm^{-2} (CFSR), while biases in climatological annual cycles of upward longwave radiation ranged from -2.7 Wm^{-2} (MERRA2) to 2.5 Wm^{-2} (JRA-55). In all cases, biases between reanalysis and satellite estimates are larger during anomalous events that exceed 1σ compared to all anomalous deviations. Furthermore, deviations during anomalous events that exceed 1σ are similar to or much greater than climatological deviations. These results

indicate that there are limitations to application of reanalysis products. Using reanalysis data to study climate processes with a signal within the bounds of errors cited in this manuscript may not be useful. Caution should be taken to fully understand the uncertainties within reanalysis products before applying them to climate analysis, since results presented here show large variability in performance between reanalyses, variables within the datasets, and sub-regions of the study domain.

Chapter 4 The Role of Clouds and Surface Heat Fluxes in the Maintenance of the 2013-2016 Northeast Pacific Marine Heatwave

4.1. Introduction & Background

From boreal fall of 2013 through early 2016, anomalously high sea surface temperatures (SSTs) were observed in the Northeast (NE) Pacific, appearing in the Gulf of Alaska waters and eventually affecting regions along the coastline of North America. The warm SSTs exceeded 6°C above normal in some locations during its multi-year duration, making it the largest and longest marine heatwave (MHW) ever observed (Bond et al., 2015; Gentemann et al., 2016; Scannell et al., 2016; Jacox et al., 2016; Frölicher and Laufkötter, 2018). MHWs often have devastating ecological and economic impacts, which can increase in severity with the length and intensity of the MHW. Anomalously warm SSTs can cause coral bleaching (Le Nohaïc et al., 2017; Hughes et al., 2017), movement of marine species to cooler water (Cavole et al., 2016; Oliver et al., 2017; Wernberg et al., 2016), mass species die offs (Jones et al., 2018; Oliver et al., 2017; Garrabou et al., 2009), and harmful algal blooms (McCabe et al., 2016). For the NE Pacific MHW in particular, the harmful algal bloom associated with the event was the largest ever recorded and caused closures of many lucrative fisheries in the U.S. Pacific Northwest (Cavole et al., 2016; McCabe et al., 2016). A better understanding of MHWs, working towards the ability to forecast the intensity and duration, could improve the adaptive capacity of communities impacted by these events.

The NE Pacific 2013/16 MHW (hereafter the NE Pacific MHW) is one of the most well-studied MHW events (Bond et al., 2015; Hartmann, 2015; Jacox et al., 2016; Gentemann et al., 2016; Di Lorenzo & Mantua, 2016; Hobday et al., 2018; Oliver et al., 2018; Myers et al., 2018), making it a good case study for understanding the maintenance mechanisms of MHWs. A MHW is defined as a period when SSTs exceed an upper threshold, typically the 90th percentile relative to local climatology, for five days or longer (Hobday et al., 2016). This NE Pacific MHW ('the Blob') is defined as a severe MHW since SST anomalies reached 3 times the 90th percentile differences from the local climatological SSTs (Hobday et al., 2018). MHWs are increasing in severity and frequency, and this trend will likely continue into the future due to climate change (Oliver et al., 2018); consequently, it is prudent to understand the physical drivers that start and maintain MHWs (Frölicher and Laufkötter, 2018; Oliver et al., 2017). The onset of the high

SSTs in the NE Pacific was associated with a ridge of high pressure that persisted over the Gulf of Alaska region for many weeks, stagnating winds and causing anomalous atmosphere-ocean heat fluxes (Bond et al., 2015; Gentemann et al., 2016; Hartmann, 2015). Less attention has been paid to why the anomalously warm SSTs lasted for so many years.

One possible process responsible for the maintenance of the MHW is a positive SST-cloud feedback. Many studies of the NE Pacific atmosphere-ocean system have observed concurrent increases in SSTs, decreases in low cloud fraction, and increases in incoming solar radiation at the ocean surface, suggestive of a positive SST-cloud feedback (Clement et al., 2009; Norris et al., 1998; Bellomo et al., 2014). In the subtropical Pacific off the coast of Baja California during the same MHW, Myers et al. (2018) observed a positive SST-cloud feedback and concluded it did indeed play a role in the persistence of the anomalous SSTs. However, they also found that further north in the NE Pacific (40-50°N and 140-160°W) from January 2013-December 2013, there was no evidence of a positive SST-cloud feedback during the onset of the MHW (Myers et al., 2018). The NE Pacific MHW offers a convenient natural experiment to study whether or not a SST-cloud feedback helped maintain the MHW in the midlatitudes – a region that was not been the focus of most previous work. Regional studies of cloud feedbacks are essential for understanding spatial patterns in these feedbacks- an important step in reducing our uncertainty of cloud feedbacks in climate models.

Here we expand on the work of Bond et al. (2015) and Myers et al. (2018) by studying a time period that encompasses the entire duration of the MHW (November 2013-January 2016), using different datasets (CFSR and GODAS) and analyzing a different study region. We seek to understand the drivers contributing to the persistence of warm SST anomalies during the entire 2013-2016 NE Pacific MHW. Specifically, we address the following questions:

1. How does the atmosphere respond to anomalously warm SSTs during the NE Pacific MHW?
2. How does the atmospheric response to anomalously warm SSTs in turn affect the SST anomalies? In other words, what processes caused the warm SSTs to *persist* for multiple years?

4.2. Data and Methods

4.2.1 Reanalysis Data

Data from the National Center for Environmental Prediction (NCEP) Climate Forecast System Reanalysis (CFSR) (Saha et al., 2010; Saha et al., 2014) are used to determine anomalies of SSTs, surface radiative heat fluxes, turbulent heat fluxes, and cloud fractions during the MHW. More details on the CFSR product are in Appendix B. We use reanalysis due to its complete spatial coverage, long time series, and comprehensive list of variables. Moreover, CFSR was found to be the most appropriate reanalysis dataset for the NE Pacific region, based on comparisons between six reanalysis datasets and NASA's CERES satellite estimates of radiative flux and cloud fraction in which CFSR included the smallest errors (Schmeisser et al., 2018). An analysis using CERES-EBAF data is included in the Appendix B so readers can see the sensitivity of results to dataset choice. Qualitatively, CERES and CFSR yield the same results (Appendix B, Table B1, Figures B4 & B5). CFSR turbulent fluxes were also compared to the OAFlux product (a dataset of best estimates of surface fluxes using satellite data and numerical weather prediction output), and the differences were small enough that the choice of dataset has minimal effect on results of this study (see Appendix B). All data are either provided as a 1°x1° gridded product, or are re-gridded to 1°x1° resolution using linear interpolation. Monthly mean data are utilized for all analyses presented here, unless otherwise noted. Climatologies were computed by averaging data from 1979-2016, and anomalies were computed by subtracting the monthly mean from the monthly climatology. The MHW time period is defined from November 2013-January 2016. Any MHW composited averages were computed by averaging data from that time period. The NE Pacific region of interest is defined here from 40-50°N and 130-150°W. We used the location of the maximum average SST anomaly to help define the study region for this analysis.

4.2.2 Marine Heatwave Identification

Here we use the MHW definition similar to Hobday et al. (2016), but we use monthly data instead of daily data. Since our focus is on the role of the atmosphere in the MHW, longer-lasting events (rather than the shorter duration events like those in Hobday et al. (2016)) presumably interact more strongly with the atmosphere and thus monthly data is sufficient.

Anytime observed SSTs exceed the monthly 90th percentile threshold, it is considered a MHW. Using this method, the MHW time period for this study is defined as starting in November 2013 and ending in January 2016.

4.2.3 Ocean Mixed Layer Heat Budget

A mixed layer heat budget was constructed to analyze the processes contributing to anomalous SSTs during the NE Pacific MHW. Following Cronin et al. (2015), the following equation the mixed layer temperature tendency is computed from:

$$\frac{\partial}{\partial t}T = \frac{Q_o}{\rho C_p h} - u_a \cdot \nabla T - \left(w_h + \frac{dh}{dt}\right)\frac{(T - T_h)}{h} - \frac{\kappa}{h}\frac{\partial T}{\partial z}\Big|_{z=h}$$

where T is sea surface temperature, Q_o is net heat flux at the ocean surface, ρC_p is the volumetric heat capacity of water ($\rho C_p = 4.088 \times 10^6$ J°C^{-1}m^{-3}), h is the mixed layer depth, $\underline{u}_a$ is ocean current velocity, w_h is vertical velocity, T_h is the temperature at the bottom of the mixed layer, κ is the diffusivity constant, and z is depth. The first term on the right side of the equation represents the contribution of ocean surface net heat flux to mixed layer temperature tendency, the second term represents the contribution by horizontal advection, the third term represents entrainment at the bottom of the mixed layer, and the fourth term represents vertical diffusivity at the bottom of the mixed layer. For the purposes of this study, the third and fourth terms on the right side of the equation are combined into one term, and are referred to as ocean processes at the bottom of the mixed layer. Given a lack of necessary data, this term is treated as the computational residual.

SSTs, radiative heat fluxes, and turbulent heat fluxes for computation of the mixed layer heat budget are from CFSR. Ocean current velocity and mixed layer depth data are from NCEP Global Ocean Data Assimilation System (GODAS). The mixed layer depth is defined as the depth where the ocean temperature does not exceed more than 0.8°C from that of the surface. This value was found to be appropriate using monthly mean data for the region of interest.

All radiative fluxes are defined with respect to the ocean mixed layer, so positive upward radiative fluxes are from the ocean to the atmosphere, and positive downward radiative fluxes are from the atmosphere to the ocean. All turbulent fluxes are defined as positive upward from the ocean to the atmosphere.

4.3. Results

4.3.1 Atmospheric response to 2013-2016 NE Pacific MHW

The CFSR data show there was a strong anomalous atmospheric response to the warm SSTs in the NE Pacific throughout the duration of the MHW. The mean SST anomaly during the MHW averaged 1.6 K throughout the study region (Figure 4.1a). The duration of the NE Pacific MHW was unprecedented (Appendix B, Figure B2), lasting for over two years (Figure 4.1b). The atmospheric response can be seen in the MHW-composited average anomalies of surface radiative fluxes, turbulent fluxes, net heat flux, and cloud fractions during the MHW (Table 4.1, Figs 4.2, 4.3 & 4.4). Upward shortwave radiative flux anomalies are not presented here because the changes are small compared to the other radiative flux terms, and mirror changes in the downward shortwave radiative flux since ocean surface albedo remains relatively constant. More details on the processes associated with the NE Pacific MHW follow.

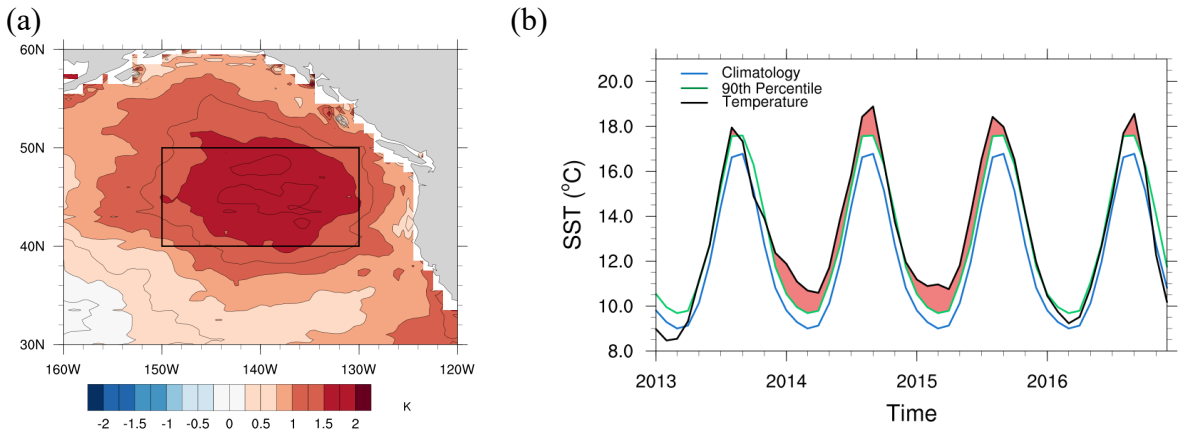

Figure 4.1 (a) Sea surface temperature anomaly from CFSR, averaged over the time period of the marine heatwave from November 2013 to January 2016, study region outlined in black; (b) Monthly averaged sea surface temperature time series from CFSR in black, SST monthly average climatology in blue and the monthly average 90th percentile in green. Red shading indicates any time period where SST exceeds the 90th percentile threshold and is thus defined as a marine heatwave.

All CFSR surface radiative fluxes had anomalous responses to the warm SSTs in the NE Pacific. During the MHW, upward longwave radiative flux increased by 8.2 Wm^{-2} on average (Table 4.1, climatological averages and standard deviations also provided in table). This increase in upward longwave radiative flux is expected given the Stefan-Boltzmann law and, unsurprisingly, the pattern of the longwave flux anomaly mirrored the pattern of the SST

anomaly (Figures 4.1a & 4.2c). During the MHW, downward longwave radiative flux increased by 4.1 Wm^{-2} on average. The largest downward longwave radiative flux anomalies were co-located with the largest anomalies in upward longwave radiative flux and SST (Figure 4.2b). The downward longwave radiative flux anomaly was due to some combination of an increase in air temperature, changes in clouds, and changes in humidity. CFSR data show changes in all of these parameters during the MHW (positive anomalies of air temperature and humidity not shown), though the relative contribution of each of these variables contributes to the increase in downward longwave radiative flux is unknown. Downward shortwave radiative flux increased by 7.1 Wm^{-2} during the event, likely due to the accompanying reduction in low cloud (Figure 4.4).

Within the region of interest, shortwave radiative flux anomalies were greatest in the southern half of the domain compared to farther north (Figure 4.2d). This pattern closely matches observed changes in low cloud (Figure 4.4). Increases in downward longwave radiative flux, upward longwave radiative flux, downward shortwave radiative flux, and upward shortwave radiative flux (not shown) result in a net radiative flux anomaly of 2.3 Wm^{-2} into the ocean mixed layer during the MHW (Figure 4.2a). Due to the spatial pattern of the shortwave radiative flux anomaly shown here, the net radiative heat flux anomaly also was strongest in the southern part of the domain compared to the north (where net radiative flux anomalies were smaller or even negative).

Table 4.1 Climatological average* and standard deviation of parameters from 1979-2016, followed by anomalies composited and averaged over the marine heatwave (11/2013-01/2016) for sea surface temperature, radiative fluxes, turbulent fluxes, and cloud cover at different levels. All values are spatially averaged over domain from 40-50°N and 130-150°W. Seasonal anomalies composited over the marine heatwave are also presented.

	Climatological average and standard deviation (1979 to 2016)	Average anomaly during MHW	Average DJF anomaly during MHW	Average MAM anomaly during MHW	Average JJA anomaly during MHW	Average SON anomaly during MHW
SST (K)	285.1 ± 5.9	1.6 ± 0.2	1.3 ± 0.2	1.7 ± 0.3	1.9 ± 0.3	1.4 ± 0.3
Upward LW (Wm^{-2})	375.2 ± 31.3	8.2 ± 1.0	6.8 ± 0.9	8.6 ± 1.6	10.1 ± 1.6	7.6 ± 1.4
Downward LW (Wm^{-2})	334.0 ± 30.4	4.1 ± 1.8	4.4 ± 1.3	3.9 ± 3.7	2.8 ± 2.2	3.8 ± 2.0
Downward SW (Wm^{-2})	133.2 ± 74.4	7.1 ± 3.3	2.8 ± 1.7	5.9 ± 7.2	17.1 ± 7.9	5.1 ± 3.0
Net radiative flux (Wm^{-2})	83.1 ± 72.9	2.3 ± 1.9	0.0 ± 1.4	0.8 ± 4.2	8.8 ± 5.4	0.9 ± 2.4
Latent heat (Wm^{-2})	56.7 ± 40.4	7.0 ± 2.5	1.4 ± 4.5	5.9 ± 3.2	9.1 ± 3.7	17.3 ± 3.7
Sensible heat (Wm^{-2})	1.8 ± 16.4	1.1 ± 1.0	-3.3 ± 1.8	1.7 ± 1.1	2.0 ± 1.2	4.4 ± 1.6
Net heat flux (Wm^{-2}) (positive into the ocean)	24.5 ± 105.4	-5.8 ± 3.6	1.9 ± 6.7	-6.8 ± 6.0	-2.4 ± 5.9	-20.8 ± 5.6
Total cloud cover (%)	79.6 ± 13.5	-3.3 ± 1.3	-2.7 ± 1.1	-2.9 ± 2.3	-6.1 ± 2.9	-2.8 ± 1.4
Boundary layer cloud cover (%)	44.9 ± 18.4	-6.9 ± 1.9	-6.3 ± 1.8	-7.6 ± 4.5	-11.0 ± 2.7	-5.4 ± 2.0
High cloud cover (%)	33.4 ± 11.9	5.3 ± 1.0	5.8 ± 2.6	6.0 ± 1.3	6.0 ± 2.3	3.2 ± 1.6

*Climatological average is computed using monthly values from CFSR averaged over the time period from 1979-2016

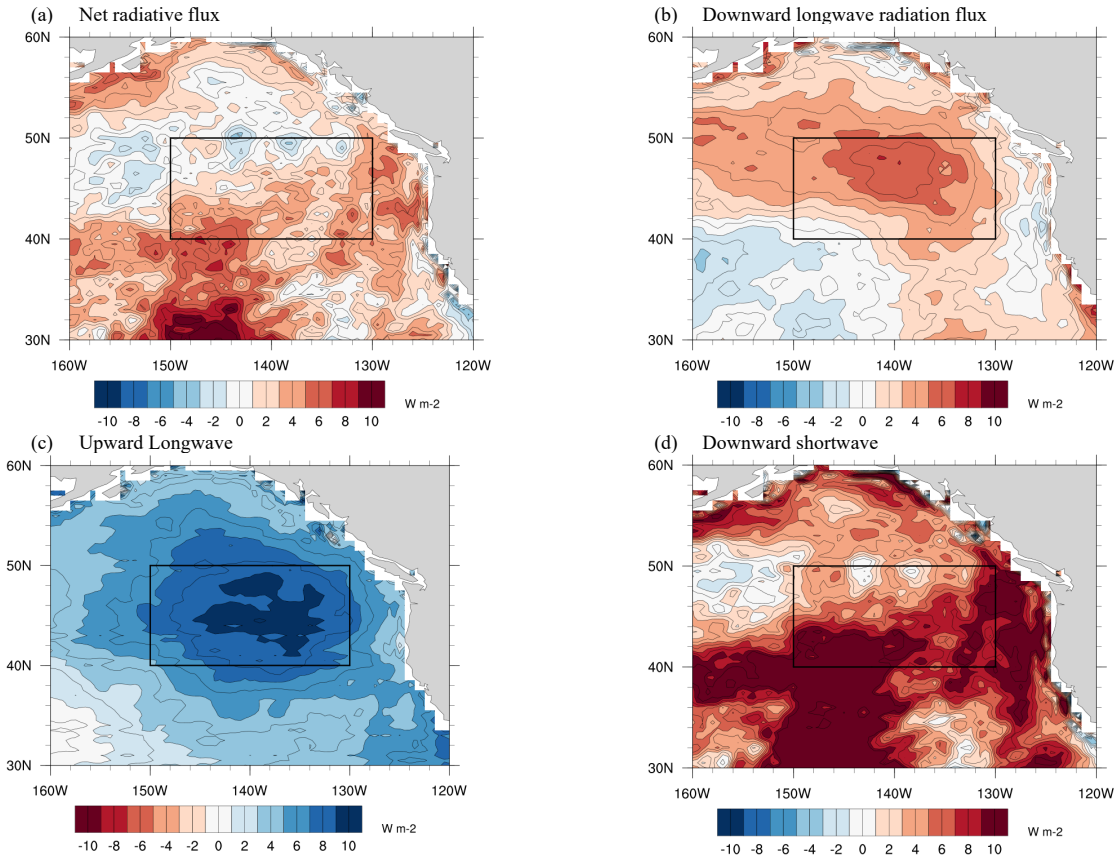

Figure 4.2 (a) Net radiative flux, (b) Downward longwave radiative flux, (c) Upward longwave radiative flux, (d) Downward shortwave flux anomalies composited and averaged over marine heatwave time period (11/2013-01/2016). The region of interest from 40-50°N and 130-150°W is boxed in black. Positive downward fluxes defined as into the ocean surface, positive upward fluxes defined as out of the ocean surface, per CFSR convention.

As with radiative flux anomalies, turbulent heat flux anomalies observed during the MHW also varied spatially and seasonally. Latent heat flux anomalies were positive throughout the entirety of the domain, and averaged an additional 7.0 Wm^{-2} flux of energy out of the ocean mixed layer during the MHW (Figure 4.3a). The latent heat flux anomaly was largest during autumn (SON) months throughout the MHW (an average of 17.3 Wm^{-2} energy loss from the ocean mixed layer), and smallest during winter (DJF) months throughout the MHW (an average of 1.4 Wm^{-2} energy loss from the ocean mixed layer) (Table 4.1). Sensible heat flux anomalies were mostly positive throughout the domain and average 1.1 Wm^{-2} energy lost from the ocean mixed layer during the MHW (Figure 4.3b). There was also a seasonal signature in sensible heat flux anomalies with the highest positive anomaly in SON (4.4 Wm^{-2}) and a negative anomaly in

DJF (-3.3 Wm^{-2}) (Table 4.1). Anomalously weak winds were observed during the MHW (Bond et al., 2015; Gentemann et al., 2016; Myers et al., 2018) and could be partially responsible for the latent and sensible heat flux anomalies during the MHW. The combination of turbulent and radiative heat fluxes yields the net flux from the ocean surface, which in this case was dominated by turbulent flux anomalies.

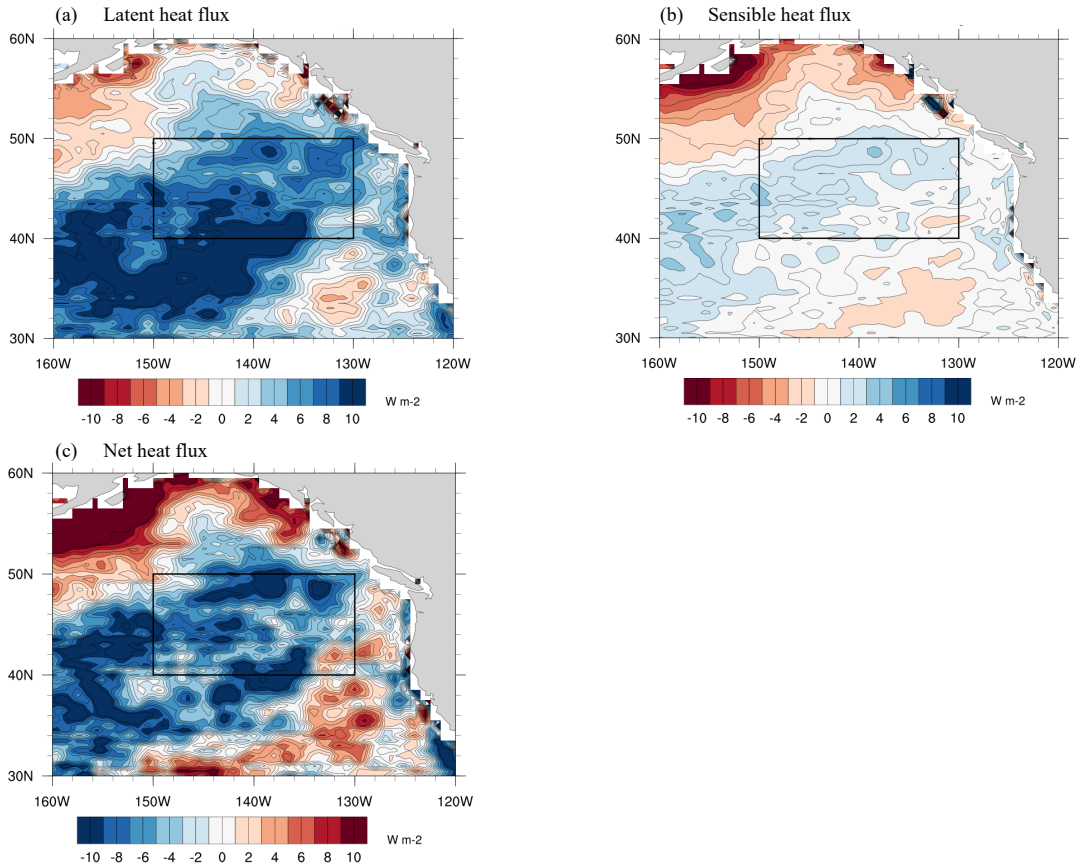

Figure 4.3 As in Figure 4.2, but for (a) latent heat flux, (b) sensible heat flux, and (c) net heat flux, including both radiative and turbulent heat fluxes. Positive turbulent fluxes defined as out of the ocean surface, positive net heat fluxes defined as out of the ocean surface, per dataset conventions.

The average net heat flux anomaly, including both radiative and turbulent heat fluxes, was negative (-5.8 Wm^{-2}) during the MHW and was dominated by the turbulent heat flux anomalies described above. While the net radiative heat flux anomaly during the MHW provided a positive anomalous heat flux of 2.3 Wm^{-2} to the ocean mixed layer, the turbulent heat flux anomaly of -8.1 Wm^{-2} more than offset this so that the ocean mixed layer experienced net anomalous cooling (-5.8 Wm^{-2}) due to the net anomalous heat flux alone (Figure 4.3c). The net

heat flux anomaly was influenced by the cloud cover response to the MHW mainly through the radiative heat flux response.

Substantial cloud changes were observed which coincide with the radiative flux anomalies during the MHW. A reduction in total cloud cover occurred during the MHW, with an average anomaly of -3.3% (Figure 4.4a). The total cloud cover anomaly was highest during summer months (JJA, an anomaly of -6.4%, Table 4.1), when total cloud cover is highest in the NE Pacific. This summer cloud anomaly resulted in an anomalous downward radiative flux of 17.1 Wm^{-2} during a time of year when the upper mixed layer is shallow and thus the heating rate is higher. The warmer surface temperatures were in turn accompanied by enhanced heat loss (primarily due to latent heat fluxes) in the summer and fall. A reduction of boundary layer cloud cover (-6.9%) was also observed throughout the domain during the MHW (Figure 4.4b). The reduction in cloud cover was largest in the southern part of the domain compared to the north, and the largest anomalies were observed during the summer (JJA, an anomaly of -11.0%, Table 4.1). This reduction in low cloud was very likely the primary driver of the observed increase in shortwave radiation at the surface during the MHW. Despite reductions in low cloud cover, clouds were not reduced throughout the entirety of the atmospheric column. High cloud cover increased during the MHW by 5.3% on average throughout the domain (Figure 4.4c). It is presumed that the most important effect of the high cloud changes was to contribute to an increase in the downward longwave radiative flux at the surface.

Although the elevated SSTs during the NE Pacific MHW coincided with a reduction in low cloud cover and an increase in radiative heat flux into the ocean surface, the turbulent heat flux anomalies offset the radiative heat flux anomalies such that the net heat flux anomalously cooled the ocean mixed layer (Figure 4.3c). Without the radiative component, however, the turbulent heat flux anomaly driven cooling would have been more efficient

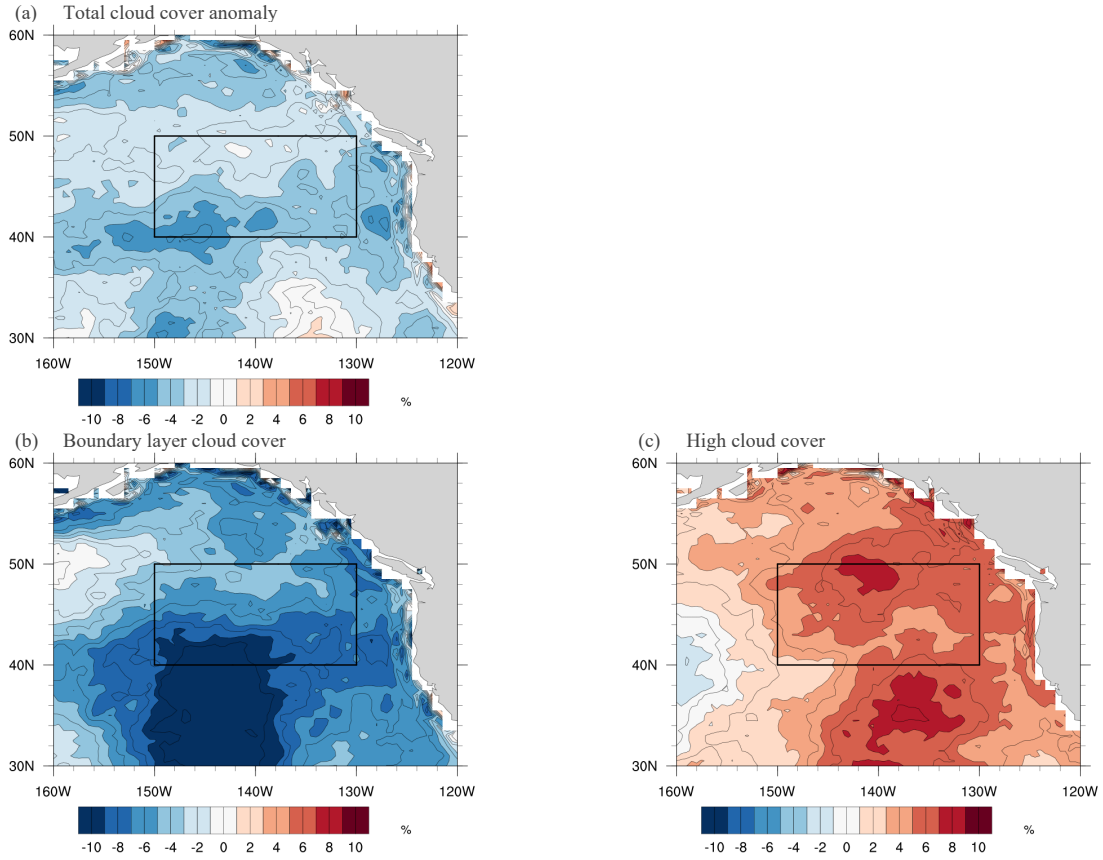

Figure 4.4 As in Figure 4.2, but for (a) total cloud cover, (b) boundary layer cloud cover, and (c) high cloud cover.

4.3.2 Ocean Mixed Layer Heat Budget During 2013-2016 NE Pacific MHW

The terms of the ocean mixed layer heat budget reveal that atmospheric processes (represented in the net heat flux term) often balance the ocean processes (represented in the advection, entrainment and diffusion terms), despite varying greatly throughout the year. The time series of ocean mixed layer temperature tendency shows it has a strong seasonality, with increasing SSTs (positive temperature tendency) from approximately February to September each year, and decreasing SSTs (negative temperature tendency) from October to January (Figure 4.5a). This temperature tendency is largely driven by the seasonality in net heat flux, which warms SSTs in the summer when insolation is highest, and cools SSTs in the winter when turbulent heat fluxes dominate (Cronin et al., 2015). Horizontal advection contributes a positive temperature tendency by advecting warmer water from the western Pacific and from lower latitudes. The bottom flux term, which is the computational residual and represents entrainment

and diffusion at the bottom of the mixed layer (in addition to any errors) balances seasonality in the other terms. In summer, when the mixed layer is shoaling and at its most shallow, the bottom processes are strongly cooling SSTs, while in the winter, when the mixed layer is deepest, bottom processes have a very minimal effect on SSTs in the mixed layer (Ronca & Battisti, 1997). Anomalies of the ocean mixed layer heat budget terms reveal that processes that control mixed layer SSTs were anomalous during the NE Pacific MHW (Table 4.2).

Furthermore, the net heat flux anomalies (Section 4.3.1 & Figure 4.5c) offset positive anomalies in ocean processes (Figure 4.5d-e) in order to maintain a near-climatological SST tendency throughout the MHW. Despite the large positive anomaly in 2013 at the beginning of the heatwave, the temperature tendency remains more or less close to 1979-2016 climatology throughout the MHW, which reflects the fact that the SSTs remained elevated after the initial forcing (Figure 4.5b). The anomalies in each heat budget term are relatively small and not consistently either positive or negative (Figure 4.5b-e). The slight seasonal variations in the anomalies of terms contributing to temperature tendency tend to offset each other, such that the temperature tendency anomaly throughout the MHW remains negligible. This analysis shows that, after the initial forcing that warms SSTs and marks the onset of the MHW, these elevated upper ocean temperatures did not just relax back to climatology in a few months' time. Instead, the anomalous atmospheric and ocean processes offset and largely balanced each other (Table 4.2; MHW-average radiative flux anomaly of 2.3 Wm^{-2}, latent heat flux anomaly of -8.1 Wm^{-2}, ocean advection anomaly of -7.8 Wm^{-2} and mixed layer entrainment and diffusion anomaly of 11.8 Wm^{-2}), resulting in the maintenance of the MHW for over 2 years. While the latter value was estimated as a residual, the sign of the term is reasonable. The warmth of the upper mixed layer during the MHW implies greater stratification near its base, consistent with suppressed exchanges between the mixed layer and cooler waters at depth. The demise of the MHW occurred in late 2016 during a period of enhanced cooling. The principal mechanisms were the surface heat fluxes (Figure 4.5c) and horizontal advection (Figure 4.5d) in association with anomalous winds from the northwest (not shown).

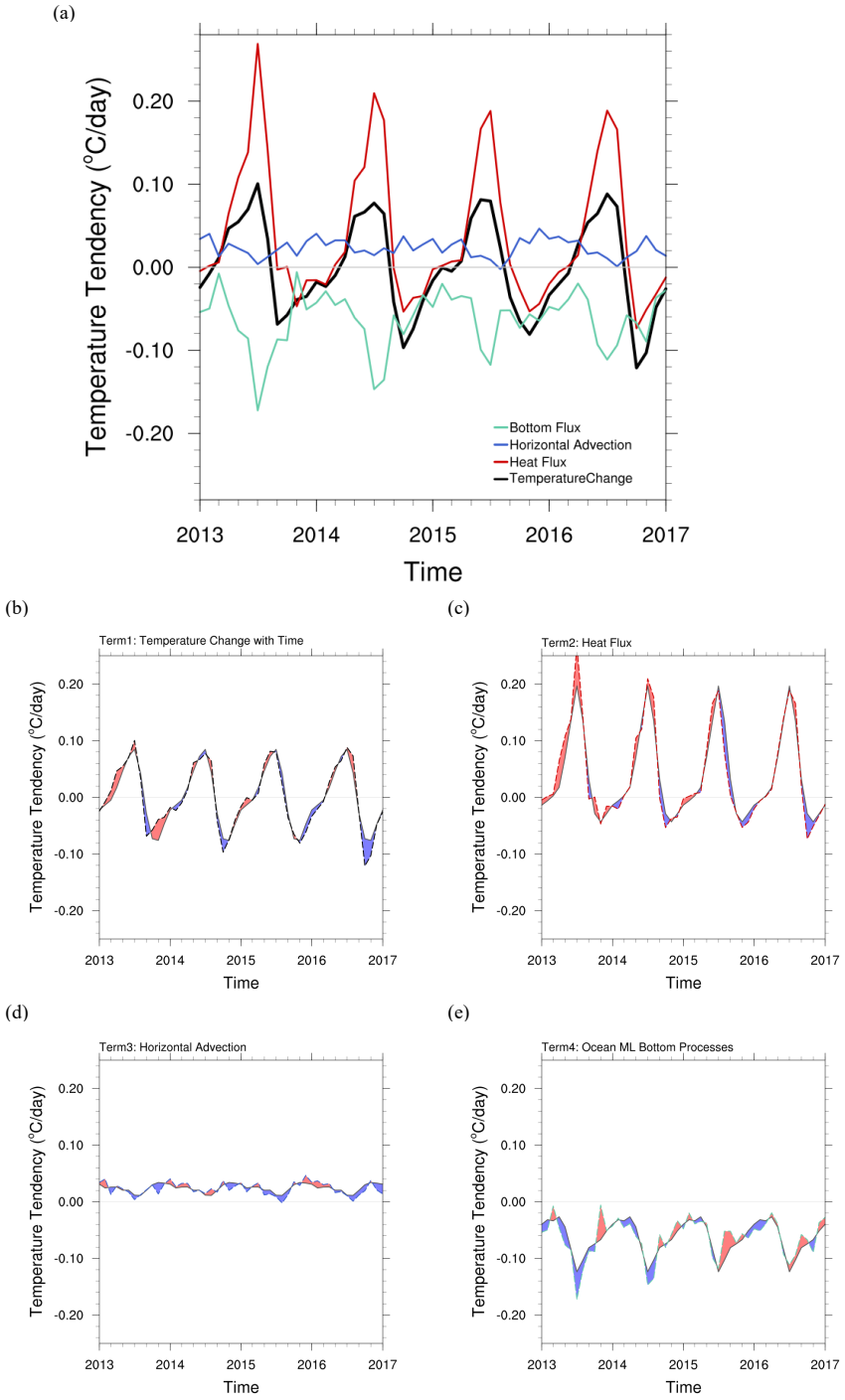

Figure 4.5 (a) Time series of ocean mixed layer heat budget components – temperature change over time (black), heat flux (red), horizontal advection in the ocean mixed layer (blue), and ocean processes at the bottom of the ocean mixed layer (light green); (b) time series of temperature tendency, where solid line is the climatology and dashed line is observed temperature tendency 2013-2016; (c) as in (b) but for heat flux component; (d) as in (b) but for horizontal advection component; (d) as in (b) but for contribution to mixed layer heat budget by ocean processes happening at the bottom of the mixed layer. In (b)-(e), positive anomalies are shaded in red, and signify additional warming (or less cooling) than typical, while negative anomalies are shaded in blue and signify less warming (or additional cooling) than typical.

Table 4.2 As in Table 4.1, but for the four terms of the ocean mixed layer heat budget. Blue shading indicates negative anomalies- less warming or more cooling than average. Orange shading indicates positive anomalies- more warming or less cooling than average.

		Climatological average and standard deviation (2001 to 2016)	Average monthly anomaly during MHW	Average DJF monthly anomaly during MHW	Average MAM monthly anomaly during MHW	Average JJA monthly anomaly during MHW	Average SON monthly anomaly during MHW
Temperature Tendency	(°C/day)	-1.0e-4 ± 5.3e-2	-2.2e-3 ± 1.5e-2	-9.3e-4 ± 9.8e-3	2.9e-3 ± 2.8e-3	1.8e-3 ± 9.8e-3	-1.3e-2 ± 1.6e-2
	(W/m^2)	-0.30 ± 160.8	-5.7 ± 39.2	-4.9 ± 51.7	12.0 ± 11.6	1.7 ± 9.1	-24.9 ± 30.6
Net Heat Flux	(°C/day)	3.9e-2 ± 7.8e-2	-3.9e-3 ± 1.9e-2	1.1e-3 ± 6.0e-3	1.6e-3 ± 1.6e-3	-1.2e-3 ± 1.5e-2	-1.7e-2 ± 6.9e-3
	(W/m^2)	118.3 ± 236.6	-10.2 ± 49.7	5.8 ± 31.6	6.6 ± 6.6	-1.1 ± 14	-32.5 ± 13.2
Horizontal Advection	(°C/day)	2.4e-2 ± 1.1e-2	-3.0e-3 ± 8.0e-3	-3.2e-3 ± 1.3e-2	1.0e-3 ± 3.0e-3	-6.1e-3 ± 2.1e-3	-3.9e-3 ± 1.7e-3
	(W/m^2)	72.8 ± 33.4	-7.8 ± 20.9	-16.9 ± 68.6	4.2 ± 12.5	-5.7 ± 2.0	-7.5 ± 3.3
Ocean ML Bottom Processes	(°C/day)	-6.3e-2 ± 3.5e-2	4.5e-3 ± 1.6e-2	3.4e-3 ± 1.5e-2	2.1e-4 ± 3.2e-3	-9.0e-3 ± 6.9e-3	8.1e-3 ± 7.7e-3
	(W/m^2)	-191.1 ± 106.2	11.8 ± 41.8	17.9 ± 79.1	0.87 ± 13.5	-8.4 ± 6.4	15.5 ± 14.7

4.4. Discussion

Analysis of the NE Pacific 2013/16 MHW using a combination of reanalysis data and a mixed layer heat budget shows that the atmosphere had a strong anomalous response to the warm SSTs. A positive regional, non-equilibrium SST-cloud feedback does play a role in reinforcing high SSTs but is offset by the large turbulent flux anomalies in the region. Anomalous ocean processes were largely balanced by atmospheric processes, which preserved the atypically warm SSTs, maintaining the MHW for over 2 years.

A remarkable result from this study is that the midlatitude NE Pacific atmosphere-ocean system has the ability to maintain itself in an anomalous state for multiple years through a subtle balance between oceanic and atmospheric processes. After the initial atmospheric forcing that caused the SST warming (Bond et al., 2015), the atmosphere responded with anomalies in radiative fluxes (2.3 Wm^{-2}) that were largely offset by anomalies in latent heat fluxes (-8.1 Wm^{-2}), and balanced by anomalies in ocean advection (-7.8 Wm^{-2}) and mixed layer entrainment and diffusion (11.8 Wm^{-2}). It is worth mentioning that anomalies in ocean advection are expected to be negative, since the analysis is formulated to look only at the MHW area where there are warm SSTs anomalies, and presumably the surrounding areas from which the ocean water is being advected are not experiencing anomalously warm SSTs. This yielded a near-climatological SST

tendency during the MHW and led to the unprecedented persistence of the warm SST anomalies. Our results also show that mechanisms that start a MHW are not necessarily the same as the combination of oceanic and atmospheric mechanisms that maintain the anomalous SSTs during a MHW or contribute to the decay of a MHW (Bond et al., 2015; Myers et al., 2018).

Myers et al. (2018) did not follow the MHW to termination and analyzed a slightly different region than the one analyzed here. Nevertheless, while magnitudes of radiative and latent heat flux anomalies during the NE Pacific MHW differed between this study and Myers et al. (2018), both analyses highlight the importance of latent heat fluxes in the mixed layer heat budget in the NE Pacific MHW. This study finds an average net radiative flux anomaly of 2.3 ± 1.9 Wm^{-2} additional energy into the ocean mixed layer from November 2013-January 2016; Myers et al. (2018) find a much smaller net radiative flux anomaly 0.4 ± 1.7 Wm^{-2} net for the region from 40-50 °N, 140-160 °W in 2013, and the 0 ± 1 Wm^{-2} anomaly in 2014. Here we find turbulent heat flux anomalies of 8.1 ± 3.5 Wm^{-2} out of the ocean from November 2013-January 2016, while Myers et al. (2018) present turbulent heat flux anomalies of -12.7 ± 4.7 Wm^{-2} (into the ocean) in 2013. Results show different processes at work at the onset of the MHW (Myers et al., 2018) compared to throughout the duration of the MHW. Here we show that positive radiative flux anomalies throughout the MHW were important in maintaining the SST anomalies, contrary to conclusions in Myers et al. (2018). In addition, turbulent heat fluxes actually contributed to the onset of anomalously warm SSTs in 2013, while throughout the duration of the MHW the turbulent fluxes provided anomalous cooling to the ocean mixed layer which offset the positive radiative flux anomalies and yielded near-climatological SST tendencies. Still, our analyses of the NE Pacific MHW agree with Bond et al. (2015) and Myers et al. (2018) on the central role of turbulent fluxes on SSTs during the event, and that radiative anomalies associated with a SST-cloud feedback do not dominate SST tendencies in this midlatitude region.

The findings presented here have important implications for the study of SST-cloud interactions in general. While the observed reduction in low cloud concurrent with elevated SSTs during the MHW further supports ample documentation of a negative SST low cloud correlation in the Northeast Pacific (Klein & Hartmann, 1993; Klein et al., 1995; Norris & Leovy, 1994; Norris et al., 1998; Norris, 2000; Clement et al., 2009), the offsetting turbulent heat fluxes show that a positive SST-cloud feedback alone does not necessarily drive SST tendencies in the region. Observations of a coincident increase in SST, decrease in low cloud, and increase in

incident shortwave radiative flux are not enough to infer additional SST warming. Turbulent fluxes play an essential role in determining how the change in heat flux actually affects SSTs and must be considered in analyses of SST-cloud interactions. The observed ocean-atmosphere interactions during the NE Pacific MHW closely follow the theoretical framework of Ronca and Battisti (1997), in which clouds respond to SST changes but do not further warm SSTs due to compensating turbulent heat fluxes. Ronca and Battisti (1997) find for the NE subtropical Pacific that net heat flux anomalies associated with SST anomalies are too small to in turn affect SSTs. In other words, the atmosphere responds to changes in SSTs, but the subsequent net heat flux anomalies are not large enough to feed back onto SSTs. This combined effect is more aptly described as a SST-cloud/atmosphere response than a SST-cloud/atmosphere feedback. Numerous studies claim positive SST-cloud feedbacks based on observations of a SST-cloud response- anomalously warm SSTs, reduction in low cloud, and increased incident solar radiation at the surface (Norris et al., 1998; Clement et al., 2009; Bellomo et al., 2014; Bellomo et al., 2016). We show here that this may not always be enough evidence to claim the presence of a true SST-cloud feedback that yields sustained anomalous SST tendencies, given the importance of turbulent fluxes and ocean processes to SST tendencies in the midlatitudes. Studies should be careful to specify the effect of SST-cloud feedbacks on SST tendency. In the case of the NE Pacific MHW, an observed positive SST-cloud feedback does not yield anomalous SST tendencies since turbulent fluxes counterbalance radiative fluxes to sustain SST anomalies.

In the context of other NE Pacific SST-cloud feedback studies, our work suggests that both SST-cloud feedbacks and turbulent flux feedbacks in this region likely have high spatio-temporal variability. While we show that a positive SST-cloud feedback did not dominate the mixed layer heat budget in the midlatitude NE Pacific during this MHW, there is evidence of a positive SST-cloud feedback dominating and driving the persistence of warm SSTs during the same MHW at lower latitudes in the subtropical NE Pacific (Myers et al., 2018). Moreover, many other studies present evidence for a positive SST-cloud feedback in the NE Pacific at lower latitudes than the region studied here (Klein & Hartmann, 1993; Klein et al., 1995; Norris & Leovy, 1994; Norris et al., 1998; Norris, 2000; Clement et al., 2009). The important role of turbulent fluxes in the midlatitudes appears to be enough to dampen positive SST-cloud feedbacks that have been documented in the lower latitudes of the subtropics (Ronca and Battisti, 1997). If SST-cloud feedbacks indeed have such high spatio-temporal variability, more work is

needed to understand what environmental variables support SST-cloud feedbacks. Regional studies like this are necessary to reduce the uncertainty in cloud feedbacks and incorporate their spatial variability more appropriately into climate models.

4.5. Conclusions

Reanalysis data show that the anomalously warm SSTs during the NE Pacific 2013/16 MHW were accompanied by increases in upward longwave, downward longwave, upward shortwave and downward shortwave radiative fluxes. The changes in downward shortwave radiative flux were associated with a reduction in low cloud fraction. The observed positive net radiative flux anomaly provides evidence for a positive SST-cloud feedback; however, this feedback does not dominate SST tendencies during the MHW. Instead, near-climatological SST tendencies were observed due to negative anomalies in turbulent fluxes that offset the radiative flux anomalies throughout the MHW. These results show the importance of turbulent fluxes to SST tendencies in the midlatitudes.

Analysis of the ocean mixed layer heat budget during the MHW reveals the essential role of ocean processes in determining the maintenance of SST anomalies during the MHW. Small anomalies in oceanic horizontal advection and processes at the bottom of the ocean mixed layer offset small anomalies in the net heat flux such that the MHW persisted for over 2 years. Through the balance in oceanic and atmospheric anomalies, the atmosphere-ocean system in the NE Pacific is able to maintain anomalous SSTs for the duration of the longest MHW ever observed.

Chapter 5 Global Marine Heatwaves Confirm Cloud Response in Global Climate Models

5.1 Introduction

Marine heatwaves (MHWs) are events of anomalously warm sea surface temperatures (SSTs) that exceed an upper SST threshold for an extended period of time (Hobday et al., 2016; Hobday et al., 2018). MHWs have already become more frequent and more severe in the last few decades due almost entirely to warming mean ocean temperatures (Oliver et al., 2018), and this trend is expected to continue with future global warming (Frölicher & Laufkötter, 2018; Frölicher et al., 2018). Although MHWs are discrete regional warming events, it is reasonable to wonder if these events offer a preview of anomalous atmosphere-ocean interactions under future warming. Here we quantify the mean local atmospheric response to MHWs, with a focus on surface heat fluxes and clouds, and evaluate whether the local responses align with changes predicted by global climate models in a warmer world.

Recent MHWs have had negative impacts on marine ecosystems and on the economies of coastal communities. Common ecological observations among recent MHWs include extreme mortality of marine species, harmful algal blooms, coral bleaching, and shifts in species ranges to cooler waters (Piatt et al., 2020; Cavole et al., 2016; McCabe et al., 2016; Le Nohaïc. et al., 2015). When fish species shift ranges during MHWs, it heavily influences the success of local fisheries, and less available catch can lead to economic devastation of fishing communities (Cavole et al., 2016; McCabe et al., 2016). Understanding atmospheric perturbations that accompany past MHWs is central to understanding and modeling the physical processes driving MHWs, which will help in anticipating and minimizing future negative environmental and socioeconomic impacts during these events.

Despite the name, MHWs are not solely oceanic phenomena. They result from coupled atmosphere-ocean interactions. MHWs can be influenced by both local and non-local, large-scale atmosphere-ocean processes. In turn, MHWs can have both local and non-local atmospheric effects. Large scale remote processes, like ENSO or the PDO, can enhance or suppress the formation of MHWs through teleconnections (Holbrook et al., 2019). Anomalous SST patterns can be started or perpetuated locally by atypical ocean currents or processes in the ocean mixed layer, as well as atypical atmospheric processes (Holbrook et al., 2019; Schmeisser et al., 2019).

In the atmosphere, the response of clouds to warm SSTs and the resulting net heat flux at the ocean surface can drive the tendency of SSTs during MHWs (Schmeisser et al., 2019). Understanding the changes in atmospheric processes during MHWs is important for determining regional differences in atmosphere-ocean interactions that drive MHW evolution, and for forecasting evolution of MHWs during future events.

An analysis of the atmospheric response to the 2013-2016 Northeast Pacific MHW showed substantial anomalies in cloud cover, radiative fluxes, and turbulent fluxes concurrent with the anomalously warm SSTs. During the approximately 2-year long MHW, low cloud cover decreased, downward shortwave radiative flux increased, upward and downward longwave radiative fluxes increased, and latent and sensible heat fluxes out of the ocean increased (Schmeisser et al., 2019). While there was a small positive net heat flux into the ocean at times during the event due to a positive SST-cloud feedback, there was a small net negative heat flux anomaly (out of the ocean, increased cooling) averaged over the lifetime of the event. The question is: does the atmosphere respond similarly during all MHW events worldwide? What can we generalize about atmospheric responses to MHWs to better understand processes that control the evolution of individual events? Does this provide insight into atmospheric adjustment to warm SSTs in a warmer future climate?

Here we: (1) detect global MHWs from 2001-2019 using satellite data and compute the additional forcing to the atmosphere during these events; (2) present local anomalous patterns in clouds and heat fluxes observed during MHW events; and (3) detail how radiative and turbulent heat flux anomalies contribute to the spatial variability in net heat flux response during MHWs. Results are compared to global climate model predictions of clouds to determine that MHWs provide an example of future anomalous atmosphere-ocean interactions.

5.2 Methods

The SST values used here are from the Hadley Centre Global Sea Ice and Sea Surface Temperature (HadISST) V1.1. The HadISST product uses in-situ and satellite SST measurements combined using an optimal interpolation procedure (Rayner et al., 2003). Grid boxes and timesteps in which sea ice was present were removed for this analysis. The HadISST

data is available from 1871 to present, but we use 1°x1° gridded monthly means from 2001-2019 to match the availability of the radiative flux and cloud satellite data.

Satellite data are used here instead of a reanalysis product (which would afford a longer time series) because a global evaluation of reanalyses products for the variables of interest is not available. Satellite data offer a shorter record, but a well-validated and 'best available' dataset for the variables needed. The surface radiative fluxes and cloud cover are from NASA's Clouds and Earth's Radiance Energy System (CERES) Energy Balanced and Filled (EBAF) Edition 4.1 satellite measurements. The CERES-EBAF Surface product is a derivative of the CERES synoptic 1° monthly means product, which calculates radiative fluxes using a 1D radiative transfer model based on inputs of temperature profiles, water vapor profiles, clouds, and other geostationary satellite observations. The data are constrained to match top of atmosphere fluxes and ocean heat storage. Detailed information on the CERES-EBAF product can be found in Kato et al. (2013) and Kato et al. (2018). CERES-EBAF data is provided on a 1°x1° grid. We use monthly means from 2001-2019. All mention of radiative fluxes here refers to fluxes at the ocean surface.

Turbulent fluxes are from the Woods Hole Oceanographic Institute (WHOI) Objectively Analyzed air-sea Fluxes (OAFlux) Project. The OAFlux product synthesizes meteorological variable estimates from various sources. The objective analysis reduces errors in individual input sources to yield an output product with minimal error. Then, the COARE 3.0 bulk flux algorithm is used to compute turbulent fluxes from the input meteorological variables. The OAFlux dataset is available over the global oceans on a 1°x1° grid and we use monthly means of latent and sensible heat fluxes from 2001-2019 to match the available time period of the CERES-EBAF data.

MHWs were detected in the HadISST dataset by first computing the climatological 95th percentile of SSTs for each month in each grid cell. Each time the mean SST in a given month exceeds the monthly 95th percentile threshold, it is flagged as a MHW in a binary file. The binary file is used to select surface heat flux and cloud cover data during MHWs. Those data are composited over all months flagged as MHWs, and averaged to yield 'MHW-averaged' variables in each grid box. Given the length of the data record used here, some especially long MHWs (like the 2013-2016 NE Pacific MHW) may not be captured in their entirety by this algorithm, which necessarily only detects 5% of months as MHWs. In this sense, we can view this analysis

as capturing the MHW months with the highest magnitude SST anomalies (as opposed to capturing all MHW months). Lowering the detection threshold to a 90th percentile threshold helps address this issue of including entire MHWs; however, a sensitivity analysis showed that changing the threshold did not significantly alter results presented here.

To help interpret any regional differences in average surface heat fluxes or cloud cover during marine heatwaves compared to average conditions, it is useful to know if the atmosphere experiences similar regional forcing due to a change in SSTs during MHWs. We assume that the forcing from the sea surface to the atmosphere can be quantified as the upwelling longwave radiative flux, computed by the Stefan-Boltzmann equation:

$$LW = \epsilon \sigma T^4 \quad [5.1]$$

We can quantify the difference in forcing by the ocean surface to the atmosphere between normal and marine heatwave conditions by differentiating the Stefan-Boltzmann equation and rearranging:

$$\frac{dLW}{dT} = 4\epsilon\, \sigma \bar{T}^3 \quad [5.2]$$

$$dLW = 4\epsilon\, \sigma \bar{T}^3 (T' - \bar{T}) \quad [5.3]$$

where LW is the upward longwave radiative flux at the ocean surface, σ is the Stefan-Boltzmann constant, ϵ is the emissivity (which we assume is unity at the ocean surface and will be dropped in further equations), $\bar{T}$ is the mean SST, and T' is the MHW SST threshold at the 95th percentile. The equation can be rearranged and reduced to a fractional representation to yield:

$$\frac{dLW}{\sigma \bar{T}^4} = 4\, \frac{(T' - \bar{T})}{\bar{T}} \quad [5.4]$$

This equation can be multiplied by 100 and used to analyze the percentage change in forcing during MHWs in different regions around the world. The hypothesis is that, if there are differences in forcing during a MHW warming, the atmosphere will show larger anomalies in regions where the forcing from SST changes is also larger.

5.3 Results

5.3.1 MHW Detection & change in forcing from ocean to atmosphere during MHWs

In 18 years, each grid cell experiences on average 11 months (~5% of an 18-year data record) of MHW conditions. For all MHWs identified across the globe, the average SST anomaly for all events was 0.8 °C.

Figure 5.1 shows the change in forcing due to anomalously warm SSTs during MHW conditions as computed in Equation 5.4, averaged over all seasons. The forcing change due to a warmer SST during MHWs is not uniform globally. Areas of strong forcing are evident in regions such as the Northeast Pacific, Northwest Atlantic, central and eastern tropical Pacific, and the Southwest Atlantic. While Figure 5.1 is computed using data from 2001-2018, and thus the 95th percentile thresholds used in the calculation may be influenced by recent large and severe MHWs, the same calculation using the full HadISST dataset (1870-2018) yields nearly the same spatial pattern (though magnitudes of percentage forcing change are larger, see Figure C1 in Appendix C). The fact that the larger forcing changes observed in some regions compared to others are robust across a long dataset highlights unique atmosphere-ocean interactions occurring in these regions.

The magnitude of the average SST anomaly during MHWs (Figure 5.2a) matches the pattern of forcing change (Figure 5.1), as expected. As we show, regions that experience a greater percentage change in forcing also experience larger anomalies in some atmospheric variables during MHWs.

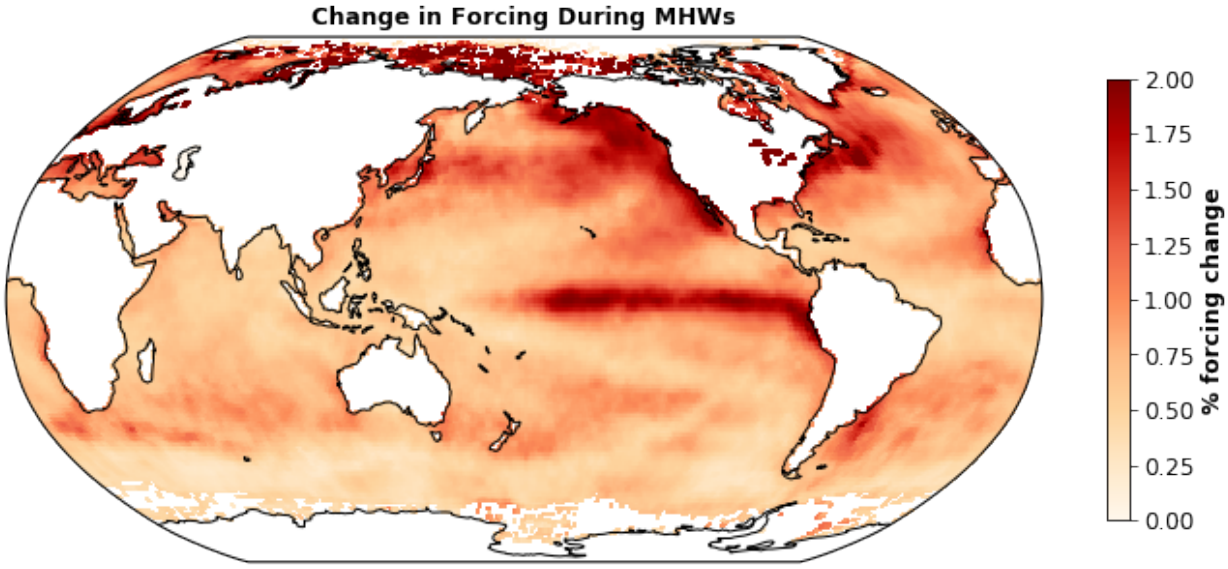

Figure 5.1 Percentage change in forcing [W/m2] from upward longwave radiative flux at the surface driven by warming of SSTs from climatological SSTs to MHW threshold, averaged over time period 2001-2019

5.3.2 Atmospheric perturbations during MHWs

Our analysis shows that there are robust atmospheric perturbations associated with MHWs. Upward longwave radiative flux increases during MHWs globally, as dictated by the Stefan-Boltzmann law (Figure 5.2c). Upward longwave radiative flux anomalies are highest in regions that experienced the highest SST anomalies during MHWs (Figure 5.2a), particularly in the NE Pacific, eastern tropical Pacific, and northwest Atlantic. Downward longwave radiative flux also increases almost everywhere worldwide (Figure 5.2d), which is largely dictated by ubiquitous and concurrent increases in air temperature (not shown) and humidity (Figure 5.2b). Cloud changes seem to have a smaller effect on this downward longwave signal.

During MHWs, low clouds decrease nearly everywhere, with the exception of a large area in the northwest Pacific, high latitudes in the Arctic and Antarctic, and scattered local coastal regions (Figure 5.3a). High cloud generally increases everywhere (Figure 5.3b). The combination of these two opposing signals results in high spatial variability in the total cloud cover response (Figure 5.3c). The cloud response is one of the key differences between atmospheric patterns during MHWs in the tropics compared to the midlatitudes. Large scale patterns show an increase in total cloud cover during MHWs in the tropics, a decrease in total

cloud cover during MHWs in the subtropics and midlatitudes, and an increase in total cloud cover in the very high latitudes (Figure 5.3c).

The cloud response dictates the downward shortwave anomalies observed during MHWs and, thus, there is large spatial variability in the shortwave flux anomalies as well. Downward shortwave radiative fluxes decrease in the tropics, increase in the subtropics and midlatitudes, and decrease in the high latitudes during MHWs (Figure 5.2e).

Latent heat flux anomalies during MHWs are regionally variable, with the largest anomalies (positive out of the ocean) in the tropical Pacific, as well as in western boundary current regions (e.g., the Kuroshio current in the northwest Pacific and the Gulf Stream current in the northwest Atlantic) (Figure 5.2g). Throughout large areas in the subtropics and midlatitudes, latent heat flux anomalies are small and negative (indicating less cooling by latent heat fluxes), with the exception of the subtropical western and central Pacific where the magnitude is substantially larger. Sensible heat fluxes are small compared to other flux terms everywhere (Figure 5.2h) except at very high latitudes, where our confidence in the data is lower due to interference by sea ice and challenges with satellite retrievals.

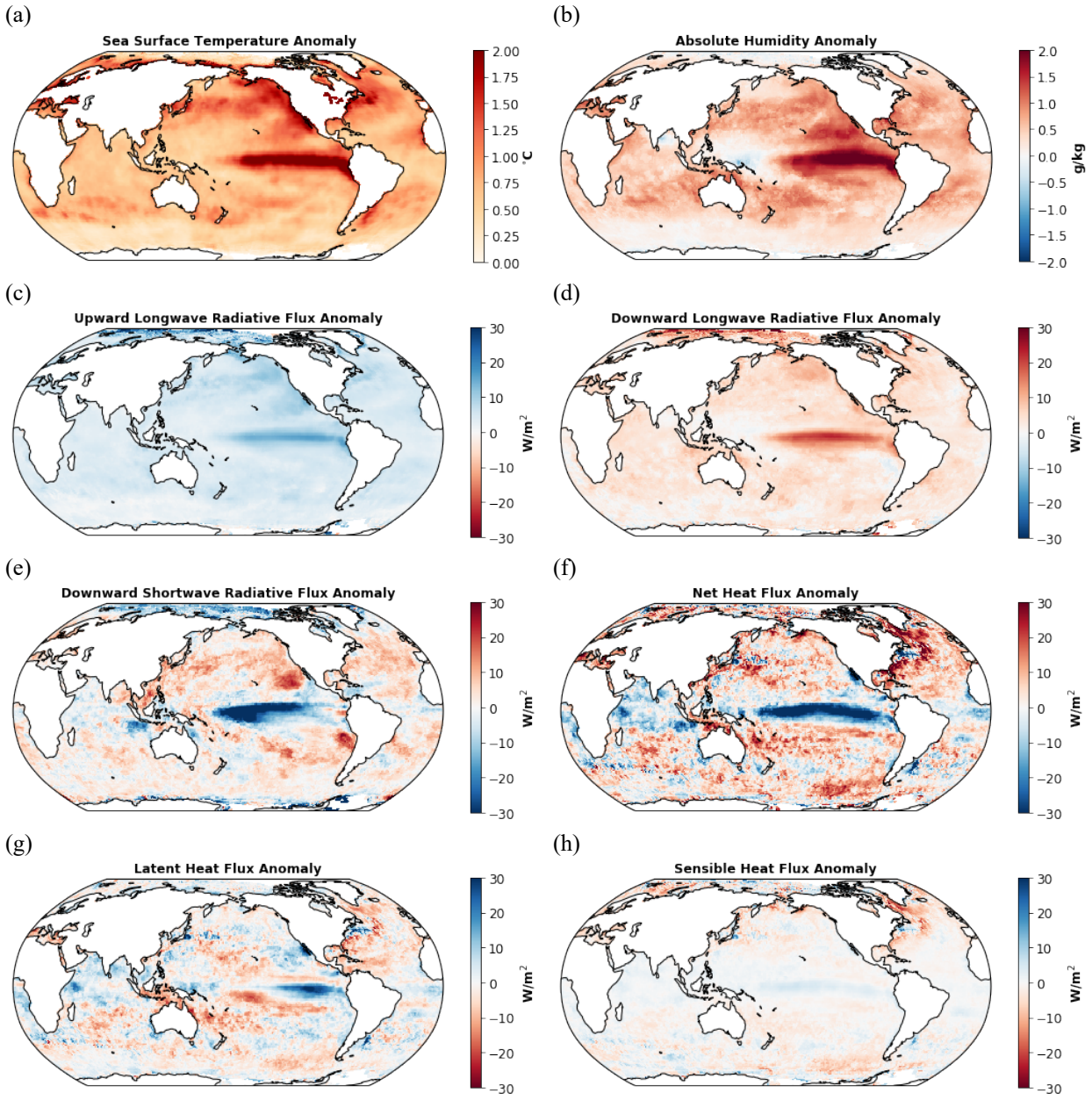

Figure 5.2 Atmospheric variable anomalies composited and averaged during MHW events: (a) SST anomalies (°C), (b) 2 m absolute humidity anomalies (g/kg), (c) upward longwave radiative flux anomalies at the surface (W/m2) (positive is up), (d) downward longwave radiative flux anomalies at the surface (positive is down), (e) downward shortwave radiative flux anomalies at the surface (positive is down), (f) net heat flux anomalies (W/m2), (g) latent heat flux anomalies (W/m2), and (h) sensible heat flux anomalies (W/m2) (positive is up).

(a)

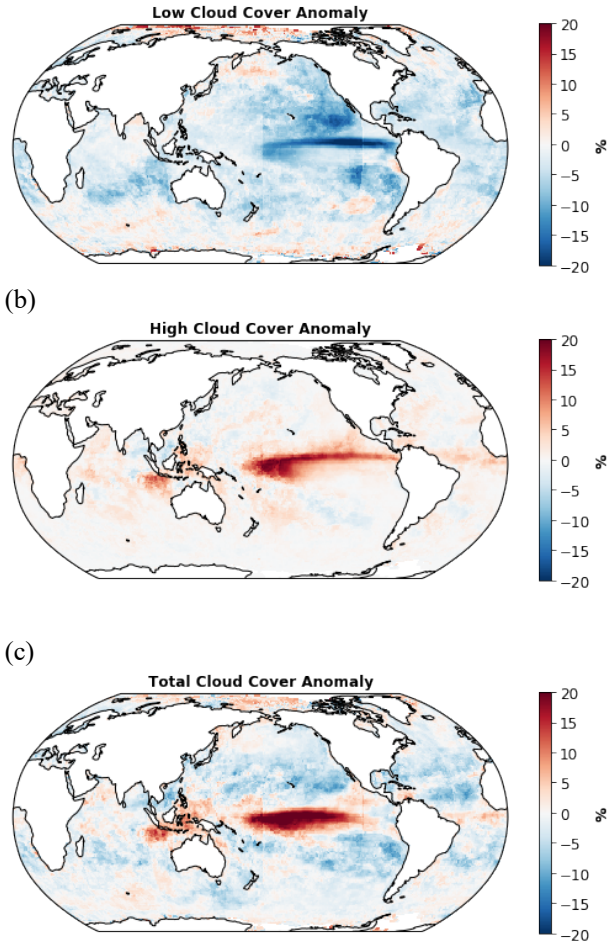

Figure 5.3 Cloud cover anomalies composited and averaged during MHW events: (a) low cloud cover anomalies (%) (b) non-low cloud cover anomalies (%), and (c) total cloud cover anomalies (%)

5.3.3 Surface net heat flux changes during MHWs

The surface net heat flux during MHWs measures the atmospheric contribution to SST tendency in the ocean mixed layer. The surface net heat flux anomaly shows large spatial variability during MHWs, indicating that the effect of the atmosphere on SSTs during MHWs is not globally uniform.

The MHW-averaged net heat flux anomaly tends to be positive (into the ocean) in the subtropics and midlatitudes, and negative (out of the ocean) in the tropics (Figure 5.2f). In general terms, the atmospheric response to warm SSTs contributes to the SST tendency by enhancing warming in the subtropics and midlatitudes with a positive net heat flux anomaly, and

damping warming in the tropics with a negative net het flux anomaly. There are some smaller regions that are exceptions (e.g., off Baja California and in the northwest Atlantic).

Comparing the contour plots of net heat flux anomaly (Figure 5.2h) and downward shortwave radiative flux anomaly (Figure 5.2e) suggests that the change in shortwave radiative flux at the surface caused by the cloud response during MHWs is largely driving the regional variability in net heat fluxes. Anomalies in latent heat fluxes also contribute substantially, particularly in western boundary current regions and the tropics. Since upward and downward longwave radiative flux anomalies have robustly similar signs (and, to a lesser extent, similar magnitudes) during MHWs in all regions of the globe (Figures 5.2c,d), they are not contributing much to the spatial structure of the net heat flux anomaly.

We can quantify the extent to which heat flux components (i.e., downward/upward longwave, downward/upward shortwave, latent, and sensible fluxes) contribute to regional variations in net heat flux anomaly by computing the percentage contribution of each heat flux component anomaly to the total net heat flux anomaly during MHWs in each grid box. We do this by dividing the absolute value of each individual net heat flux component anomaly by the sum of the absolute value of all net heat flux component anomalies. Results of this calculation are shown in Figure 5.4. In many places, downward shortwave radiative flux anomalies (Figure 4d) and latent heat flux anomalies (Figure 5.4e) are the dominant contributors to net heat flux anomalies during MHWs. The fact that latent heat fluxes account for 20-40% of the anomalous net heat flux response during MHWs is particularly notable since under climatological conditions, latent heat fluxes are a much smaller contributor to net heat fluxes (5-10%, not shown).

Downward and upward longwave radiative flux anomalies contribute secondarily to the net heat flux anomaly spatial variation in most regions (Figures 5.4a,b). Sensible heat flux anomalies and upward shortwave radiative flux anomalies only contribute substantially in very high latitudes where sea ice is often present (Figures 5.4c,f).

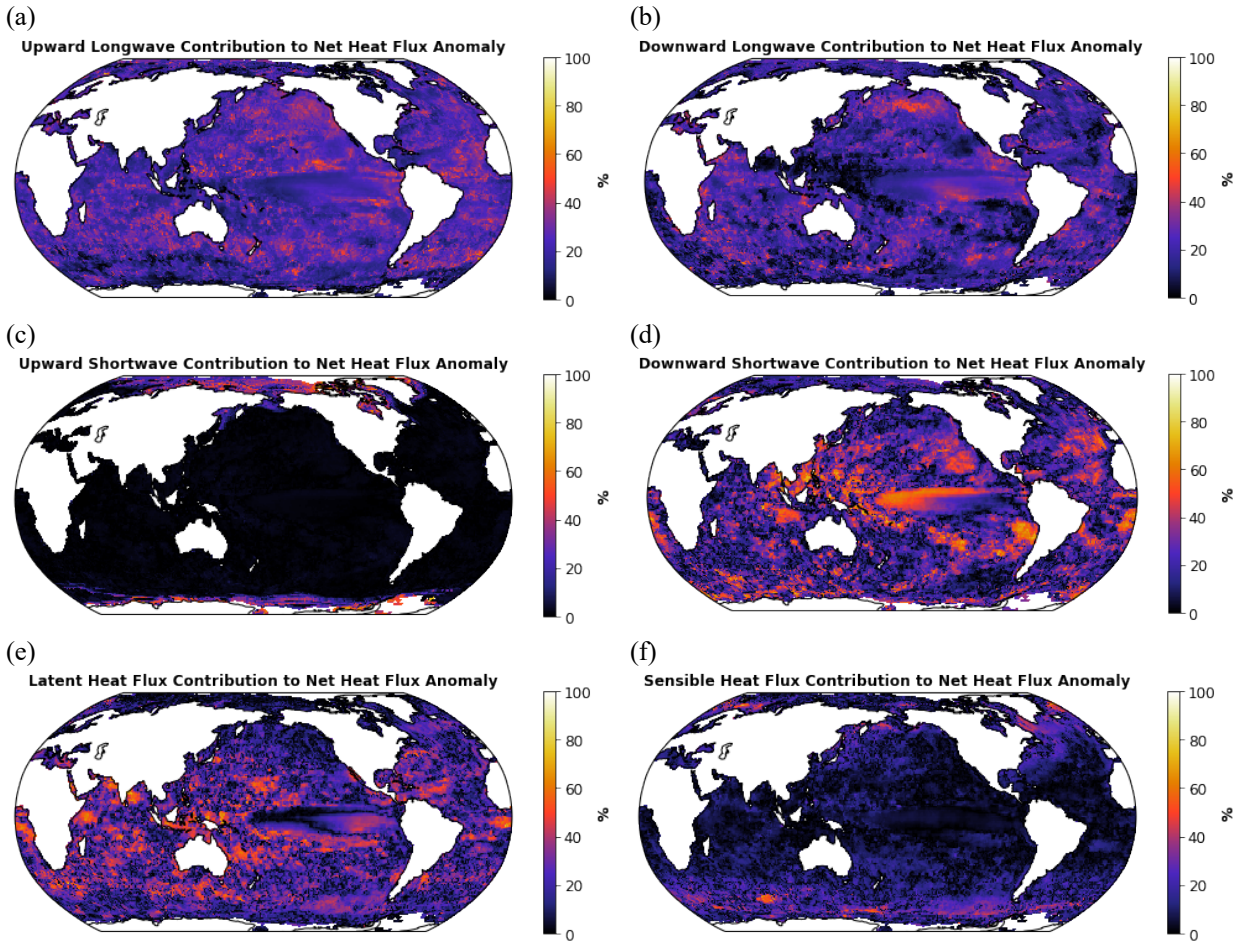

Figure 5.4 Percentage contribution of (a) upward longwave radiative flux anomaly, (b) downward longwave radiative flux anomaly, (c) upward shortwave radiative flux anomaly, (d) downward shortwave radiative flux anomaly, (e) latent heat flux anomaly, and (f) sensible heat flux anomaly to the MHW-averaged net heat flux anomaly.

5.4 Discussion & Conclusions

5.4.1 Changes in forcing from the ocean to the atmosphere during MHWs

Our analysis shows that anomalous local forcing from the sea surface to the atmosphere during MHWs is regionally variable. Regions experiencing the highest SST anomalies and, thus, upward radiative flux anomalies during MHWs were also the regions that had the highest change in percentage forcing from the ocean surface to the atmosphere. This isn't an inevitable conclusion, given that the change in forcing is normalized by the average temperature of a

region. This indicates that certain regions are prone to experiencing especially warm SST anomalies relative to other regions with similar average temperatures, and as a consequence, the forcing on the atmosphere from anomalous SSTs during MHWs is larger in these regions. Furthermore, ocean-atmosphere interactions have an amplified response in these places. For some atmospheric variables (downward longwave radiative flux, cloud cover and latent heat fluxes), the larger forcing may be associated with larger atmospheric anomalies. The implication is that the world's oceans are not uniform in response to MHWs, and our analyses and modeling efforts should reflect the heterogeneity in regional evolution of these extreme events.

5.4.2 Atmospheric patterns during MHWs

Our results capture MHW months with only the most extreme SSTs; they represent only the highest 5% of SST anomalies during the data period. In some extreme cases when the MHW persists for many months or years, like that of the 2013-2016 NE Pacific MHW, the entire event is not captured in this analysis since the duration is longer than could be captured by the MHW detection algorithm given the length of the data record. (For analyses of individual events with longer duration, the threshold for MHW detection can be reduced to, say, the 90th percentile or below, in order to analyze the full consecutive event; alternatively, the detection algorithm can be altered so that time periods in which SSTs drop below the threshold can be included in the event if the anomalies are bookended on both sides by MHW conditions). Throughout the evolution of an entire MHW, the atmospheric patterns may vary. For example, in the 2013-2016 NE Pacific MHW, the average net heat flux anomaly over the duration of the event was net negative (Schmeisser et al., 2019). However, the analysis here shows the net heat flux anomaly in that same region is net positive. A careful look at the time series of net heat flux anomalies during the event indicates that during the time periods of most intense SST anomalies (also captured in this analysis), the net heat flux anomaly is indeed positive. However, averaging over the lifetime of the MHW yields a negative net heat flux anomaly, as this includes months when the SSTs were cooling back to below the MHW threshold. While composited MHW results are useful, a careful time series analysis of individual events is also crucial in understanding dynamics that are at play throughout the build-up, duration, and decay of the MHW. The

dynamics during each phase will be different and not necessarily the same as the processes represented in event-composited results.

It is also prudent to note that the atmospheric anomalies shown here are almost certainly a combination of both local effects (from underlying warm SSTs) and remote effects (from large scale climate variability). The anomalies shown here are important because they document that indeed the atmosphere is perturbed from its mean state during MHWs. However, diagnostic work will be key to picking apart remote and local effects, and then properly incorporate these physical mechanisms into models that aim to forecast MHWs. While not addressed here, this is an important area of future research.

Regional patterns in MHW-averaged cloud anomalies presented here generally align well with SST-cloud relationships published in the literature. As SSTs increase during a MHW, low clouds decrease almost everywhere (e.g., Klein et al., 1995; de Szoeke and Verlinden, 2016; Clement et al., 2009; Bellomo et al., 2014). One notable exception is the northwest Pacific (Sea of Okhotsk and Bering Sea regions), for which the literature on SST-cloud relationships is sparse, though it is reasonable to assume this area is intermittently affected by sea ice and/or cold air outbreaks from the Siberian region that could influence clouds. The Southern Ocean also experiences increases in low cloud in some areas, which could be attributed to sea ice interaction or poor data quality at high latitudes. We show that high clouds generally increase everywhere during MHWs. This is expected given the SST-high cloud relationships outlined in the literature which suggest deep convection generally increases with warming ocean waters (e.g., Zhang et al., 1995; Ramanthan & Collins, 1991). This is especially apparent in our high cloud results in the central and eastern Pacific, when warm waters typically associated with El Niño and a shift in the Walker circulation bring deep convection and precipitation to these areas. Increases in high cloud cover in the subtropics or midlatitudes associated with warm SSTs (e.g., Zhang et al., 1995; Ramanthan & Collins, 1991) or MHWs (e.g., Myers et al., 2018; Schmeisser et al., 2019) have been observed by many other studies as well. Our MHW-composited cloud anomaly results show that, even at the tail end of the SST distribution (MHW events), our understanding of cloud behavior under warm SSTs is consistent with the observations.

The influence of the El Niño-Southern Oscillation is apparent in the tropical Pacific in many of the figures presented. We note that a strong El Niño event can technically be classified as a MHW in the east and central equatorial Pacific, so El Niño events are rightly included in the

analysis, since we are interested to see how extreme SSTs influence the atmosphere. While the driving forces of El Niño-related MHWs could certainly be different than the driving forces of other MHWs globally, we are not concerned here with what drives the spin-up of the MHW; rather, we are focused on the overlying atmospheric anomalies associated with warm SST events. In fact, including El Niño-influenced events provides an excellent confirmation of our results. The increased convection in the central and eastern tropical Pacific, represented by decreased low cloud and increased high cloud fractional coverages, aligns with our expectations of El Niño behavior. Additionally, the increase in humidity in the eastern and tropical Pacific aligns with the changes in the Walker circulation during El Niño events.

In the case of downward longwave radiative flux, a near universal increase during MHWs is somewhat surprising given the spatial differences in cloud changes regionally. Since downward longwave radiative flux is determined mainly by air temperature, humidity levels, and cloud cover, regional variability in the magnitude of cloud cover anomalies during MHWs might be expected to yield regional variability in downward longwave radiative flux anomalies at the surface. Rather, the widespread increases in air temperature and humidity dominate the downward longwave response. Cloud changes are of secondary importance on downward longwave radiative flux anomalies during MHWs. These results provide observational evidence during natural warming events that support the idea that downward longwave radiative flux is largely set by surface temperatures and the resulting turbulent fluxes that warm and moisten the overlying atmosphere; cloud changes make a much smaller contribution.

It is worth mentioning that the seasonal dependence of these results is not analyzed here, as the relatively short time series of MHW events does not allow for sufficient data points in each season to provide robust results. However, there is good reason to think that these results are seasonally dependent. For example, outside of the tropics when the oceanic mixed layer is shallow, it may be easier to warm the ocean water to MHW levels and thus a disproportionate fraction of MHWs could occur in the warm season. Additionally, climatological cloud cover differs from season to season in many parts of the world, so cloud response, and more importantly- the impact of that cloud response on net heat flux at the ocean surface- could depend heavily on the season. Future work analyzing seasonal dependence of the atmospheric response to MHWs using longer datasets should be prioritized.

5.4.3 Implications

There are two important implications of this analysis. First, we show that the role of the atmosphere in MHWs is regionally variable and, because of these regional differences in atmosphere-ocean interactions, we do not expect MHWs to evolve similarly in all regions. Second, we argue that the MHW-averaged atmospheric responses shown here are similar to global climate model predictions of those atmospheric variables in a warmer world, suggesting that MHWs provide an observational surrogate of what surface flux and atmospheric changes will look like in a warmer world. The results of our analysis show that some atmospheric variables have a similar and robust local response to MHWs in all regions globally, while other atmospheric variables behave differently in the tropics, subtropics, and midlatitudes. These differences combine to produce spatial variability in the net heat flux response during MHWs. The net heat flux during MHWs encompasses the atmospheric effects on SST tendency; consequently, the local atmospheric contribution to MHWs is regionally variable.

Atmospheric variables like downward and upward longwave radiative fluxes at the surface, low cloud cover, high cloud cover, and humidity anomalies are robustly uniform in sign during MHWs in nearly all regions. But atmospheric variables like latent heat flux, total cloud cover, and downward shortwave radiative flux anomalies show large regional differences in sign. It is the latter variables that drive the global spatial differences in net heat flux response at the surface during MHWs. Generally speaking, the atmosphere tends to cool SSTs through a negative surface net heat flux anomaly during MHWs in the tropics; the opposite is the case during MHWs in the subtropics and midlatitudes. Differences in tropical versus subtropical vs. midlatitude atmosphere-ocean interactions are largely dictated by cloud response and latent heat fluxes, which emphasizes the importance of understanding clouds and latent heat fluxes to properly model the coupled climate system.

Average SSTs in most ocean basins will warm 1°C above 1986-2006 historical averages by the end of the century in an RCP4.5 scenario, and by 2050 in an RCP8.5 scenario (Hoegh-Guldberg et al., 2014). The SST anomalies during MHWs presented here average about 0.8 °C, and thus are a conservative representation of the future ocean conditions under global warming. The global response of total cloud cover to MHWs in our data set closely resembles the global response of total cloud cover per degree warming in the global climate model ensemble mean

from the Cloud Feedback Model Intercomparison Project (CFMIP; Zelinka et al., 2012, Figure 1). Models and observational data from MHWs both show an increase in total cloud cover over the tropical oceans, a decrease in the subtropics and midlatitudes, and an increase in the high latitudes. Regional changes in low cloud and non-low cloud fraction (which make up changes in total cloud fraction) during MHWs are also consistent with those from global climate model ensemble means (Mark Zelinka, personal communication).

We do not claim MHWs are exact replicas of future ocean conditions. For example, large-scale SST gradients that exist currently between MHW regions and neighboring non-MHW regions will either not be present or very significantly reduced when future SST warming happens on a global scale. Nevertheless, MHW events provide valuable insight into the potential atmospheric response to future warming of SSTs. It is a reasonable hypothesis that radiative fluxes, turbulent fluxes, clouds, and humidity will respond similarly to future warm SSTs as observed in the MHWs analyzed here. Furthermore, MHWs can help validate atmospheric response to warming SSTs in global climate models. We show that cloud response is a key factor in determining the net het flux response to MHWs and, thus, the atmospheric contribution to SST tendency during MHWs. Correctly modeling clouds in global climate models is fundamental to properly representing atmosphere-ocean interactions and net heat fluxes in global climate models; therefore, it is encouraging to see the consistency between the results in this MHW analysis and model ensemble means.

Chapter 6 Net Heat Flux Feedbacks During Marine Heatwaves

6.1 Introduction

The net surface heat flux at the ocean surface is a key component of temperature tendency in the ocean mixed layer. Changes in the net surface heat flux can cause sea surface temperature (SST) anomalies, and those SST anomalies can in turn change the net surface heat flux. This amplification or damping of the SST anomalies from the net heat flux response defines the net heat flux feedback.

Marine heat waves (MHW) are extreme climate events in the ocean when SSTs exceed an upper threshold (Hobday et al., 2016). MHWs can be initiated by either oceanic or atmospheric processes. Changes in ocean currents or entrainment at the bottom of the ocean mixed layer, for example, can cause SST anomalies. On the atmospheric side, reduction in wind, decrease in cloud cover, or a stalled high pressure ridge can all can change the net heat flux at the ocean surface and contribute to warm SST anomalies (e.g., Bond et al., 2014; Oliver et al., 2018; Holbrook et al., 2019). Regardless of whether the surface net heat flux triggers a MHW, it is inevitably affected by the abnormally warm SSTs of a MHW, and can in turn affect those SSTs.

The average net surface heat flux feedback is negative over the world's oceans. This is anticipated given an enhancement of upward longwave radiative flux and turbulent heat flux accompanying increased SSTs; furthermore, this mostly negative feedback is demonstrated in observational data (Park et al., 2005; Frankignoul & Kestenare, 2002; Hausmann et al., 2016) and modeling studies (Frankignoul et al., 1998). However, anomalous atmospheric responses to SSTs that can modulate the feedback (Park et al., 2005) and thus there are certain regions and certain seasons that deviate from the global average and experience positive net heat flux feedbacks. For example, in response to warm SST anomalies, the negative surface heat flux feedback weakens if atmospheric moisture and/or temperature increases, wind speed decreases, or low cloud cover decreases over warm SST anomalies. Understanding the dominant heat flux components (i.e., latent, sensible, longwave or shortwave radiative fluxes) in the feedback further elucidates features of the local coupled atmosphere-ocean system.

The regions and seasons predisposed to positive net surface heat flux feedbacks are of particular interest in MHW applications. The hypothesis is that if a MHW is triggered in a region and season that has a positive net heat flux feedback, the MHW could be more persistent. There

is some preliminary evidence that surface heat flux feedbacks may indeed be important in determining MHW persistence. For example, Bond et al. (2015), Schmeisser et al. (2019) and Myers et al. (2018) analyzed the 2013-16 MHW in the midlatitude Northeast Pacific and found suppressed latent heat fluxes led to the start of the MHW. While the surface heat flux response to the warm SSTs was a net negative feedback in the midlatitudes, the damping was weakened by a positive SST-cloud feedback that contributed to the persistence of the MHW (Schmeisser et al., 2019). The subtropical extension of the same NE Pacific MHW was analyzed by Myers et al. (2018), and results show that the radiative heat flux anomaly dominated the SST tendency and drove SST anomalies higher, while latent heat flux anomalies played a smaller role (and did not damp anomalies as expected) during the persistence of the MHW. Oliver et al. (2017) analyzed the 2015/16 Tasman Sea MHW and found the net surface heat flux anomalies were negligible; instead anomalous ocean advection was primarily responsible for the MHW development. Holbrook et al. (2019) provides the first assessment of global MHWs and their drivers. They found strong correlations between some climate modes and MHWs in certain ocean basins; however, they showed that local processes are the most important in driving each MHW. There is still ample work to be done to systematically understand the details of the atmospheric processes and feedbacks at play during MHWs worldwide.

Synthesis of the literature suggests that spatio-temporal variability in the net heat flux feedback is to be expected. Furthermore, the importance of the net heat flux feedback in evolution of SST anomalies (compared to the effect of ocean processes) is also likely to have high geographic variability. This informs the hypothesis that the spatio-temporal variability in surface net heat flux feedbacks dictates that *when* and *where* warm SST anomalies build to MHW levels will influence the persistence of the event. Here we aim to establish the variability in net heat flux feedbacks during normal conditions and also during MHW conditions, and analyze statistical relationships between MHW duration and net heat flux feedbacks.

Three primary research questions will be addressed here:

1. How do climatological net heat flux feedback parameters computed using updated datasets and more recent time series compare to past analyses of surface heat flux feedbacks (e.g., Park et al., 2005)?
2. Do net surface heat flux feedbacks change during a MHW compared to climatological conditions for that region and season?

3. Are regions and seasons with positive net surface heat flux feedbacks more susceptible to persistent MHWs than regions with negative net surface heat flux feedbacks?

6.2 Methods

The methods used here closely follow that of Park et al. (2005) and Frankignoul & Kestenare (2002); however, datasets, data resolution, and years of analysis differ. Park et al. (2005) improved on the Frankignoul and Kestenare (2002) estimates of net heat flux feedback parameters by using International Satellite Cloud Climatology Project (ISCCP) satellite-derived radiative fluxes instead of indirect estimates using conversion formulas on the Comprehensive Ocean and Atmosphere Dataset (COADS). We improve on the Park et al. (2005) estimates of feedback parameters by using the best available satellite measurements of SSTs and heat fluxes at a much higher spatial resolution.

SST data are from the HadISST dataset, turbulent fluxes are from the OAFlux dataset, and surface radiative fluxes are from the CERES EBAF dataset. Additional information on these products is available in Chapter 5.2. The ocean mixed layer depth used in the analysis is from NCEP Global Ocean Data Assimilation System (GODAS). More information on GODAS can be found in Chapter 4.2. All data used are monthly averages interpolated to a 1° x 1° global grid.

Computations of net heat flux feedbacks are based on the theoretical work from Frankignoul & Hasselman (1977), who develop a simple model of SST:

$$\frac{dT'}{dt} = F - \lambda T'$$

where T' is the SST anomaly, F is the forcing anomaly and λ is the heat flux feedback parameter. Their work suggests that feedback estimates are accurate only when atmospheric persistence times are small. In other words, the data have to be filtered of low-frequency atmospheric changes that can bias the net heat flux feedbacks toward positive values. Since El Niño-Southern Oscillation (ENSO) is a low-frequency atmospheric variation that can create this bias, the ENSO signal is removed from all datasets before computing feedback parameters. ENSO signal removal is performed following the methods from Park et al. (2005) and Frankignoul & Kestenare (2002). First, a covariance-based EOF analysis was performed to yield ENSO indices and the first three principal components of SSTs between 20 °S and 20 °N. In each grid box, a

linear regression between time series of the principal components and the variables of interest (SSTs and net heat flux components) was performed using three consecutive monthly values centered on each month (e.g., February regression was done using January, February, and March). The regression values were subtracted from the data to yield the ENSO-removed dataset. The data were detrended after removing the ENSO signal in order to remove bias from a global warming signal.

The net heat flux feedback parameter, λ, is computed with an analysis of the lagged covariance between temperature anomalies and net heat flux anomalies, using the following equation from Park et al. (2005), Frankignoul and Kestenare (2002) and Frankignoul et al. (1998) (based on the original Frankignoul & Hasselman (1977) work):

$$\lambda(i) = -\frac{Cov[T'(i-1), Q'(i)]}{Cov[T'(i-1), T'(i)]} = -\frac{\sum T'(i-1) * Q'(i)}{\sum T'(i-1) * T'(i)}$$

where T' is the SST anomaly, Q' is the net surface heat flux anomaly, *i* represents a certain month and *i-1* represents the month preceding *i.* Seasonal averages of the net heat flux feedback parameter are computed using the same methodology but with data from three consecutive months. An example of the seasonal feedback parameter computation is presented in the following equation for autumn:

$$\lambda(SON) = -\frac{Cov[T'(ASO), Q'(SON)]}{Cov[T'(ASO), T'(SON)]} = -\frac{\sum T'(ASO) * Q'(SON)}{\sum T'(ASO) * T'(SON)}$$

where SON stands for September, October, November and ASO stands for August, September, October. The heat flux feedback parameter is also computed for each component of the net heat flux, replacing net heat flux in the above equations with one flux component- downward shortwave, upward shortwave, downward longwave, upward longwave, turbulent and sensible heat fluxes.

The inverse of the e-folding times of SST anomalies due to the net heat flux feedback can be computed with the following equation:

$$\tau = \frac{\lambda}{\rho c_p h}$$

where λ is the net heat flux feedback parameter, ρc_p is the volumetric heat capacity of water (equal to 4.088×10^6 J °C^{-1} m^{-3}) and h is the depth of the ocean mixed layer.

MHWs are defined here as any month when SSTs exceed the 90th percentile threshold as computed from the 2001-2019 HadISST time series. The 90th percentile is computed for the

SSTs within each grid cell, thus the MHW definition is regionally specific. Since 10% of the time series qualifies as MHW conditions, approximately 21 months qualify as MHWs in each grid cell. The results shown here are generally not sensitive to the MHW threshold, though some sensitivity analysis is presented to show the difference in results between MHWs defined with the 90^{th} percentile threshold and those defined with a 95^{th} percentile threshold.

To compare how climatological net heat flux feedbacks compare to those during MHWs, net heat flux feedback parameters are computed for the entire available time series (total average net heat flux feedback parameter), and then again for only the portions of the time series designated as MHWs (total average MHW net heat flux feedback parameter). Then, differences between the MHW net heat flux feedback parameter and the average net heat flux feedback parameter are computed to directly compare differences in MHW conditions to climatological conditions in all regions. Seasonal MHW feedback parameters are not computed since there aren't enough MHW months per season for results to be robust.

In order to analyze the relationship between climatological net heat flux feedback and the maximum length of MHW experienced in that place, the Pearson correlation coefficient is computed between both datasets. The length of a MHW is computed by adding up the number of consecutive months that meet the MHW criteria.

6.3 Results

6.3.1 Average seasonal net heat flux feedback parameter

In this section we present global seasonal net heat flux feedback parameters as well as the associated inverse e-folding times of SST anomalies. Figure 6.1 shows the net heat flux feedback parameter for each of the four seasons in units of W/ m^2/K. A negative feedback parameter indicates amplification of SST anomalies (a positive feedback) and a positive feedback parameter indicates damping of SST anomalies (a negative feedback). Although the figures present feedback parameters, the discussion will center around feedbacks, as feedbacks are more intuitive. During all seasons, the net heat flux feedback is broadly negative, as would be expected, for example, with an enhancement of upward longwave radiative and turbulent heat

fluxes accompanying a warm SST anomaly. However, there are many notable exceptions to this broad pattern, as positive feedbacks are observed in some regions.

The Northeast Pacific calculations show a tendency for near-zero or positive feedbacks in much of the region during DJF, MAM, and JJA. The Northwest Atlantic as well as the western tropical Atlantic have positive net heat flux feedbacks in DJF and MAM. There are positive net heat flux feedbacks throughout a decent portion of the Southern Ocean during all months, with a particular region southwest of South America that shows a strong positive feedback much of the year. The net heat flux components contributing most to the positive net heat feedbacks are presented in the next section.

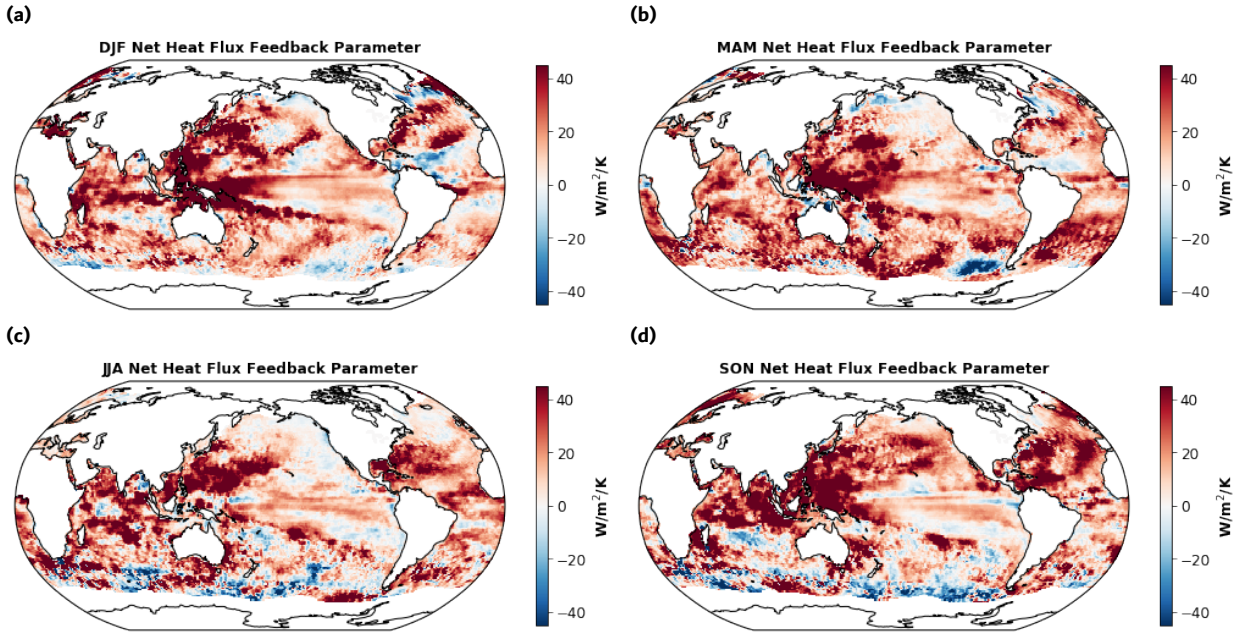

Figure 6.1 (a) DJF, (b) MAM, (c) JJA, and (d) SON net heat flux feedback parameters (in $W/m^2/K$) across the globe, averaged over years 2001-2018. Negative heat flux feedback parameters indicate a positive feedback and vice versa.

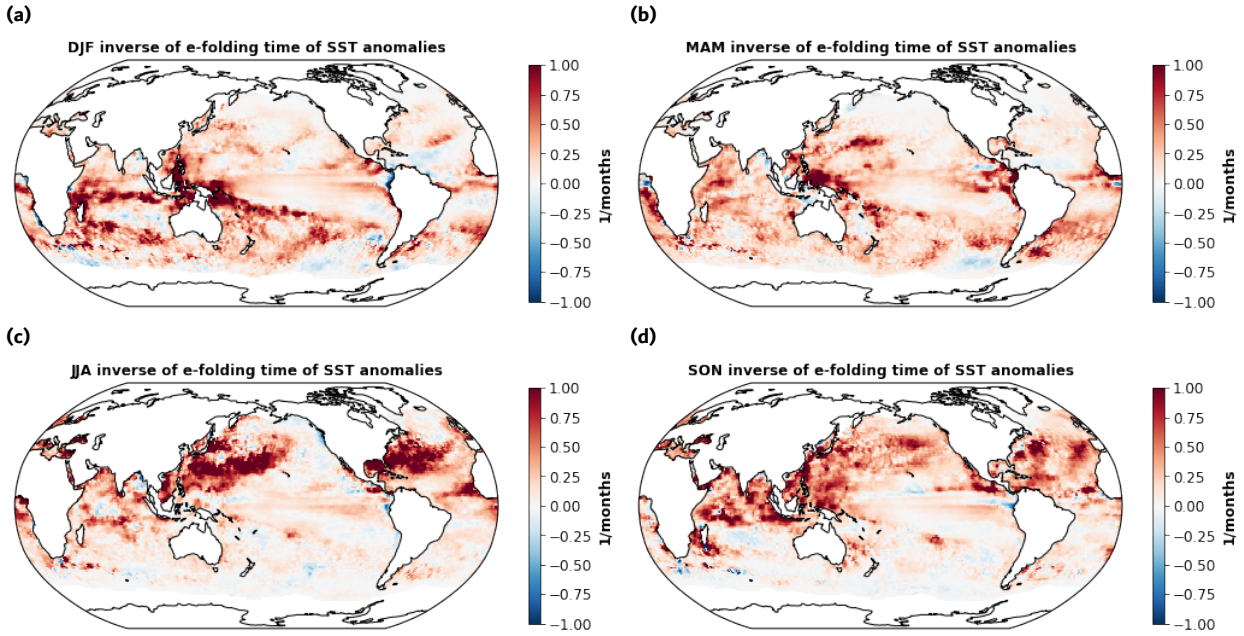

Figure 6.2 (a) DJF, (b) MAM, (c) JJA, and (d) SON inverse of the e-folding times (in months^{-1}) of SST anomalies from net heat flux feedback. A value of 0.25 indicates an e-folding time of 4 months

The seasonal inverse e-folding times of SST anomalies due to influence of net heat flux feedbacks are presented in Figure 6.2. Inverse e-folding times are shown in months^{-1}, so values of 1 indicate that SSTs are damped in 1 month, while values of 0.25 indicate that SSTs are damped in 4 months, etc. Negative inverse e-folding times signify that the net heat flux feedback does not damp SST anomalies in that region. As anticipated, areas that have negative inverse e-folding times of SST anomalies are areas that show positive feedbacks.

6.3.2 Average seasonal heat flux feedback parameter by component

To gain insight into the physical mechanisms driving the seasonal net heat flux feedback patterns (Figure 6.1), this section shows the individual contributing components to the net heat flux feedback. Figure 6.3 shows the downward shortwave radiative flux feedback parameter for each season. The downward shortwave feedback is strongly negative in the tropics and especially so in the tropical Western Pacific. This aligns with the widely accepted mechanism that warm SSTs in the tropics enhance convection and overall increase in cloud cover, thus decreasing the shortwave radiative flux at the surface and damping SST anomalies. Much of the midlatitudes exhibit a positive shortwave heat flux feedback (inferring a positive SST-cloud feedback). In

some regions like the Northeast Pacific, this positive SST-cloud feedback is persistent throughout the year, while in other regions, like near the Kuroshio current, the positive SST-cloud feedback is seasonal (strongest in JJA). In the tropics, and especially the western equatorial Pacific, the shortwave feedback is a large component in the net heat flux feedback. In the mid- to high latitudes, the magnitude of the shortwave feedback is on par with contributions from the other heat flux components.

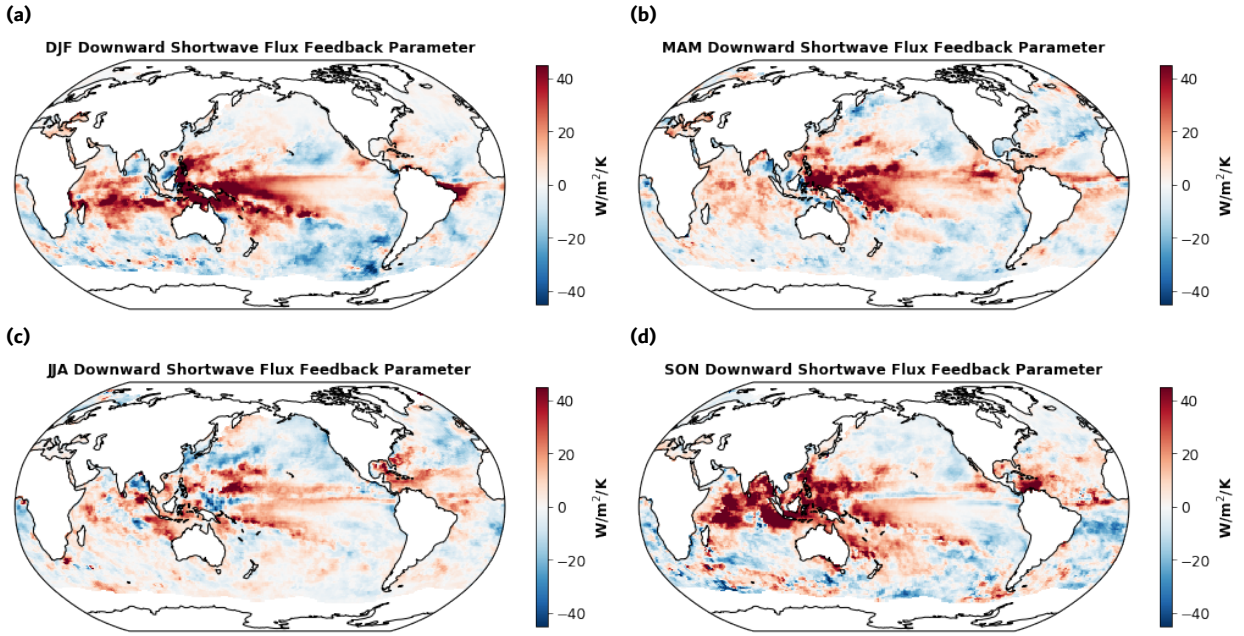

Figure 6.3 As in Figure 6.1, but for downward shortwave radiative heat flux.

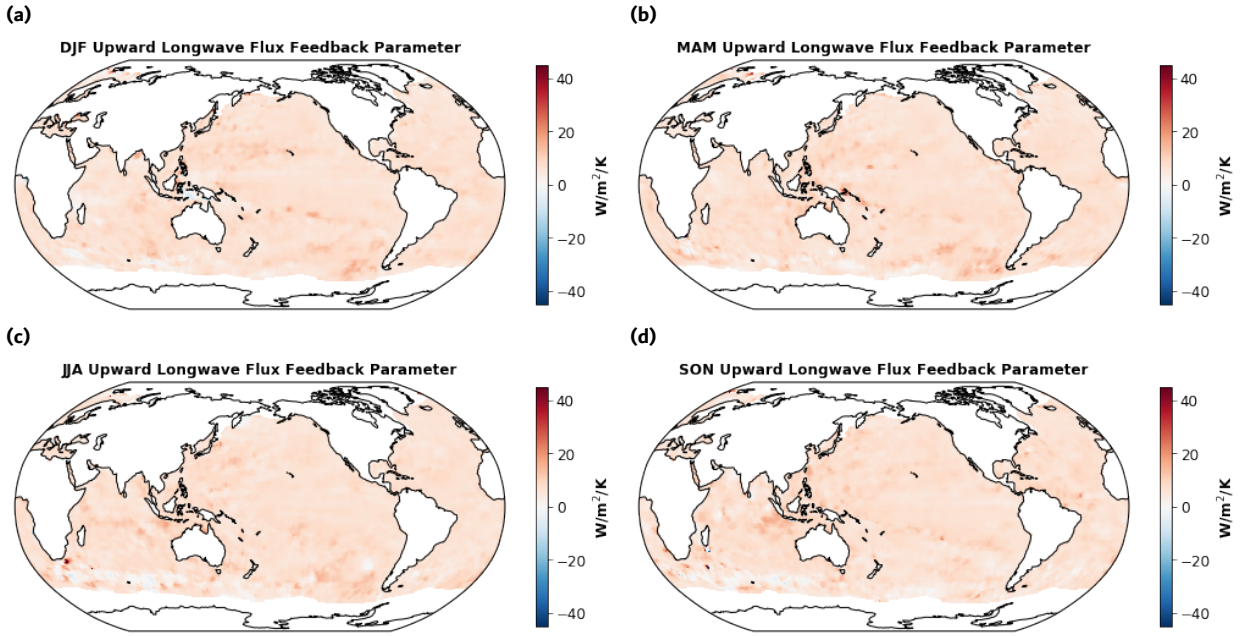

Figure 6.4 As in Figure 6.2, but for upward longwave radiative heat flux.

Figure 6.4 presents the upward longwave radiative flux feedback parameters for each of the four seasons. The longwave radiative flux feedback parameter is approximately uniform throughout all regions and seasons, with some regional enhancements. This is consistent with theoretical expectations that warm SST anomalies will cool with an upward longwave enhancement that scales with $4\sigma SST^3$ (where σ is the Stefan-Boltzmann constant equal to 5.67 x 10^{-8} W m^{-2} K^{-4}).

Figure 6.5 presents the downward longwave radiative flux feedback parameters for each of the four seasons. The downward longwave radiative flux feedback parameter, like the upward longwave radiative flux feedback parameter, is approximately uniform throughout all regions and seasons, though of the opposite sign. There are some regions in the subtropics that show enhancement of the feedback. Downward longwave feedbacks are positive. This indicates that the response of the atmosphere, through some combination of changes in clouds, humidity, and air temperature, acts to amplify SST anomalies. The near-uniformity of sign of the downward longwave radiative flux feedback is perhaps surprising, especially since the changes in clouds with SST anomalies (as inferred from Figure 6.3) are not uniform. The magnitude is also similar globally, though there is enhancement of the feedback parameters in warm water regions of the subtropics. This suggests that in most regions an atmospheric column experiences increased air temperature and humidity due to a warmer SST, and these changes in column properties cause a corresponding increase in downward longwave radiative flux. Unscrambling the effects of changes in column properties on the downward longwave flux from the effects of cloud changes is quite challenging, but the uniformity of the results in Figure 6.5 argues for the dominance of the former, rather than the latter.

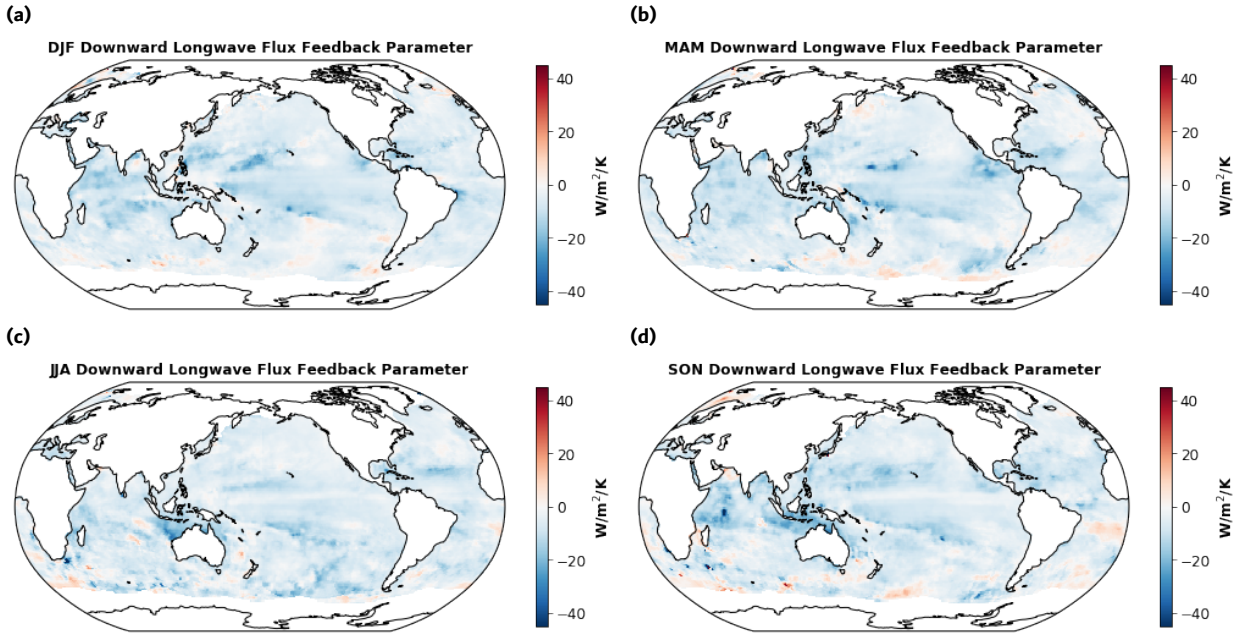

Figure 6.5 As in Figure 6.2, but for downward longwave radiative heat flux.

The combination of the upward and downward longwave radiative flux feedbacks is shown in in Figure 6.6. In regions where the net longwave feedback is negative, the upward longwave feedback dominates, and in regions where the net longwave feedback is positive, the upward longwave feedback dominates. There is significant spatial variability in the net longwave feedback. Generally speaking, there is a tendency for the tropics to have a positive longwave feedback (the downward longwave feedback dominates), while the mid-latitudes tend towards a negative longwave feedback (the upward longwave feedback dominates). The positive feedback in the tropics may be due to an increase in downward longwave radiation from increased cloud cover. More research looking at cloud property datasets and/or model process studies is needed to pick apart the physics driving the latitudinal differences in these feedbacks.

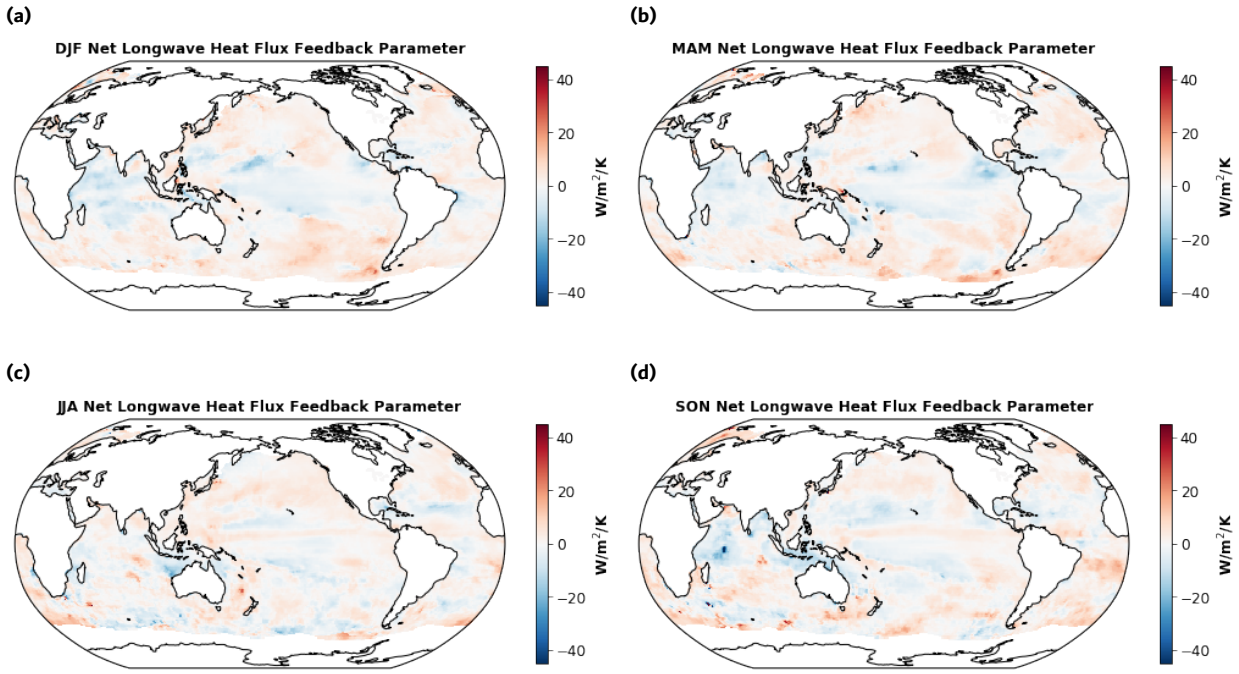

Figure 6.6 As in Figure 6.2, but for net longwave radiative heat flux.

Figure 6.7 shows the seasonal latent heat flux feedback parameters. The magnitude of the latent heat flux feedback is large in comparison to the other net heat flux components, except for the shortwave feedback which has a similar magnitude as the latent heat feedback in some tropical regions. Latent heat flux feedbacks are mostly negative around the globe (e.g., latent heat fluxes increase with warmer SST anomalies and thus act to damp anomalies). Some regions of the Southern Ocean experience positive latent heat flux feedbacks throughout the year. In

addition, the tropical western Atlantic shows persistent positive latent heat flux feedbacks during all seasons. This positive latent feedback appears to be the dominant component of the positive net heat flux feedback is this region, particularly in DJF and MAM (see Figure 6.1). The region near the South Pacific Convergence Zone (SPCZ), and to some extent the Intertropical Convergence Zone (ITCZ), also shows positive latent heat flux feedbacks. This would indicate that latent heat fluxes are suppressed during warm SST anomalies, which could occur if winds decrease or atmospheric humidity increases concurrently. This signal could be indicative, for example, of a positive wind-evaporation-sea surface temperature (WES) feedback.

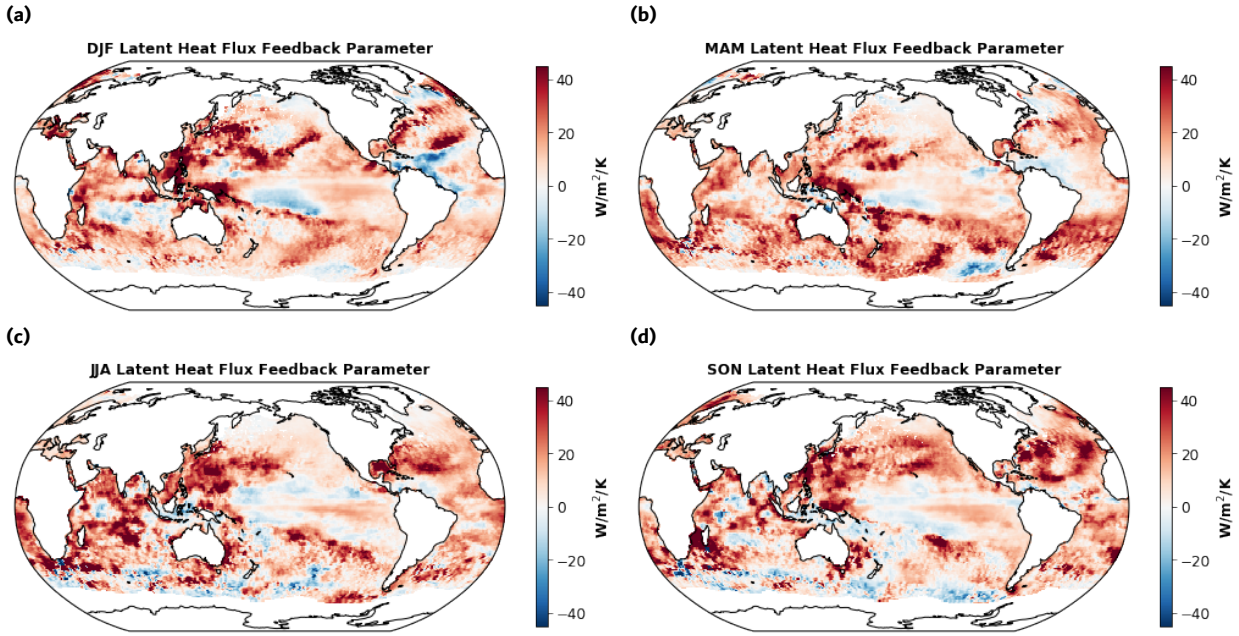

Figure 6.7 As in Figure 6.2, but latent heat flux.

Sensible heat flux feedback parameters are presented in Figure 6.8. Globally, the sensible heat flux feedback is mostly negative and magnitudes are mostly small. However, areas in the North Pacific, North Atlantic, and Southern Ocean show a positive sensible feedback during some seasons.

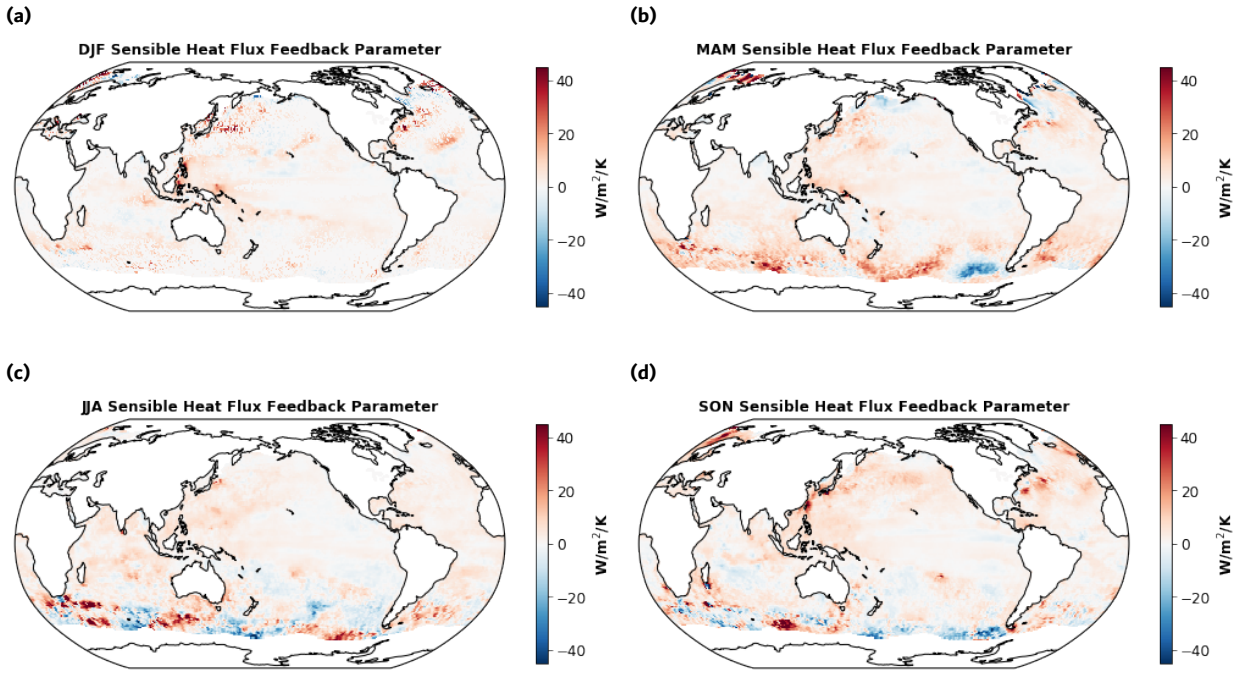

Figure 6.8 As in Figure 6.2, but for sensible heat flux.

6.3.3 Net heat flux feedback parameters during marine heat waves

The average net heat flux feedback parameter for the entire time series of data from 2001-2019 is presented in Figure 6.9a. As expected, this map approximately averages out the seasonal variability in feedback parameter shown in Figure 6.1, with almost all regions showing a negative feedback (positive λ), and only some regions exhibiting a near-zero or slightly negative feedback. The net heat flux feedback parameter for all months that meet the 95th percentile MHW threshold and the 90th percentile MHW threshold are presented in Figures 6.9b and 6.9c, respectively.

Net heat flux feedback parameters during MHWs have much higher spatial variability compared to climatological conditions. Furthermore, positive net heat flux feedbacks are more common during MHWs compared to climatological conditions. The difference between MHW and climatological net heat flux feedback parameters is shown in Figures 6.9d and 6.9e for MHWs defined with the 95th percentile threshold and 90th percentile threshold, respectively. The difference is largely negative over most of the globe, indicating that during MHWs net heat flux feedbacks are less positive or more negative, depending on the climatological feedback of that region. The MHW feedback parameters are largely insensitive to the two MHW definition

thresholds shown here (Figure 6.9b vs Figure 6.9c). Results show that net surface heat flux feedbacks change during a MHW compared to climatological net surface heat flux feedbacks for a given region and season.

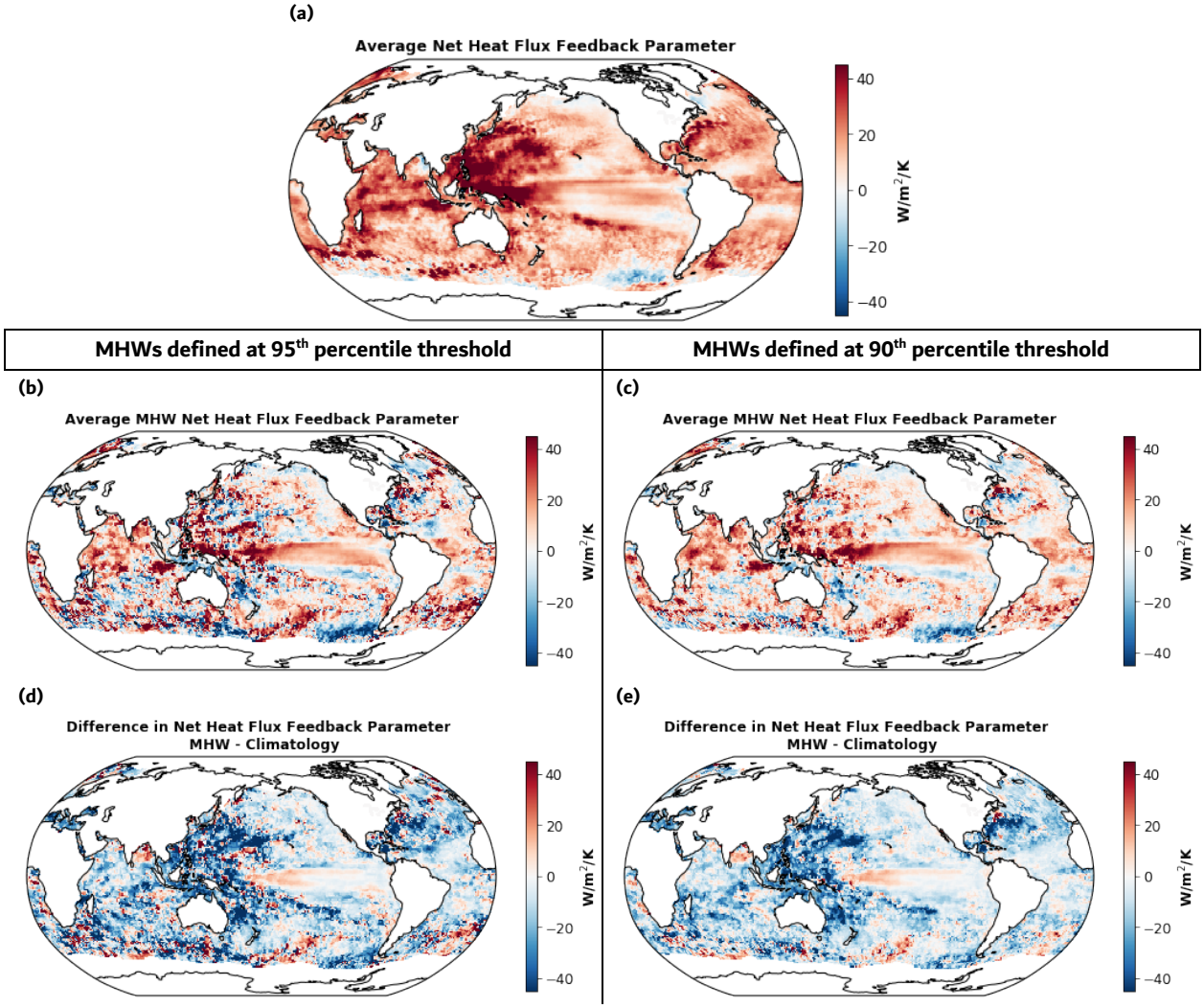

Figure 6.9 (a) The average net heat flux feedback parameter computed using the entire time series of heat flux data from 2001-2018. (b) The average net heat flux feedback parameter computed only using data during MHW months that meet the 95th percentile threshold and (c) the 90th percentile. The difference between the net heat flux feedbacks during MHWs and during climatology is shown in (d) for MHWs at the 95th percentile threshold and (e) the 90th percentile threshold.

The average inverse e-folding times of SST anomalies due to net heat flux feedbacks are presented in Figure 6.10a for the entire length of the time series (2001-2019), and in Figure 6.10b for only times that are identified as MHWs. The difference between inverse e-folding times during MHWs and climatological conditions is presented in Figure 6.10c. Inverse e-folding

times during MHWs are consistently lower than during climatological conditions, meaning that SST anomalies generally take longer to damp or are instead amplified due to heat flux feedbacks during MHWs. Keep in mind that the e-folding times here only represent the influence of the net heat flux feedback on SST anomalies, and exclude the influence of oceanic process, which will also influence the decay of SST anomalies during MHWs.

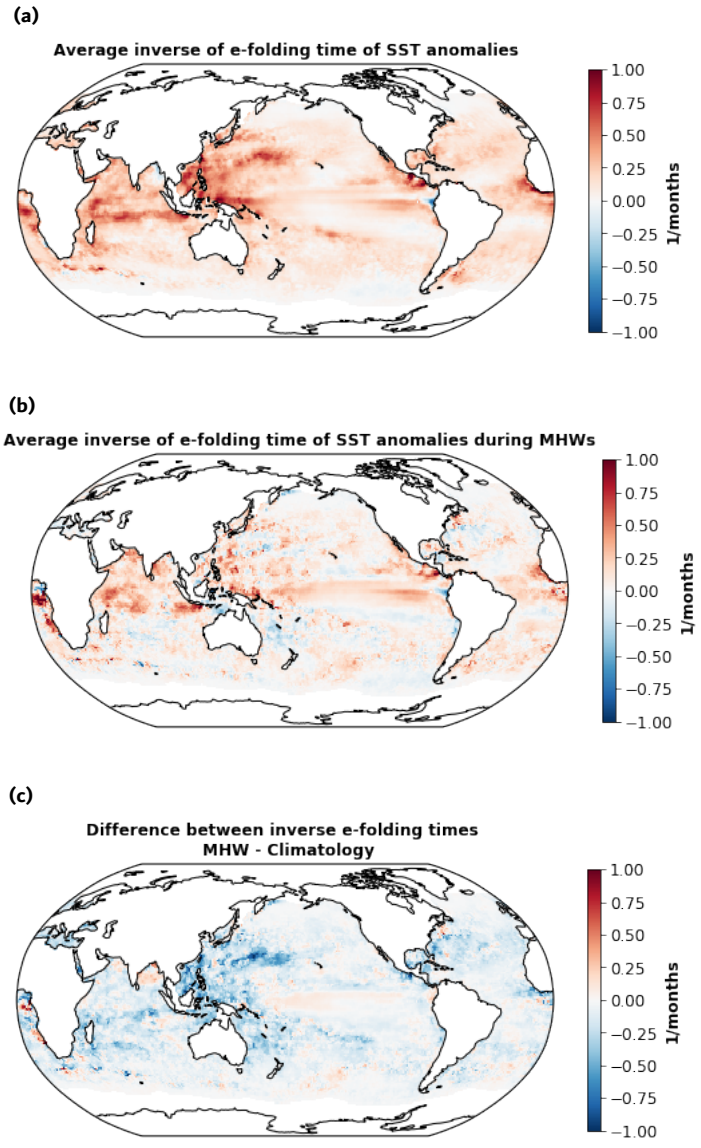

Figure 6.10 (a) Inverse of e-folding times (in months^{-1}) of SST anomalies due to the influence of net heat flux feedbacks averaged over the entire time series from 2001-2018; (b) as in (a), but for time periods designated as MHWs; and (c) the difference in inverse of e-folding times during MHWs compared to climatological conditions.

The maximum length of a MHW in the data record was computed for each individual grid cell by summing the longest consecutive number of months that meet the 90th percentile MHW threshold criteria. The maximum MHW length observed in each grid cell is presented in Figure 6.11. When Figure 6.11 is analyzed in the context of average net heat flux feedbacks for each region (Figure 6.9a), many areas with positive feedbacks or small negative feedbacks (like the tropical Eastern Pacific, Northeast Pacific, western tropical Atlantic, and the Southern Ocean off of southwest South America) experience longer MHWs, while many areas with large negative feedbacks (like the tropical western Pacific) experience MHWs of shorter duration.

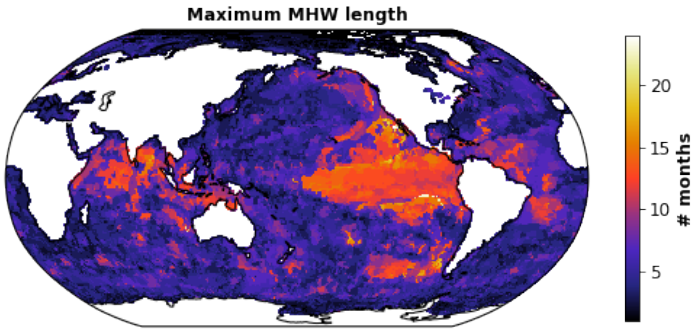

Figure 6.11 The maximum length of a MHW, in months, observed in each grid cell.

To better understand any statistical relationship between average net heat flux feedback of a grid cell and maximum MHW length, the Pearson correlation coefficient and related p-value were computed. MHW length and average net heat flux feedback are negatively correlated with a coefficient of -0.22 and a p-value of 0 (indicating a near-zero chance that the statistical correlation could be produced from a random distribution of numbers) (Table 6.1). This indicates that lower heat flux feedback parameters (positive or near-zero feedbacks) are associated with longer MHWs. This negative correlation holds true for grid cells with positive net heat flux feedback parameters as well as grid cells with negative heat flux feedback parameters, though the negative correlation is strongest where heat flux feedback parameters are positive. See Appendix D for statistics between MHW-averaged feedbacks and maximum length of MHWs. Note that most of the ocean has negative feedbacks, thus the statistics are more robust in this regime. These results confirm that areas with small negative net heat flux feedbacks or positive net heat flux feedbacks of any magnitude are more susceptible to more persistent MHWs.

Table 6.1 Pearson correlation coefficients between maximum MHW length and average net heat flux feedback parameters, p-value is the probability that an uncorrelated dataset would produce the Pearson correlation coefficient, and n is the number of data points that went into computing the statistic. Statistics are presented for all grid points, only grid points that exhibit an average positive net heat flux feedback parameter, and only grid points that exhibit on average a negative net heat flux feedback parameter.

	Pearson correlation coefficient	p-value	n
All data	-0.22	0*	31718
Positive net heat flux feedback parameters	-0.23	0*	28791
Negative net heat flux feedback parameters	-0.09	1.4e-5	2077

The negative correlation between MHW length and average net heat flux feedback parameter is also apparent in Figure 6.12, which shows a scatter plot of maximum MHW length in each grid cell vs. the average net heat flux feedback in each grid cell, with binned medians of the net heat flux feedback parameter shown in orange for each maximum MHW length. Figure 6.12a shows the entire spread of the data, and Figure 6.12b zooms in on data ranging from -40 to 40 $W/m^2/K$ to better visualize the trend in the binned medians. The data show that the grid cell's average heat flux feedback parameter decreases as its maximum MHW length increases. It is also apparent in Figure 6.12 that the variability of the net heat flux feedback parameter data is much greater at lower maximum MHW lengths, which is logical since the number of data points is much greater in the lower maximum MHW length bins compared to the high maximum MHW length bins.

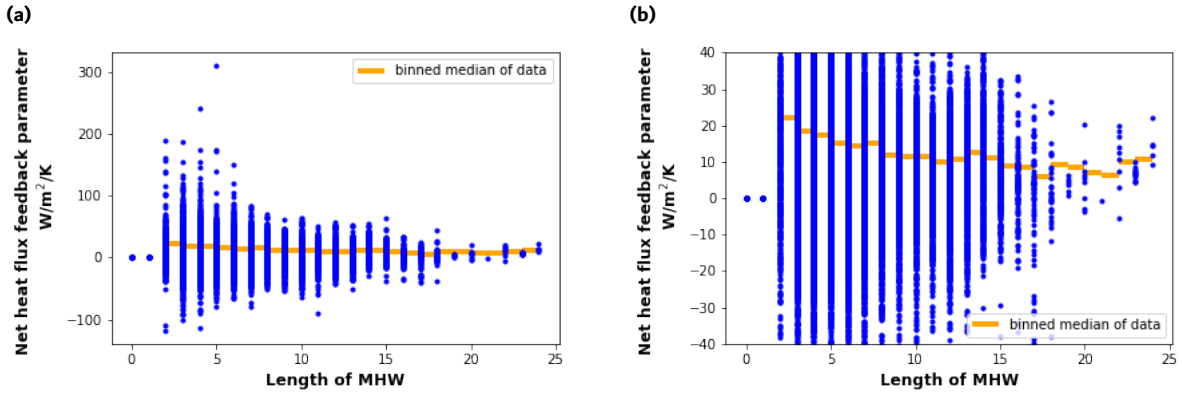

Figure 6.12 Maximum length of MHW (in months) in each grid cell vs. the average net heat flux feedback parameter (in W/m^2/K) in each grid cell. Scatter plot points are in blue, and the binned median of the net heat flux feedback parameter for each binned maximum MHW length are in orange. All data are shown in (a) and data bounded between net heat flux feedback parameters of -40 and 40 W/m^2/K are shown in (b), where it is easier to see changes in binned medians with length of MHW.

6.4 Discussion

6.4.1 Annual and seasonal net heat flux feedback climatology compared to past studies

Where geographic overlap is available, the annual and seasonal climatologies of net heat flux feedback parameters presented here are mostly in good agreement with past studies (Park et al., 2005; Frankignoul and Kestenare, 2002). Global averages of net heat flux feedbacks are generally negative, with most places in the ocean experiencing damping by net heat fluxes in response to SST anomalies. While net heat flux feedbacks are largely negative globally, there are regions and seasons in which net heat flux feedbacks are positive. Some of those key regions and the potential mechanisms driving the net heat flux feedbacks toward positive are discussed here.

Over the northeast Pacific the net heat flux feedback is positive or very weakly negative for DJF, MAM and JJA. This positive feedback is largely driven by a positive shortwave radiative feedback year-round, and a smaller positive turbulent heat flux feedback contributing somewhat during DJF and MAM. The positive shortwave radiative feedback observed in the data is driven by a positive SST-cloud feedback that is well documented in the region (e.g., Norris & Leovy, 1994; Klein et al., 1995; Norris et al., 1998; Myers et al., 2018; Schmeisser et al., 2019). Some of this literature on SST-cloud relationships in the Northeast Pacific also notes the influence of upstream SST on clouds, which is not accounted for in this study and thus the local

feedbacks presented here may be underestimates (e.g., Norris et al., 1998; Park et al., 2005). Our feedback results confirm findings from Latif & Barnett (1994), but are slightly different from the analysis of the North Pacific in Frankignoul and Kestenare (2002) (using NCEP and COADS data at resolutions of 2°x2° and 5°x5°, respectively) and that of Park et al. (2005) (using EECRA and ISCCP data at a resolution of 5°x10°). Frankignoul and Kestenare (2002) and Park et al. (2005) both find negative net heat flux feedbacks in the North Pacific, with the turbulent fluxes providing a strong net negative feedback and radiative fluxes providing a weaker positive feedback during all seasons. The more recent time series and higher resolution data analyzed here suggest that the positive radiative flux feedback dominates negative turbulent flux feedbacks in most seasons. The discrepancy indicates how magnitudes, not just signs, of heat flux feedbacks are very important in getting an accurate estimate of the net feedback. Studies that get the proper signs of radiative and turbulent heat flux feedbacks can end up with different net heat flux feedbacks in regions of the world like the northeast Pacific where the two terms are similar in magnitude but of opposing signs. The influence of the climatological net heat flux feedbacks in the Northeast Pacific on MHWs in the region is discussed in the next section.

A few areas of interest exist in the Atlantic Ocean – one in the western tropical Atlantic near the Caribbean Sea and one in the far Northwest Atlantic. Both regions exhibit positive net heat flux feedbacks for DJF and MAM. Unlike in the North Pacific, these positive heat flux feedbacks are not dominated by the shortwave heat flux feedback. In the western tropical Atlantic, the shortwave heat flux feedback is strongly negative, likely due to enhanced convection associated with warm SSTs in the Atlantic ITCZ region (Park et al., 2005). The Northwest Atlantic experiences near-zero shortwave heat flux feedbacks. Instead, positive latent heat flux feedbacks are observed in both of these regions in the Atlantic during DJF and MAM. In addition, the Northwest Atlantic shows a positive sensible heat flux feedback during DJF and MAM and the western tropical Atlantic has a positive longwave feedback during MAM, both of which enhance the effects of the positive latent heat flux feedbacks. Previous studies do not provide information on feedbacks in the Northwest Atlantic due to coarse resolution and missing data, so our results cannot be compared with others. However, in the western tropical Atlantic, Park et al. (2005) find similar results as ours for net heat flux feedbacks, turbulent heat flux feedbacks, and longwave heat flux feedbacks during DJF and MAM. Park et al. (2005) find the

positive net heat flux feedback extends year-round in this region, while our data show that the net heat flux feedback flips negative for JJA and SON.

The Southern Ocean exhibits the largest seasonal variability in net heat flux feedback parameters of any region. With the exception of one study (Hausmann et al., 2016), previous feedback studies do not analyze this area due to lack of available data. While we have continuous SST, turbulent, and radiative heat flux data over the Southern Ocean from which to compute feedbacks, the reliability of data in this region is less robust than other regions of the globe. Data are sometimes less dependable in the Southern Ocean since satellite retrievals are made more difficult with frequent cloud cover and presence of sea ice (e.g., Bourassa et al., 2013); furthermore, there are fewer in-situ datasets with which to validate satellite products. Consequently, caution must be taken not to overinterpret results in this region. Large patches of the Southern Ocean have positive net heat flux feedbacks throughout the entire year, particularly during JJA and SON. Magnitudes of positive feedbacks are especially high in the region off the southwest coast of South America. Positive shortwave heat flux feedbacks and latent heat flux feedbacks appear to be the largest contributors to the positive net heat flux feedback. Hausmann et al. (2016) find mostly negative turbulent and radiative heat flux feedbacks in the Southern Ocean, using a time period from 1980-2013 and two reanalysis datasets (ERA-Interim and OAFlux). These differences could be due to the different time periods analyzed, or different handling of the potential influence of sea ice in the region. It is clear that more research is needed in this region to better constrain net heat flux feedback estimates and understand the physical mechanisms influencing the feedbacks.

It is important to note that this study does not explicitly consider the influence of ocean processes on SST anomalies. Though this is by design, to narrow focus solely onto the effect of the atmosphere on air-sea feedbacks, it is possible that that ocean processes, like horizontal advection or changes in the mixed layer depth, may dominate the ocean mixed layer heat budget in some areas of the ocean during some seasons. While understanding the net heat flux feedback is essential in order to obtain a complete picture of the atmosphere-ocean system, it is important to keep in mind that ocean processes are acting in parallel with net heat flux feedbacks to either damp or amplify SST anomalies. One future direction of this work is to include ocean-induced feedbacks on SSTs and outline the areas of the world where net heat flux feedbacks dominate over ocean feedbacks and vice versa.

6.4.2 Net heat flux feedbacks during MHWs

The evolution of SST anomalies during MHWs depends on the surface net heat flux and ocean processes including advection, entrainment at the bottom of the ocean mixed layer, and diffusion at the bottom of the mixed layer. Net heat flux feedbacks represent the local role of the atmosphere during marine heatwaves, and, in combination with the effects from the ocean and remote atmospheric forcing, can be used to predict the likely evolution of SSTs during a MHW. As these results show, net heat flux feedbacks have high spatio-temporal variability. This means that when and where SST anomalies arise influences the relative role of the atmosphere in the persistence of the anomalies.

One aim of this research was to analyze whether net heat flux feedback parameters change during MHWs compared to climatological conditions. Results show that this is true; average MHW net heat flux feedback parameters are lower (feedbacks tend to be less negative or more positive) compared to climatological conditions. One interpretation might be that the net heat flux feedback parameter is not constant throughout the SST anomaly distribution. However, preliminary analysis suggests that the nature of the atmosphere-ocean system is for net heat flux feedbacks to tend toward zero at lower frequencies, as is this case with persistent MHWs. The Barsugli and Battisti (1995) stochastic model of midlatitude atmosphere-ocean interactions show a reduction in net heat flux feedbacks with increasing duration of MHWs, driven by reduced thermal damping at longer time scales (Battisti, personal communication). This is early indication that the difference in net heat flux feedback observed during MHWs may be an inherent feature of the atmosphere-ocean system, and not necessarily an indication of exotic physics happening during MHWs. Diagnostic and modeling studies will be necessary to further understand these features both in the tropics and midlatitudes to rule out any potential changes in physics driving a different net heat flux feedback parameter at the upper tail end of the SST anomaly distribution. Similarly, analysis into the net heat flux feedbacks and associated physics at the lower tail end of the distribution (marine ‘cold snaps’) could be equally enlightening and help elucidate any non-linearity in the atmosphere-ocean system.

Another aim of this research was to determine if regions with positive net surface heat flux feedbacks are more susceptible to longer, more persistent MHWs. The results show that

indeed there is a negative (positive) correlation between net heat flux feedback parameter (net heat flux feedback) and maximum MHW length observed in a grid cell. This means that areas that have a climatological near-zero or negative heat flux feedback have a tendency for longer MHWs. Although the time series used here is not long enough for robust seasonal MHW statistics, one interpretation is that for certain regions, the season in which the SST anomaly arises may also help dictate the persistence of the anomaly. For example, in a region like the Northeast Pacific where the net heat flux feedback is positive in DJF, MAM, and JJA, but negative in SON, these results suggest that an SST anomaly arising in DJF, MAM, and JJA is more likely to persist longer than if it arises in SON. More exploration of how timing of SST anomaly formation relates to the net heat flux feedback and MHW persistence will be necessary as longer time series of reliable data become available.

The most persistent MHW (as well as the largest in area) ever recorded was the 2013-2016 Northeast Pacific MHW. The analyses presented here suggest that the tendency of that region to have near-zero or positive net heat flux feedbacks most of the year (dominated by a positive SST-cloud feedback) very likely played a role in the long e-folding times of SST anomalies. In addition, the net heat flux feedbacks in that region tend to be even more positive during times of MHWs, further amplifying this effect.

6.5 Conclusions

Surface heat flux feedback parameters were computed using the best available SST, radiative flux, and turbulent flux data. The net surface heat flux feedback is negative over almost all of the world's oceans, damping SST anomalies. However, there are certain regions and seasons where a positive net heat flux feedback is observed. Here we are particularly interested in regions that depart from the average behavior of global net heat flux feedbacks (in other words, regions with positive net heat flux feedbacks) for two reasons. First, understanding the spatio-temporal variability of net heat flux feedbacks and properly representing that variability in models is essential for accurately modeling the atmosphere-ocean system. Second, the knowledge of net heat flux feedbacks is useful in understanding areas and seasons that may be prone to persistent MHWs.

Regions such as the northeast Pacific, northwest Atlantic, tropical western Atlantic, and areas of the Southern Ocean (especially southwest of South America) all show positive net heat

flux feedbacks during some, if not all, seasons. Analysis of the net heat flux feedback components (shortwave, longwave, latent, and sensible heat flux feedbacks) elucidate which factors are the largest contributors to positive net heat flux feedbacks. The dominate heat flux components differ from region to region, and thus do the physical mechanisms in the atmosphere that drive the net heat flux feedback. Some regions (like the northeast Pacific) experience large positive shortwave radiative feedbacks that originate from positive SST-cloud feedbacks in the region. Other areas (like the tropical western Atlantic) have positive latent and longwave heat flux feedbacks that likely originate from suppression of winds and/or enhancement of humidity in the air overlying SST anomalies. While this analysis provides an excellent big picture understanding of the spatio-temporal variability of heat flux feedbacks, local and regional studies are needed to better understand the intricate physics in the coupled atmosphere-ocean system that dictate the net heat flux feedbacks in a given location.

Across most of the globe, net heat flux feedbacks tend to be more positive during MHWs, indicating longer e-folding times for the warm SST anomalies. It is unlikely that this means atmosphere-ocean interactions change at the high tail-end of the SST distribution. Instead, this observation likely confirms the finding of simple atmosphere-ocean models that show net heat flux feedback parameters tend towards zero as MHWs becoming longer (lower atmospheric frequencies).

Regions that have negative or near-zero net heat flux feedbacks tend to experience longer MHWs compared to regions with large positive net heat flux feedbacks. This finding is very important for modeling efforts seeking to be able to predict the evolution of MHWs. The net heat flux feedback clearly plays an important role in how SSTs evolve, and properly representing the role of the atmosphere (through net heat flux feedbacks) will be essential to predicting the persistence of MHWs. Providing robust climatologies of net heat flux feedbacks during average and MHW conditions, like those presented here, will enhance modeling efforts that could eventually lead to better preparation of coastal regions to minimize the negative effects of MHWs.

Chapter 7 Implications & Conclusions

Although the science of MHWs is still in its infancy, it is now well established that the impacts of these extreme events can be detrimental. Mortality and shifts in ranges of marine species, harmful algal blooms, closures of fisheries, and coral bleaching from anomalously warm SSTs can all leave marine ecosystems and coastal communities devastated (e.g., Cavole et al., 2016; McCabe et al., 2016; Oliver et al., 2017; Wernberg et al., 2017; Le Nohaïc et al., 2017; Jones et al., 2017; Ritzman et al., 2018; Smale et al., 2019). There is urgency to better understand the physics of MHWs, particularly so we can better predict their onset and progression and give risk managers a better chance at adapting to and preparing for the negative impacts of these extreme events. While processes in both the ocean and atmosphere influence the evolution of MHWs, the goal of this dissertation was to advance our understanding of how MHWs influence the atmosphere, and how induced changes in the atmosphere influence SST anomalies during MHWs.

One overarching conclusion from the analyses presented here is: **The role of the atmosphere in MHWs is regionally variable and, because of these regional differences in air-sea interactions, we do not expect MHWs to evolve similarly in all regions.** This finding has large implications for proper modeling of MHWs, as the unique balance between atmospheric processes (radiative and turbulent heat fluxes) and ocean processes (advection, entrainment, and diffusion) in individual locations must be well understood in order to accurately project the evolution of SST anomalies.

There are multiple lines of evidence to support the regional variability in the atmosphere's role in MHWs. Results from Chapter 5 show that the forcing on the atmosphere from anomalously SST during MHWs is not uniform globally. Hot spots of particularly high forcing exist especially along the coasts of North America and in the eastern and central tropical Pacific. Consequences of this regionally variable forcing are apparent in heat flux and cloud cover anomalies during MHWs, which have unique geographic signatures. The tropics tend to have negative shortwave flux anomalies during MHWs (likely due to enhanced convection), while the mid-latitudes tend to have positive shortwave flux anomalies during MHWs (likely due to reduction in low cloud cover with warmer SSTs). Latent heat flux anomalies during MHWs have high spatial variability and little discernible geographic pattern. Although the net impact on

the atmosphere (net heat flux) is variable in space, it is worth mentioning that some atmospheric variables show surprisingly uniform responses during MHWs. For example, atmospheric humidity increases almost everywhere during a MHW, as do both upward and downward radiative fluxes. These are important because they determine which atmospheric variables set the spatial variability, and which do not. Shortwave radiative flux and latent heat fluxes are the most important factors in determining geographic differences in net heat flux during MHWs.

The results of Chapter 6 extend those of Chapter 5 and provide more evidence showing regional variability in the role of the atmosphere during MHWs. Surface net heat flux feedbacks provide an excellent framework for understanding how the net heat flux changes with changes in SST and how those SSTs are in turn damped or amplified by net heat flux changes. While the net heat flux feedback is negative and damps SST anomalies over most of the world's oceans, there are some regions and seasons that experience positive net heat flux feedbacks which would amplify SST anomalies. This is very important for understanding areas that may be particularly prone to persistent SSTs. Areas of the Northeast Pacific, tropical East Pacific, tropical West Atlantic, northwest Atlantic, and Southern Ocean exhibit near-zero or positive net heat flux feedbacks during parts of the year.

Another robust conclusion emerging from the results is that: **The Northeast Pacific has unique atmosphere-ocean interactions that make it particularly susceptible to persistent MHWs**. The changes in forcing from the ocean to the atmosphere during MHWs are particularly high in the Northeast Pacific. A decrease in low cloud amount that accompanies an increase in SSTs yields a positive radiative flux that is not quite offset by enhanced turbulent fluxes during average MHW conditions. This behavior is confirmed with a near-zero or positive net heat flux feedback most of the year in this region, largely dominated by the shortwave radiative feedback and slightly less so by the turbulent heat flux feedback. This effect is more important in summer, when cloudiness and shortwave radiative flux are both at their peaks, than in winter, when cloudiness and shortwave radiative flux are both reduced. During the 2013-2016 Northeast Pacific MHW, the most persistent MHW ever recorded, we computed these unique atmosphere-ocean interactions on a month-to-month basis as the event developed. The ocean mixed layer heat analysis reveals that positive SST-cloud feedbacks produced a net radiative heat flux comparable to the net turbulent heat fluxes at the surface, yielding a near-zero net heat flux that allowed SSTs to remain elevated for a couple of years. Including an analysis of the ocean

processes during the event showed that atmospheric and oceanic anomalies often offset each to produce a balance in which the atmosphere-ocean system was able to maintain itself in an anomalous state. We now understand that this region, with its unique SST-cloud relationship and near zero net heat flux feedback, is primed to produce a persistent MHW event like this.

One final intriguing conclusion from the dissertation is: **There is preliminary evidence that MHWs provide an observational proxy for future atmosphere-ocean interactions expected under global warming**. Cloud changes observed during MHWs show a robust decrease in low cloud cover globally, an increase in high cloud cover globally, and anomalies in total cloud cover that are positive in the tropics, negative in the subtropics and mid-latitudes, and positive in the high latitudes (Chapter 5). These cloud changes closely resemble those predicted by the CFMIP climate models per one degree of warming. The implication of this is that MHWs can provide valuable insight into the potential atmospheric response to future warming of SSTs. In particular MHWs might be able to constrain local responses to warming, though they will not provide insight into changes in large scale dynamics or dynamical patterns, such as the Pacific Decadal Oscillation (PDO). Further research is needed to understand the extent to which MHWs might provide an observational surrogate of what surface flux and atmospheric changes will look like in a warmer world.

These dissertation results lead in many interesting research directions. Perhaps most pressing is the need to start analyzing how global climate models represent the atmosphere-ocean physics of historical MHWs, and then utilize those models to look at atmosphere-ocean interactions during future MHWs. Are the atmospheric processes observed during past MHWs similar during future MHWs? Or do atmosphere-ocean physics start to look different at the far tail end of the SST anomaly distribution, or in SST regimes not-yet-observed? There is a realistic possibility that MHWs on top of global warming could push the atmosphere-ocean system into an unprecedented state, in which case we don't know if the combination of physics in air-sea interactions will remain constant, or if non-linearities will emerge. Application of the net heat flux feedback climatology (and the MHW net heat flux feedback climatology) could be particularly fruitful in helping model development. If models do an adequate job of capturing the regions of the world that experience near-zero or positive net heat flux feedbacks, they are more likely to be able to model the formation and duration of MHWs, which could be especially useful in a world trying to manage the risks of damaging MHWs.

Continuation of event-specific MHW analyses will also be needed. The atmospheric and oceanic physics of particularly large or persistent MHW events need to be well understood. The detailed physics of individual events should be compared and contrasted to events in other regions to understand how different atmosphere-ocean regimes affect SST anomaly evolution. Equally important will be the comparison of different events that occur in the same region. This will help to elucidate what components of atmosphere-ocean interactions are consistent and predictable, and what previously observed MHW processes may themselves be anomalous extreme events. An excellent example of this is a comparison of the 2013-2016 Northeast Pacific MHW to the shorter 2019-2020 Northeast Pacific MHW. We need to understand why one MHW was so persistent, while the other MHW was much shorter in time but even more intense in terms of SST anomalies.

Finally, more analyses that assess both atmosphere and ocean processes during MHWs will be key. One challenge will lie in finding datasets that accurately represent both the atmosphere and ocean without introducing large residuals. Another challenge will be building teams of interdisciplinary experts that can properly synthesize processes in the coupled atmosphere-ocean system that occur during MHWs.

As mean ocean temperatures increase with global warming, so will the frequency, duration, and intensity of MHWs as defined by historical MHW thresholds. There is a pressing need to understand the physical drivers dictating the evolution of MHWs, not only to better understand the extreme end of the atmosphere-ocean state but also so modelers can better predict MHWs and project future MHW changes. MHW science is moving quickly, and we are learning more and more every year about these extreme events. This research shows that the atmosphere plays an important role in MHWs. Everywhere around the globe, atmospheric anomalies are observed concurrent with MHWs, and those atmospheric changes affect the evolution of SST anomalies. Any comprehensive analysis of a MHW, or MHW modeling effort, should include analysis of the atmosphere for a full understanding of the atmosphere-ocean environment that dictates the progression of a MHW.

Bibliography

Arakawa, O., & Kitoh, A. (2004). Comparison of local precipitation–SST relationship between the observation and a reanalysis dataset. *Geophysical research letters*, *31*(12). https://doi.org/10.1029/2004GL020283

Bao, X., & Zhang, F. (2013). Evaluation of NCEP–CFSR, NCEP–NCAR, ERA-Interim, and ERA-40 reanalysis datasets against independent sounding observations over the Tibetan Plateau. *Journal of Climate*, *26*(1), 206-214. https://doi.org/10.1175/JCLI-D-12-00056.1

Barsugli, J. J., & Battisti, D. S. (1998). The basic effects of atmosphere-ocean thermal coupling on midlatitude variability. *Journal of the Atmospheric Sciences*, 55(4), 477-493.

Betts, A. K., Viterbo, P., Beljaars, A., Pan, H. L., Hong, S. Y., Goulden, M., & Wofsy, S. (1998). Evaluation of land-surface interaction in ECMWF and NCEP/NCAR reanalysis models over grassland (FIFE) and boreal forest (BOREAS). *Journal of Geophysical Research: Atmospheres*, *103*(D18), 23079-23085. https://doi.org/10.1029/98JD02023

Betts, A. K., M. Zhao, P. A. Dirmeyer, & A. C. M. Beljaars (2006), Comparison of ERA40 and NCEP/DOE near-surface data sets with other ISLSCP-II data sets, *Journal of Geophysical Research*, 111, D22S04. https://doi.org/10.1029/2006JD007174

Bellomo, K., Clement, A. C., Norris, J. R., & Soden, B. J. (2014). Observational and model estimates of cloud amount feedback over the Indian and Pacific Oceans, *Journal of Climate, 27(2),* 925-940, doi:10.1175/JCLI-D-13-00548.1

Bellomo, K., Clement, A. C., Murphy, L. N., Polvani, L. M., & Cane, M. A. (2016). New observational evidence for a positive cloud feedback that amplifies the Atlantic Multidecadal Oscillation, *Geophysical Research Letters*, 43(18), 9852-9859, doi:10.1002/2016GL069961

Bond, N. A., Cronin, M. F., Freeland, H., & Mantua, N. (2015). Causes and impacts of the 2014 warm anomaly in the NE Pacific, *Geophys. Res. Lett., 42,* 3414-3420, doi:10.1002/2015GL063306Bond, N. A., Cronin, M. F., Freeland, H. & Mantua, N. (2015). Causes and impacts of the 2014 warm anomaly in the NE Pacific. *Geophysical Research Letters,* 42 (9), 3414-3420. https://doi.org/10.1002/2015GL063306

Bosilovich, M. G., Chen, J., Robertson, F. R., & Adler, R. F. (2008). Evaluation of global precipitation in reanalyses. *Journal of Applied Meteorology and Climatology*, *47*(9), 2279-2299. https://doi.org/10.1175/2008JAMC1921.1

Bosilovich, M., Akella, S., Coy, L., Cullather, R., Draper, C., Gelaro, R., et al. (2015). MERRA-2: Initial evaluation of the climate. *NASA Tech. Rep. Series on Global Modeling and Data Assimilation* (NASA/TM-2015-104606, Vol. 43). Greenbelt, MD: NASA Goddard Space Flight Center.

Bourassa, M. A., Gille, S. T., Bitz, C., Carlson, D., Cerovecki, I., Clayson, C. A., Cronin, M. F., Drennan, W. M., Fairall, C. W., Hoffman, R. N., Magnusdottir, G., Pinker, R. T., Renfrew, I. A., Serreze, M., Speer, K., Talley, L. D. & Wick, G. A. (2013). High-Latitude Ocean and Sea Ice Surface Fluxes: Challenges for Climate Research. *Bull. Amer. Meteor. Soc.*, **94**, 403–423, https://doi.org/10.1175/BAMS-D-11-00244.1.

Bromwich, D. H., Fogt, R. L., Hodges, K. I., & Walsh, J. E. (2007). A tropospheric assessment of the ERA-40, NCEP, and JRA-25 global reanalyses in the polar regions. *Journal of Geophysical Research: Atmospheres*, *112*(D10). https://doi.org/10.1029/2006JD007859

Cavole, L. M., Demko, A. M., Diner, R. E., Giddings, A., Koester, I., Pagniello, C. M. L. S., Paulsen, M.-L., Ramirez-Valdez, A., Schwenck, S. M., Yen, N. K., Zill, M. E., & Franks, P. J. S. (2016). Biological impacts of the 2013-2015 warm-water anomaly in the Northeast Pacific: Winners, losers and the future. *Oceanography,* 29(2), 273-285, doi:10.5670/oceanog.2016.32

Clement, A. C., Burgman, R., & Norris, J. R. (2009). Observational and model evidence for positive low-level cloud feedback, *Science*, 325(5939), 460-464, doi:10.1126/science.1171255

Cronin, M. F., Pelland, N. A., Emerson, S. R. & Crawford, W. R. (2015). Estimating diffusivity from the mixed layer heat and salt balances in the North Pacific*, Journal of Geophysical Research Oceans*, 120, 7346-7362, doi:10.1002/2015JC011010

De Szoeke, S. P., Verlinden, K. L., Yuter, S. E., & Mechem, D. B. The time scales of variability of marine low clouds. *J. Clim.* **29,** 6463-6481 (2016).

Decker, M., Brunke, M. A., Wang, Z., Sakaguchi, K., Zeng, X., and Bosilovich, M. G. (2012). Evaluation of the reanalysis products from GSFC, NCEP, and ECMWF using flux tower observations. *Journal of Climate*, *25*, 1916-1944. https://doi.org/10.1175/JCLI-D-11-00004.1

Dee, D. P., Uppala, S. M., Simmons, A. J., Berrisford, P., Poli, P., Kobayashi, S., et al. (2011). The ERA-Interim reanalysis: Configuration and performance of the data assimilation system. *Quarterly Journal of the Royal Meteorological Society*, *137*(656), 553-597. https://doi.org/10.1002/qj.828

Deser, C. & National Center for Atmospheric Research Staff (Eds.). Last modified 28 Jan 2019. *The Climate Data Guide: ICOADS Surface Marine Weather Observations*. Retrieved from https://climatedataguide.ucar.edu/climate-data/icoads-surface-marine-weather-observations

Di Lorenzo, E., & Manuta, N. (2016). Multi-year persistence of the 2014-2015 North Pacific marine heatwave, *Nature Climate Change,* 6(11), 1042, doi:10.1038/nclimate3082

Donat, M. G., Sillmann, J., Wild, S., Alexander, L. V., Lippmann, T., & Zwiers, F. W. (2014). Consistency of temperature and precipitation extremes across various global gridded in situ and reanalysis datasets. *Journal of Climate*, *27*(13), 5019-5035. https://doi.org/10.1175/JCLI-D-13-00405.1

Dulière, V., Zhang, Y., & Salathé Jr, E. P. (2011). Extreme precipitation and temperature over the US Pacific Northwest: A comparison between observations, reanalysis data, and regional models. *Journal of Climate*, *24*(7), 1950-1964. https://doi.org/10.1175/2010JCLI3224.1

Fassbender, A. J., Sabine, C. L., & Cronin, M. F. (2016). Net community production and calcification from 7 years of NOAA Station Papa Mooring measurements. *Global Biogeochem Cycles,* 30, 250-267, doi:10.1002/2015GB005205

Fordyce, A. J., Ainsworth, T. D., Heron, S. F. & Leggat, W. (2019). Marine heatwave hotspots in coral reef environments: physical drivers, ecophysiological outcomes, and impact upon structural complexity. *Frontiers in Marine Science*, 6(498), 1-17, doi:10.3389/fmars/2019.00498

Frankignoul, C., and K.Hasselmann (1977). Stochastic climate models. Part II: Application to sea-surface temperature anomalies and thermocline variability. *Tellus*, **29A**, 289–305, doi:https://doi.org/10.1111/j.2153-3490.1977.tb00740.x.

Frankignoul, C., Czaja, A., & L'Heveder, B. (1998). Air–sea feedback in the North Atlantic and surface boundary conditions for ocean models. *Journal of climate*, *11*(9), 2310-2324, doi:10.1175/1520-0442(1998)011<2310:ASFITN>2.0.CO;2

Frankignoul, C., & Kestenare, E. (2002). The surface heat flux feedback. Part I: Estimates from observations in the Atlantic and the North Pacific. *Climate dynamics*, *19*(8), 633-647, doi:10.1007/s00382-002-0252-x

Freeland, H. (2007). A short history of Ocean Station Papa and Line P. *Progress in Oceanography*, *75*(2), 120-125.

Freeman, E., Woodruff, S. D., Worley, S. J., Lubker, S. J., Kent, E. C., Angel, W. E., ... & Gloeden, W. (2017). ICOADS Release 3.0: a major update to the historical marine climate record. *International Journal of Climatology*, *37*(5), 2211-2232.

Frölicher, T. L., & Laufkötter, C. (2018). Emerging risks from marine heat waves. *Nature communications*, *9*(1), 650, doi: 10.1038/s41467-018-03163-6

Frölicher, T. L., Fischer, E. M., & Gruber, N. (2018). Marine heatwaves under global warming. *Nature*, 560, 360-364. Doi: 10.1038/s41586-018-0383-9

Fujiwara, M., Wright, J.S., Manney, G.L., Gray, L.J., Anstey, J., Birner, T., et al. (2017). Introduction to the SPARC Reanalysis Intercomparison Project (S-RIP) and overview of the reanalysis systems. *Atmospheric Chemistry and Physics*, 17, 1417-1452. https://doi.org/10.5194/acp-17-1417-2017

Garrabou, J., Coma, R., Bensoussan, N., Bally, M., Chevaldonné, P., Cigliano, M., Diaz, D., Harmelin, J. G., Gambi, M. C., Kersting, D. K., Ledoux, J. B., Lejeusne, C., Linares, C., Marschal, C., Pérez, T., Ribes, M., Romano, J. C., Serrano, E., Teixido, N., Torrents, O., Zabala, M., Zuberer, F., & Cerrano, C. (2009). Mass mortality in Northwestern Mediterranean rocky benthic communities: effects of the 2003 heatwave, *Global Change Biology*, 15, 1090-1103, doi:10.1111/j.1365-2486.2008.01823

Gelaro, R., McCarty, W., Suárez, M.J., Todling, R., Molod, A., Takacs, L., et al. (2017). The modern-era retrospective analysis for research and applications, version 2 (MERRA-2). *Journal of Climate*, *30*(14), pp.5419-5454. https://doi.org/10.1175/JCLI-D-16-0758.1

Gentemann, C. L., Fewings, M. R., & García-Reyes, M. (2017). Satellite sea surface temperatures along the West Coast of the United States during the 2014-2016 Northeast Pacific marine heatwave, *Geophysical Research Letters, 44(1),* 312-319, doi:10.1002/2016GL071039.

Hausmann, U., A. Czaja, and J. Marshall. (2016). Estimates of Air–Sea Feedbacks on Sea Surface Temperature Anomalies in the Southern Ocean. *J. Climate*, **29**, 439–454, https://doi.org/10.1175/JCLI-D-15-0015.1.

Hartmann, D. (2015). Pacific sea surface temperature and the winter of 2014, *Geophysical Research Letters, 42,* 1894-1902, doi:10.1002/2015GL063083

Hobday, A. J., Alexander, L. V., Perkins, S. E., Smale, D. A., Straub, S. C., Oliver, E. C. J., Benthuysen, J. A., Burrows, M. T., Donat, M. G., Feng, M., Holbrook, N. J., Moore, P. J., Scannell, H. A., Sen Gupta, A., & Wernberg, T. (2016). A hierarchical approach to defining marine heatwaves. *Progress in Oceanography*, 141, 227-238. doi:10.1016/j.pocean.2015.12.014

Hobday, A. J., Oliver, E. C. J, Sen Gupta, A., Benthuysen, J. A., Burrows, M. T., Donat, M. G., Holbrook, N. J., Moore, P. J., Thomsen, M. S., Wernberg, T., & Smale, D. A. (2018). Categorizing and naming marine heatwaves. *Oceanography*, 31(2), doi:10.5670/oceanog.2018.205

Hoegh-Guldberg, O., et al., 2014: The Ocean. In: *Climate Change 2014: Impacts, Adaptation, and Vulnerability. Part B: Regional Aspects. Contribution of Working Group II to the Fifth Assessment Report of the Intergovernmental Panel on Climate Change* [Barros, V.R., C.B. Field, D.J. Dokken, M.D. Mastrandrea, K.J. Mach, T.E. Bilir, M. Chatterjee, K.L. Ebi, Y.O. Estrada, R.C. Genova, B. Girma, E.S. Kissel, A.N. Levy, S. MacCracken, P.R. Mastrandrea, and L.L. White (eds.)]. Cambridge University Press, Cambridge, United Kingdom and New York, NY, USA, pp. 1655-1731.

Holbrook, N. J., Scannell, H. A., Sen Gupta, A., Benthuysen, J. A., Feng, M., Oliver, E. C. J., Alexander, L. V., Burrows, M. T., Donat, M. G., Hobday, A. J., Moore, P. J. Perkins-Kirkpatrick, S. E., Smale, D. A., Straub, S. C., & Wernberg, T. (2019). A global assessment of marine heatwaves and their drivers. *Nature Communications,* 10:2624, doi:10.1038/s4167-019-10206-z

Hu, Z.-Z., Huang, B., & Pegion, K. (2008). Low cloud errors over the southeastern Atlantic in the NCEP CFS and their association with lower-tropospheric stability and air-sea interaction. *Journal of Geophysical Research: Atmospheres*, 113(D12114), doi:10.1029/2007JD009514

Hughes, T. P., Kerry, J. T., Álvarez-Noriega, M., Álvarez-Romero, J. G., Anderson, K. D., Baird, A. H., Babcock, R. C., Beger, M., Bellwood, D. R., Berkelmans, R., Bridge, T. C., Butler, I. R., Byrne, M., Cantin, N. E., Comeau, S., Connolly, S. R., Cumming, Graeme, S., Dalton, S. J., Diaz-Pulido, G., Eakin, C. M., Figueira, W. F., Gilmour, J. P., Harrison, H. B., Heron, S. F., Hoey, A. S., Hobbs, J.-P. A., Hoggenboom, M. O., Kennedy, E. V., Kuo, C.-y., Lough, J. M., Lowe, R. J., Liu, G., McCulloch, M. T., Malcolm, H. A., McWilliam, M. J., Pandolfi, J. M., Pears, R. J., Pratchett, M. S., Schoepf, V., Simpson, T., Skirving, W. J., Sommer, B., Torda, G., Wachenfeld, D. R., Willis, B. L., & Wilson, S. K. (2017). Global warming and recurrent mass bleaching of corals, *Nature*, 543, 373-378, doi: 10.1038/nature21707

IPCC, 2012: Summary for Policymakers. In: *Managing the Risks of Extreme Events and Disasters to Advance Climate Change Adaptation* [Field, C. B., V. Barros, T. F. Stocker, D. Qin, D. J. Dokken, K. L. Ebi, M. D. Mastrandrea, K. J. Mach, G.-K. Plattner, S. K. Allen, M. Tignor, and P. M. Midgley (eds.)]. A Special Report of Working Groups I and II of the Intergovernmental Panel on Climate Change. Cambridge University Press, Cambridge, UK, and New York, NY, USA, pp. 1-19

IPCC SREX, 2012: Summary for Policymakers. In: *Managing the Risks of Extreme Events and Disasters to Advance Climate Change Adaptation* [Field, C. B., V. Barros, T. F. Stocker, D. Qin, D. J. Dokken, K. L. Ebi, M. D. Mastrandrea, K. J. Mach, G.-K. Plattner, S. K. Allen, M. Tignor, and P. M. Midgley (eds.)]. A Special Report of Working Groups I and II of the Intergovernmental Panel on Climate Change. Cambridge University Press, Cambridge, UK, and New York, NY, USA, pp. 1-19

Jacox, M. G., Hazen, E. L., Zaba, K. D., Rudnick, D. L., Edwards, C. A., Moore, A. M., & Bograd, S. J. (2016). Impacts of the 2015-2016 El Niño on the California Current System: Early assessment and comparison to past events. *Geophysical Research Letters*, 43, 7072-7080, doi:10.1002/2016GL069716

Jakobson, E., Vihma, T., Palo, T., Jakobson, L., Keernik, H., & Jaagus, J. (2012). Validation of atmospheric reanalyses over the central Arctic Ocean. *Geophysical Research Letters*, *39*(10). https://doi.org/10.129/2012GL051591

Jiang, J. H., Su, H., Zhai, C., Wu, L., Minschwaner, K., Molod, A. M., & Tompkins, A. M. (2015). An assessment of upper-troposphere and lower-stratosphere water vapor in MERRA, MERRA2 and ECMWF reanalyses using Aura MLS observations. *Journal of Geophysical Research: Atmospheres, 120, https://doi.org/10.1002/2015JD023752*

Jin-Huan, Z., Shu-Po, M., Han, Z., Li-Bo, Z., & Peng, L. (2014). Evaluation of reanalysis products with in situ GPS sounding observations in the Eastern Himalayas. *Atmospheric and Oceanic Science Letters*, *7*(1), 17-22. https://doi.org/10.3878/j.issn.1674-2834.13.0050

Jones, T., Parrish, J. K., Peterson, W. T., Bjorkstedt, E. P., Bond, N. A., Ballance, L. T., Bowes, V., Hipfner, J. M., Burgess, H. K., Dolliver, J. E., Lindquist, K., Lindsey, J., Nevins, H. M., Robertson, R. R., Roletto, J., Wilson, L., Joyce, T., & Harvey, J. (2018). Massive mortality of a planktivorous seabird in response to a marine heatwave. *Geophysical Research Letters*, 45, 3193-3202, doi: 10.1002/2017GL076164

Josey, S.A. (2001). *A comparison of ECMWF, NCEP-NCAR, and SOC heat fluxes with moored buoy measurements in the subduction region of the Northeast Atlantic.* Journal of Climate, 13, 1780-1789. https://doi.org/10.1175/1520-0442(2001)014<1780:ACOENN>2.0.CO;2

Josey, S. A., Kent, E. C., & Taylor, P. K. (2002). Wind stress forcing of the ocean in the SOC climatology: Comparisons with the NCEP–NCAR, ECMWF, UWM/COADS, and Hellerman and Rosenstein datasets. *Journal of physical oceanography*, *32*(7), 1993-2019. https://doi.org/10.1175/1520-0485(2002)032<1993:WSFOTO>2.0.CO;2

Kalnay, E., Kanamitsu, M., Kistler, R., Collins, W., Deaven, D., Gandin, L., et al. (1996). The NCEP/NCAR 40-year reanalysis project. *Bulletin of the American Meteorological Society*, *77*(3), 437-471. https://doi.org/10.1175/1520-0477(1996)077<0437:TNYRP>2.0.CO;2

Kanamitsu, M., Ebisuzaki, W., Woollen, J., Yang, S. K., Hnilo, J. J., Fiorino, M., & Potter, G. L. (2002). NCEP–DOE AMIP-II Reanalysis (R-2). *Bulletin of the American Meteorological Society*, *83*(11), 1631-1643. https://doi.org/10.1175/BAMS-83-11-1631

Kato, S., N. G. Loeb, F. G. Rose, D. R. Doelling, D. A. Rutan, and T. E. Caldwell (2012a), Modeled surface irradiances consistent with CERES-derived top-of-atmosphere shortwave and longwave irradiances. *Journal of Climate,* 26, 2719-2740. https://doi.org/10.1175/JCLI-D-12-00436.1

Kato, S., Loeb, N. G., Rutan, D. A., Rose, F. G., Sun-Mack, S., Miller, W. F., & Chen, Y. (2012b). Uncertainty estimate of surface irradiances computed with MODIS-, CALIPSO-, and CloudSat-derived cloud and aerosol properties. *Surveys in Geophysics*, *33*(3-4), 395-412. https://doi.org/10.1007/s10712-012-9179-x

Kato, S., Rose, F. G., Rutan, D. A., Thorsen, T. J., Loeb, N. G., Doelling, D. R., Huang, X., Smith, W. L., Su, W., & Ham, S. (2018). Surface Irradiances of Edition 4.0 Clouds and the Earth's Radiant Energy System (CERES) Energy Balanced and Filled (EBAF) Data Product. *Journal of Climate*, 31, 4501-4527. https://doi.org/10.1175/JCLI-D-0523.1

Klein, S. A., & Hartmann, D. L. (1993). The seasonal cycle of low stratiform clouds, *Journal of Climate*, *6(8)*, 1587-1606.

Klein, S. A., Hartmann, D. L., & Norris, J. R. (1995). On the relationships among low-cloud structure, sea surface temperature, and atmospheric circulation in the summertime northeast Pacific, *Journal of Climate, 8(5)*, 1140-1155, doi:10.1175/1520-0442(1995)008<1140:OTRALC>2.0.CO;2

Kobayashi, S., Ota, Y., Harada, Y., Ebita, A., Moriya, M., Onoda, H., Onogi, K., Kamahori, H., Kobayashi, C., Endo, H. and Miyaoka, K., 2015. The JRA-55 reanalysis: General specifications and basic characteristics. *Journal of the Meteorological Society of Japan. Ser. II*, *93*(1), pp.5-48. https://doi.org/10.2151/jmsj/2015-001

Kumar, A., & Hu, Z.-Z. (2012). Uncertainty in the ocean-atmosphere feedbacks associated with ENSO in the reanalysis products. *Climate Dynamics*, 39, 575-588. https://doi.org/10.1007/s00382-011-1104-3

Ladd, C., & Bond, N.A. (2002). Evaluation of the NCEP/NCAR reanalysis in the NE Pacific and the Bering Sea. *Journal of Geophysical Research*, 107(C10), 3158. https://doi.org/10.1029/2001JC001157

Latif, M. & Barnett, T. P. (1994). Caution of decadal climate variability in the North Pacific/North American sector. *Science*, 266, 634-637.

Le Nohaïc, M., Ross, C. L., Cornwall, C. E., Comeau, S., Lowe, R., McCulloch, M. T., & Schoepf, V. (2017). Marine heatwave causes unprecedented regional mass bleaching of thermally resistant corals in northwestern Australia. *Nature Scientific Reports*, 7(14999), doi:10.1038/s41598-017-14794-y

Li, Jui-Lin & E. Waliser, D & Stephens, Graeme & Lee, Seungwon. (2016). Characterizing and Understanding Cloud Ice and Radiation Budget Biases in Global Climate Models and Reanalysis. Meteorological Monographs. 56. 13.1-13.20. 10.1175/AMSMONOGRAPHS-D-15-0007.1.

Lindsay, R., Wensnahan, M., Schweiger, A., & Zhang, J. (2014). Evaluation of seven different atmospheric reanalysis products in the Arctic. *Journal of Climate*, 27, 2588-2606. https://doi.org/10.1175/JCLI-D-13-00014.1

Loeb, N. G., Wielicki, B. A., Doelling, D. R., Smith, G. L., Keyes, D. F., Kato, S., ... & Wong, T. (2009). Toward optimal closure of the Earth's top-of-atmosphere radiation budget. *Journal of Climate*, *22*(3), 748-766.

Lüpkes, C., Vihma, T., Jakobson, E., König-Langlo, G., & Tetzlaff, A. (2010). Meteorological observations from ship cruises during summer to the central Arctic: A comparison with reanalysis data. *Geophysical Research Letters*, *37*(9). https://doi.org/10.1029/2010GL042724

Ma, L., Zhang, T., Li, Q., Frauenfeld, O. W., & Qin, D. (2008). Evaluation of ERA-40, NCEP-1, and NCEP-2 reanalysis air temperatures with ground-based measurements in China. *Journal of Geophysical Research: Atmospheres*, *113*(D15). https://doi.org/10.1029/2007JD009549

McCabe, R. M., Hickey, B. M., Kudela, R. M., Lefebvre, K. A., Adams, N. G., Bill, B. D., Gulland, F. M. D., Thomson, R. E., Cochlan, W. P., & Trainer, V. L. (2016). An unprecedented coastwide toxic algal bloom linked to anomalous ocean conditions. *Geophysical Research Letters*, 43(10), 10366-10376, doi:10.1002/2016GL070023

Meindl, E. A., & Hamilton, G. D. (1992). Programs of the National Data Buoy Center. *Bulletin of the American Meteorological Society*, 73(7), 985-993.

Ming, L., Qinghua, Y., Jiechen, Z., Lin, Z., Chunhua, L., & Shang, M. (2013). Evaluation of reanalysis and satellite-based sea surface winds using in situ measurements from Chinese Antarctic Expeditions. *Chinese Journal of Polar Research*, *24*(3-English), 147-152. https://doi.org/10.3724/SP.J.1085.2013.00147

Myers, T. A., Mechoso, C. R., Cesana, G. V., DeFlorio, M. J., & Waliser, D. E. (2018). Cloud feedback key to marine heatwave off Baja California, *Geophysical Research Letters*, 45(9), 4345-4352, doi:10.1029/2018GL078242

Newman, M., Sardeshmukh, P. D., & Bergman, J. W. (2000). An assessment of the NCEP, NASA, and ECMWF reanalyses over the tropical west Pacific warm pool. *Bulletin of the American Meteorological Society*, *81*(1), 41-48. https://doi.org/10.1175/1520-0477(2000)081<0041:AAOTNN>2.3.CO;2

Norris, J. R. (2000). Interannual and interdecadal variability in the storm track, cloudiness, and sea surface temperature over the summertime North Pacific, *Journal of Climate*, 13(2), 422-430, doi:10.1175/1520-0442(2000)013<04222:IAIVIT>2.0.CO;2

Norris, J. R., & Leovy, C. B. (1994). Interannual variability in stratiform cloudiness and sea surface temperature, *J. of Climate, 7(12)*, 1915-1925, doi:10.1175/1520-0442(1994)007<1915:IVISCA>2.0.CO;2

Norris, J. R., Zhang, Y., & Wallace, J. M. (1998). Role of low clouds in summertime atmosphere-ocean interactions over the North Pacific, *Journal of Climate, 11(10),* 2482-2490, doi:10.1175/1520-0442(1998)011<2482:ROLCIS>2.0.CO;2

Oliver, E. C. J., Donat, M. G., Burrows, M. T., Moore, P. J, Smale, D. A., Alexander, L. V., et al. (2018). Longer and more frequent marine heatwaves over the past century, *Nature Communications, 9:1324*, doi:10.1038/s41467-018-03732-9

Oliver, E. C. J., Perkins-Kirkpatrick, S. E., Holbrook, N. J., & Bindoff, N. L. (2018). Anthropogenic and natural influences on record 2016 marine heatwaves, *Bulletin of the American Meteorological Society*, 99(1), S44-S48, doi:10.1175/BAMS-D-17-0093.1

Oliver, E. C., Benthuysen, J. A., Bindoff, N. L., Hobday, A. J., Holbrook, N. J., Mundy, C. N., & Perkins-Kirkpatrick, S. E. (2018). The unprecedented 2015/16 Tasman Sea marine heatwave, *Nature communications,* 8, 16101, doi:10.1038/ncomms16101

Park, S., Deser, C., & Alexander, M. A. (2005). Estimation of the surface heat flux response to sea surface temperature anomalies over the global oceans. *Journal of Climate,* 18, 4582-4599, doi:10.1175/JCLI3521.1

Piatt, J. F., et al. Extreme mortality and reproductive failure of common murres resulting from the northeast Pacific marine heatwave of 2014-2016. *PLoS One* **15,** 1, (2020).

Pfeifroth, U., Mueller, R., & Ahrens, B. (2013). Evaluation of satellite-based and reanalysis precipitation data in the tropical Pacific. *Journal of Applied Meteorology and Climatology*, *52*(3), 634-644. https://doi.org/10.1175/JAMC-D-12-049.1

Porter, David F., John J. Cassano, and Mark C. Serreze. "Analysis of the Arctic atmospheric energy budget in WRF: A comparison with reanalyses and satellite observations." *Journal of Geophysical Research: Atmospheres* 116.D22 (2011). https://doi.org/10.1029/2011JD016622

Ramanthan, V. & Collins, W. Thermodynamic regulation of ocean warming by cirrus clouds deduced from observations of the 1987 El Niño. *Nature* **353,** 737-740 (1991).

Randles, C. A., Da Silva, A. M., Buchard, V., Colarco, P. R., Darmenov, A., Govidaraju, R., Smirnov, A., Holben, B., Ferrare, R., Hair, J., Shinozuka, Y., & Flynn, C. J. (2017). The MERRA-2 aerosol reanalysis, 1980 onward. Part I: System description and data assimilation evaluation. *Journal of Climate, 30*, 6823-6850. https://doi.org/10.1175/JCLI-D-16-0609.s1

Rayner, N. A., et al. Global analyses of sea surface temperature, sea ice, and night marine air temperature since the late nineteenth century *J. Geophys. Res. Vol*. **108,** 4407 (2003).

Ritzman, J., Brodbeck, A., Brostrom, S., McGrew, S., Dreyer, S., Klinger, T., & Moore, S. K. (2018). Economic and sociocultural impacts of fisheries closures in two fishing-dependent communities following the massive 2015 US West Coast harmful algal bloom. *Harmful Algae*, *80*, 35-45, doi:10.1016/j.hal.2018.09.002

Ronca, R. E. & Battisti, D. S. (1997). Anomalous sea surface temperatures and local air-sea energy exchange on intraanual timescales in the Northeastern subtropical Pacific, *Journal of Climate*, 10, 102-117, doi:10.1175/1520-0442(1997)010<0102:ASSTAL>2.0.CO;2

Rutan, D. A., Kato, S., Doelling, D. R., Rose, F. G., Nguyen, L. T., Caldwell, T. E., & Loeb, N. G. (2015). CERES synoptic product: Methodology and validation of surface radiant flux. *Journal of Atmospheric and Oceanic Technology*, *32*(6), 1121-1143. https://doi.org/10.1175/JTECH-D-14-00165.1

Saha, S., Moorthi, S., Pan, H. L., Wu, X., Wang, J., Nadiga, S., et al. (2010). The NCEP climate forecast system reanalysis, *Bulletin of the American Meteorological Society*, 91(8), 1015-1058, doi:10.1175/2010BAMS3001.1

Saha, S., Moorthi, S., Wu, X., Wang, J., Nadiga, S., Tripp, P., et al., (2014). The NCEP climate forecast system version 2, *Journal of Climate*, 27(6), 2185-2208, doi:10.1175/JCLI-D-12-00823.1Schmeisser, L., Hinkelman, L. M., & Ackerman, T. P. (2018). Evaluation of radiation and clouds from five reanalysis products in the Northeast Pacific Ocean. *Journal of Geophyscial Research: Atmospheres*, 123, doi:10.1029/2018JD028805

Sanford, E., Sones, J. L, García-Reyes, M., Goddard, J. H. R., & Largier, J. L. (2019). Widespread shifts in the coastal biota of northern California during the 2014-2016 marine heatwaves. *Scientific Reports, 9(4216)*, doi:10.1038/s41598-019-40784-3

Scannell, J. A., Pershing, A. J., Alexander, M. A., Thomas, A. C., & Mills, K. E. (2016). Frequency of marine heatwaves in the North Atlantic and North Pacific since 1950, *Geophysical Research Letters*, 43, 2069-2076, doi:10.1002/2015GL067308

Schmeisser, L., Bond, N. A., Siedlecki, S. A., & Ackerman, T. P. The role of clouds and surface heat fluxes in the maintenance of the 2013–2016 Northeast Pacific marine heatwave. *J. Geophys. Res. Atmos.* **124,** 10772-10783 (2019).

Smale, D. A., Wernberg, T., Oliver, E. C. J., Thomsen, M., Harvey, B. P., Straub, S. C., Burrows, M. T., Alexander, L. V., Benthuysen, J. A., Donat, M. G., Feng, M., Hobday, A. J., Holbrook, N. J., Perkins-Kirkpatrick, S. E., Scannell, H. A., Sen Gupta, A., Payne, B. L., & Moore, P. J. (2019). Marine heatwaves threaten global biodiversity and the provision of ecosystem services. *Nature Climate Change,* 9(4), 306. doi:10.1038/s41558-019-0412-1

Tareghian, R., & Rasmussen, P. F. (2013). Statistical downscaling of precipitation using quantile regression. *Journal of hydrology*, *487*, 122-135, doi: 10.1016/j.jhydrol.2013.02.029

Teng, C. C., Cucullu, S., McArthur, S., Kohler, C., Burnett, B., & Bernard, L. (2009, October). Buoy vandalism experienced by NOAA national data buoy center. In *OCEANS 2009* (pp. 1-8). IEEE.

Trainer, V. L., Moore, S. K., Hallegraeff, G., Kudela, R. M., Clement, A., Mardones, J. I., & Cochlan, W. P. (2019). Pelagic harmful algal blooms and climate change: Lessons from nature's experiments with extremes. *Harmful Algae*, doi:10.1016/j.hal.2019.03.009

Uppala, S. M., Kållberg, P. W., Simmons, A. J., Andrae, U., Bechtold, V. D., Fiorino, M., et al. (2005). The ERA-40 re-analysis. *Quarterly Journal of the royal meteorological society*, *131*(612), 2961-3012. https://doi.org/10.1256/qj.04.176

Vargas Zeppetello, L. R., Donohoe, A., & Battisti, D. S. Does surface temperature respond to or determine downwelling longwave radiation?. *Geo. Res. Lett.* **46,** 2781-2789 (2019).

Vey, S., Dietrich, R., Rülke, A., Fritsche, M., Steigenberger, P., & Rothacher, M. (2010). Validation of precipitable water vapor within the NCEP/DOE reanalysis using global GPS observations from one decade. *Journal of Climate*, *23*(7), 1675-1695. https://doi.org/10.1175/2009JCLI2787.1

Walsh, J. E., Chapman, W. L., & Portis, D. H. (2009). Arctic cloud fraction and radiative fluxes in atmospheric reanalyses. *Journal of Climate*, *22*(9), 2316-2334. https://doi.org/10.1175/2008JCLI2213.1

Wang, K., & Dickinson, R. E.. (2013)Global atmospheric downward longwave radiation at the surface from ground-based observations, satellite retrievals, and reanalyses. *Reviews of Geophysics,* 51.2, 150-185. https://doi.org/10.1002/rog.20009

Wernberg, T., Bennnett, S., Babcock, R. C., de Bettignies, T., Cure, K., Depczynski, M., Dufois, F., Fromont, J., Fulton, C. J., Hovey, R. K., Harvey, E. S., Homes, T. H., Kendrick, G. A., Radford, B., Santana-Garcon, J., Saunders, B. J., Smale, D. A., Thomsen, M. S., Tuckett, C. A., Tuya, F., Vanderklift, M. A., & Wilson, S. (2016). Climate-driven regime shift of a temperature marine ecosystem. *Science*, 353(6295), 169-172, doi:10.1126/science.aad8745

Wielicki, B. A, Barkstrom, B. R., Harrison, E. F., Lee, R. B., Louis Smith, G., and Cooper, J. E. (1996). Clouds and the Earth's Radiant Energy System (CERES): An Earth Observing System Experiment. *Bulletin of American Meteorological Society* 77, 853-868. https://doi.org/10.1175/1520-0477(1996)077<0853:CATERE>2.0.CO;2

Yang, S. K., Hou, Y. T., Miller, A. J., & Campana, K. A. (1999). Evaluation of the earth radiation budget in NCEP–NCAR reanalysis with ERBE. *Journal of Climate*, *12*(2), 477-493. https://doi.org/10.1175/1520-0442(1999)012<0477:EOTERB>2.0.CO;2

Yu, L., Zhang, Z., Zhou, M., Zhong, S., Lenschow, D., Hsu, H., et al. (2010). Validation of ECMWF and NCEP-NCAR reanalysis data in Antarctica. *Advances in Atmospheric Sciences*, *27*(5), 1151-1168. https://doi.org/10.1007/s00376-010-9140-1

Zelinka, M. D., Klein, S. A., & Hartmann, D. L. Computing and partitioning cloud feedbacks using cloud property histograms. Part II: Attribution to changes in cloud amount, altitude, and optical depth. *J. Clim.* **25,** 3736-3754 (2012).

Zhang, C. Large-scale variability of atmospheric deep convection in relation to sea surface temperature in the tropics. *J. Clim.* **6,** 1898-1913 (1993).

Zhang, Y. C., Rossow, W. B., & Lacis, A. A. (1995). Calculation of surface and top of atmosphere radiative fluxes from physical quantities based on ISCCP data sets: 1. Method and sensitivity to input data uncertainties. *Journal of Geophysical Research: Atmospheres*, *100*(D1), 1149-1165. https://doi.org/10.129/94JD02747

Zhang, T., Stackhouse Jr, P. W., Gupta, S. K., Cox, S. J., Mikovitz, J. C., & Hinkelman, L. M. (2013). The validation of the GEWEX SRB surface shortwave flux data products using BSRN measurements: A systematic quality control, production and application approach. *Journal of Quantitative Spectroscopy and Radiative Transfer*, *122*, 127-140. https://doi.org/10.1016/j.jqsrt.2012.10.004

Zhang, X., Liang, S., Wang, G., Yao, Y., Jiang, B, & Cheng, J. (2016). Evaluation of the reanalysis surface incident shortwave radiation products from NCEP, ECMWF, GSFC, and JMA using satellite and surface observations. *Remote Sensing,* 8.3(225). https://doi.org/10.3390/rs8030225

Zib, B. J., Dong, X., Xi, B., & Kennedy, A. (2012). Evaluation and intercomparison of cloud fraction and radiative fluxes in recent reanalyses over the Arctic using BSRN surface observations. *Journal of Climate*, *25*(7), 2291-2305. https://doi.org/10.1175/JCLI-D-11-00147.1

Data/Funding Acknowledgements

I would like to thank the University of Washington IGERT Program on Ocean Change award #NSF1068839 for partial funding of this work. I would also like to thank the Joint Institute for Study of the Atmosphere and Ocean graduate fellowship program, in conjunction with the University of Washington College of the Environment, for partial funding

All data used in this study are available publicly. CERES EBAF satellite estimates can be downloaded from the NASA CERES website at: https://ceres.larc.nasa.gov/order_data.php. ECMWF ERA-Interim reanalysis are available from the ECMWF website at: https://www.ecmwf.int/en/forecasts/datasets/reanalysis-datasets/era-interim . MERRA2 reanalysis datasets are available at: https://gmao.gsfc.nasa.gov/reanalysis/MERRA-2/data_access/. JRA-55 reanalysis data can be downloaded from: http://jra.kishou.go.jp/JRA-55/index_en.html. NCEP2 reanalysis data is available from NOAA/OAR/ESRL PSD, Boulder, Colorado, USA and can be downloaded from: https://www.esrl.noaa.gov/psd/data. Finally, CFSR data are available from: https://rda.ucar.edu/pub/cfsr.html and https://rda.ucar.edu/datasets/ds094.2/ (for CFSRv2). The CFSR reanalysis data were developed by NOAA's National Centers for Environmental Prediction (NCEP). The data for this study are from the Research Data Archive (RDA) which is maintained by the Computational and Information Systems Laboratory (CISL) at the National Center for Atmospheric Research (NCAR). NCAR is sponsored by the National Science Foundation (NSF). The original data are available from the RDA (http://dss.ucar.ed) in dataset number ds093.2. GODAS data are provided by the NOAA/OAR/ESRL Physical Sciences Division (PSD) in Boulder, Colorado, USA from there website at https://www.esrl.noaa.gov/psd/. The OAFlux global ocean heat flux and evaporation products were provided by the WHOI OAFlux project (http://oaflux.whoi.edu) funded by the NOAA Climate Observations and Monitoring (COM) program. Sea surface temperatures from the HadISST dataset are available from the Met Office Hadley Centre website https://www.metoffice.gov.uk/hadobs/hadisst/.

Appendix A
Supplementary information for Chapter 3

Appendix A provides modelers a chain of evidence between the cloud fraction (CF) bias and surface shortwave (SW) radiative flux bias. CERES EBAF-TOA and –Surface measurements are used for CERES data shown here, see full descriptions in Chapter 3.3.1. All data for reanalysis is described in Section 3.3.2. Figure A1 shows total cloud fraction versus top of atmosphere (TOA) albedo in attempt to give a sense of the extent to which reanalyses are defining clouds fraction in the same way as the CERES estimates. Figure A2 shows the relationship between total cloud fraction and normalized downward shortwave at the surface. Finally, Figure A3 shows the relationship between total cloud fraction bias and normalized downward shortwave radiative flux bias at the surface. Figure A3 shows that, given the weak relationship between CF bias and SW bias in some of the reanalysis products, factors other than CF bias must be contributing to the SW bias.

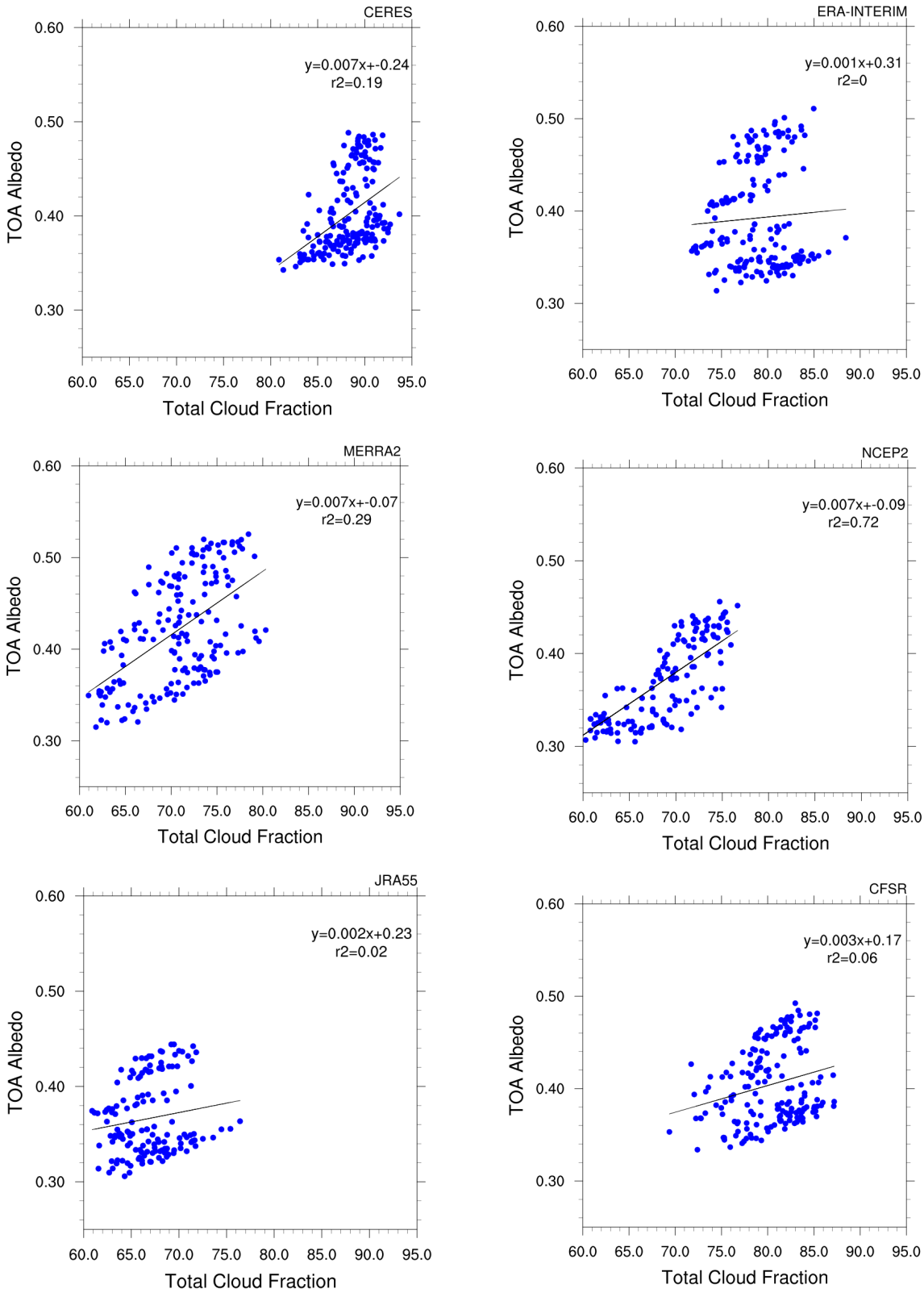

Figure A1. Total cloud fraction vs. albedo at the top of the atmosphere for CERES satellite observations and five reanalyses

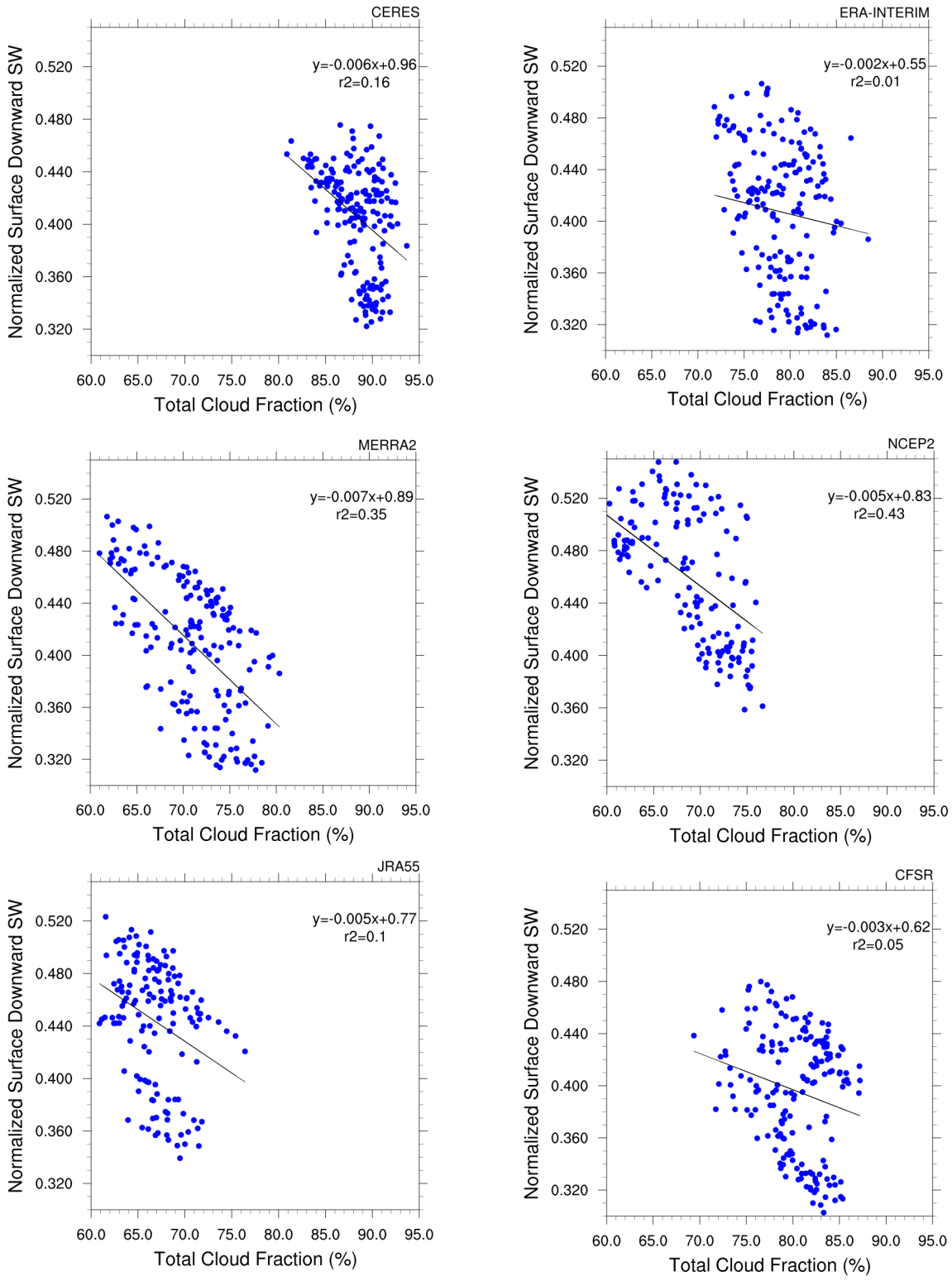

Figure A2. Total cloud fraction vs. downward shortwave radiative flux at the surface normalized by incident shortwave at the top of the atmosphere for CERES satellite observations and five reanalyses.

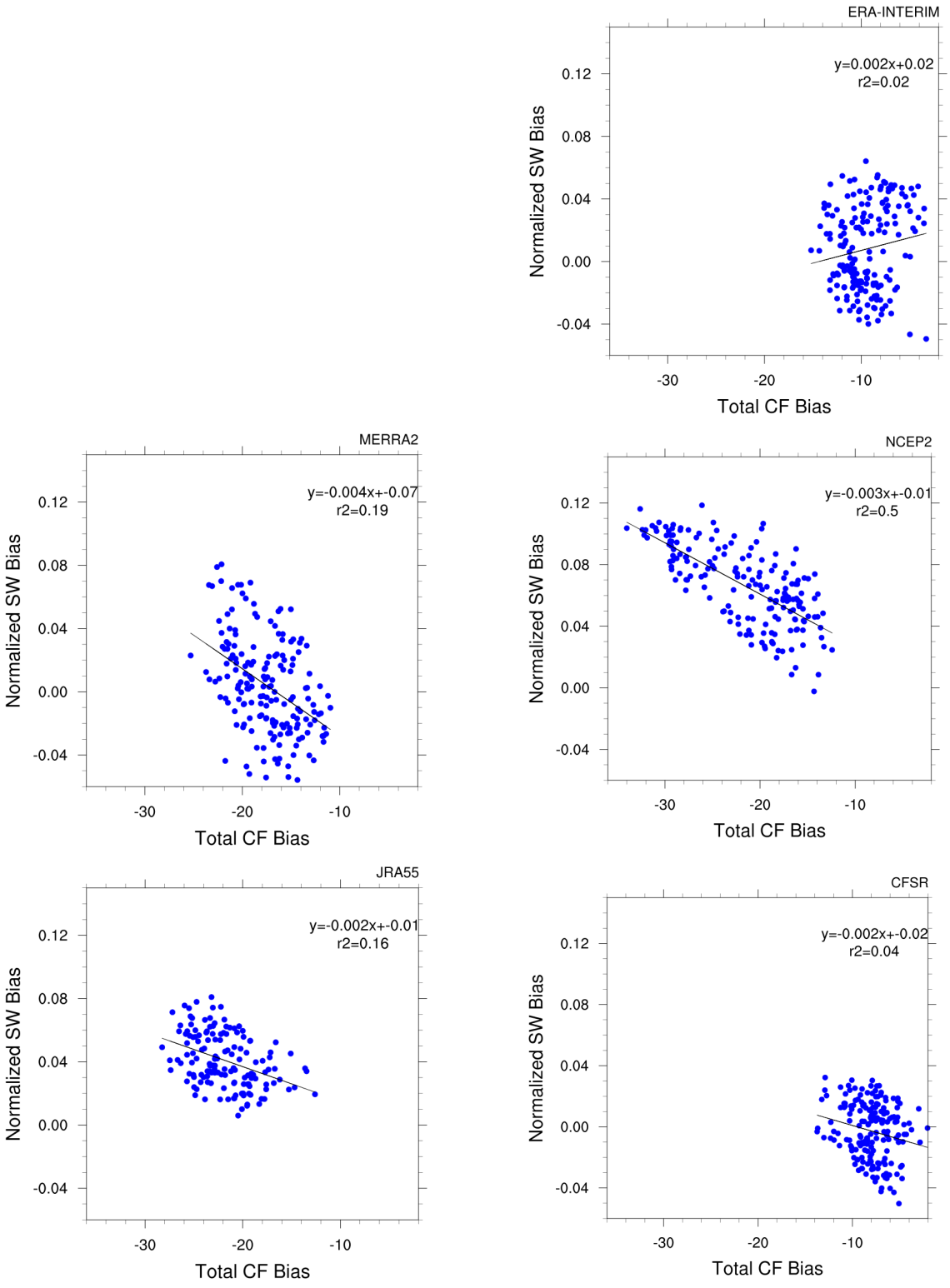

Figure A3. Total cloud fraction bias (reanalysis – satellite) vs. shortwave radiative flux bias at the surface normalized by incident shortwave radiative flux at the top of the atmosphere for five reanalyses.

Appendix B
Supplementary information for Chapter 4

Appendix B includes a description of the CFSR atmospheric reanalysis product used in the analysis. Appendix B also includes text and two figures providing historical context of the SST and cloud anomalies observed during the MHW. There is a comparison of two turbulent flux datasets to motivate our use of CFSR in Chapter 4, which includes a text description of the results and one supplemental figure of the results. In addition, there are results for the analysis of atmospheric response to the MHW using CERES-EBAF satellite data instead of CFSR data. That section includes a description of differences in results using the two different datasets, as well as two figures and one table showing results.

Details on the CFSR Product

The Climate Forecast System Reanalysis (CFSR) product is a coupled atmosphere-ocean-land-sea ice reanalysis product from NOAA NCEP. CFSR data is available from 1979 to present, with an upgrade to the operational model in March 2011. Details about the CFSR model and reanalysis process is available in Saha et al. (2010) and Saha et al. (2014). The CFSR model should represent climate changes due to its assimilation of atmospheric concentrations of carbon dioxide, trace gases, and aerosols. CFSR boundary layer clouds are defined as clouds that occupy the lowest 10% of the atmosphere by mass, while high clouds are defined at 350hPa and above (Hu et al., 2008).

2013-16 NE Pacific MHW in context of historical climatology

The 2013-2016 NE Pacific MHW is unprecedented in the historical record of observations of the region. HadISST version 1.1 data were used to provide a long time series of SST for the region from 1870-2017. The HadISST dataset was created using a combination of SST measurements from ships, in situ SST measurements and satellite observations. Figure S1 shows monthly SST anomalies. The magnitudes of the strongest SST anomalies observed during the MHW have never been observed in the historical record, and the persistence of warm SST anomalies above 1°C during the MHW was the longest ever in this region. Figure S2 shows monthly low cloud cover anomalies from CFSR. The magnitudes of the strongest low cloud

cover anomalies during the MHW were also unprecedented, and the persistence of the low cloud anomalies was notable. An event of low cloud cover anomalies in 1996-1998 persisted almost as long as those during the MHW, though magnitudes of the anomalies were not as large.

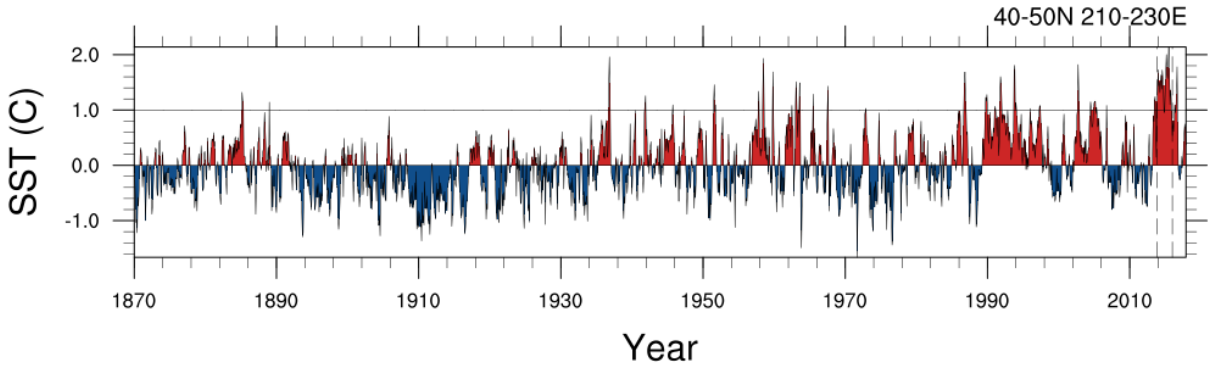

Figure B1. Time series of HadISST anomalies from 1970-2018. The duration of the marine heat wave in the NE Pacific is delineated with vertical dashed lines from November 2013-January 2016. A horizontal reference line at an SST anomaly of 1°C is provided as a visual guide.

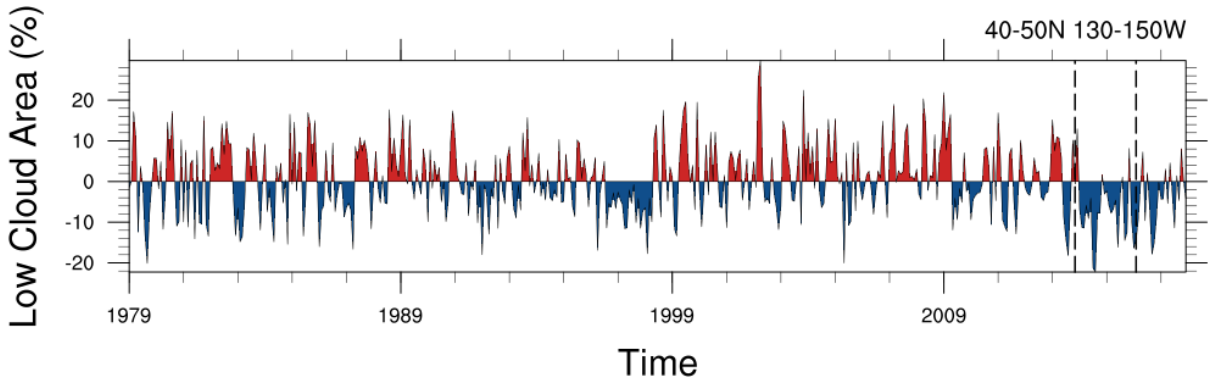

Figure B2. Time series of CFSR low cloud cover anomalies from 1979-2017. The duration of the marine heat wave in the NE Pacific is delineated with vertical dashed lines from November 2013-January 2016.

Comparison of CFSR to OAFlux product

To determine whether or not there was a substantial difference between using turbulent fluxes from CFSR or the OAFlux product for this analysis, sensible and latent heat fluxes from both products are compared. Figure S3a presents the monthly climatology of latent heat fluxes from 2000-2016 for CFSR (green line) and OAFlux (black line). CFSR estimates of latent heat flux are consistently higher than OAFlux estimates, with the largest differences in the winter

when turbulent heat fluxes are the highest. Figure S1b present the monthly climatology of sensible heat fluxes from 2000-2016 for CFSR (green line) and OAFlux (black line). CFSR estimates of sensible heat flux are consistently lower than OAFlux estimates, with the largest differences in the winter when turbulent fluxes are the highest. Differences between the products are relatively small and, what's more, the net turbulent heat fluxes are very similar, given that CFSR estimates higher latent heat fluxes and lower sensible heat fluxes compared to OAFlux. Since differences between the products are small, CFSR is utilized in the analysis given the long timeseries available and the dynamical consistency with the other CFSR variables used here.

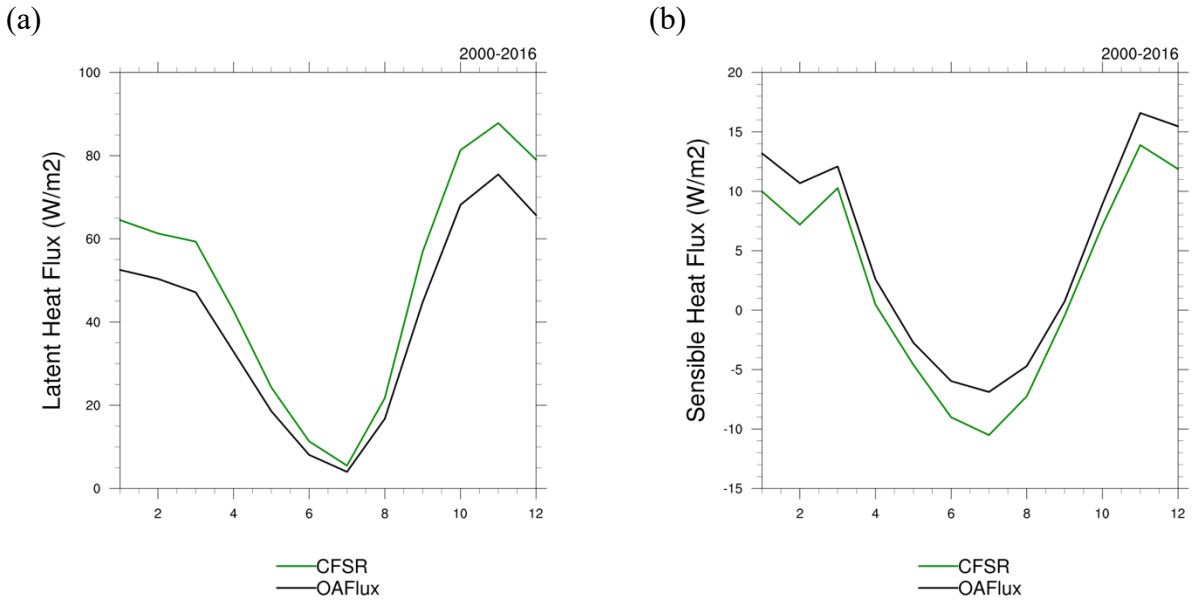

Figure B3. (a) Comparison of monthly climatologies of latent heat flux from OAFlux product (black line) and CFSR (green line) from 2000-2016. (b) Comparison of monthly climatologies of sensible heat flux from OAFlux (black line) and CFSR (green line) using data from 2000-2016.

Analysis results using CERES-EBAF satellite observations

To understand the sensitivity of the results to dataset choice, the analysis of the atmospheric response to the 2013-16 NE Pacific MHW was repeated using CERES-EBAF version 4.0 satellite estimates. CERES-EBAF4.0 provides monthly means of globally gridded radiative fluxes and cloud data at 1°x1° resolution. More information on the CERES-EBAF4.0

satellite estimates can be found in Kato et al., 2013. CERES satellite estimates were not used for the primary analysis in the manuscript due to the shorter time series (the MHW event accounts for 15% of the total CERES time series, which can skew anomalies), and it was desirable to have the turbulent and radiative fluxes from the same physically constrained CFSR reanalysis dataset. In addition, we understand that differences in anomalies calculated using different versions of the CERES EBAF products is comparable to the difference in anomalies calculated using CERES and reanalysis data, indicating that there is no optimal dataset choice. However, since CERES satellite estimates are some of the best available observations of radiative fluxes, it is prudent to see how they compare to those from CFSR. An in-depth comparison of reanalysis products to CERES satellite estimates in the NE Pacific can be found in Schmeisser et al., 2018.

Average anomalies of radiative fluxes and cloud cover observed during the MHW from both the CFSR and CERES-EBAF4.0 datasets are provided in Table S1. Qualitatively, the anomalies from CERES-EBAF data are the same as those from CFSR during the MHW. Namely, there were increases in upward and downward longwave radiative fluxes, as well as increases in downward shortwave radiative flux. The difference in MHW-averaged net heat flux between the different datasets is 2 Wm^{-2} (4.3 Wm^{-2} from CERES-EBAF and 2.3 Wm^{-2} from CFSR). Cloud changes during the MHW were qualitatively the same for both datasets- a decrease in total cloud cover and low cloud cover, and an increase in high cloud cover. The results of the sensitivity analysis show that the choice of dataset does not change the conclusions of the analysis qualitatively; however, the CERES data suggest that the net radiative flux anomaly played an even more important role in the evolution of the SSTs than suggested by the CFSR data.

Table B1. As in Table 4.1 but showing data from CFSR and CERES-EBAF.

	Climatological average and standard deviation (1979 to 2016)	Average CFSR (1979-2016) anomaly during MHW	Average CERES (2001-2016) anomaly during MHW
SST (K)	285.1 ± 5.9	1.6	1.6
Upward LW (Wm^{-2})	375.2 ± 31.3	8.2	8.0
Downward LW (Wm^{-2})	334.0 ± 30.4	4.1	7.7
Downward SW (Wm^{-2})	133.2 ± 74.4	7.1	5.1
Net radiative flux (Wm^{-2})	83.1 ± 72.9	2.3	4.3
Latent heat (Wm^{-2})	56.7 ± 40.4	7.0	--
Sensible heat (Wm^{-2})	1.8 ± 16.4	1.1	--
Net heat flux (Wm^{-2})	24.5 ± 105.4	-5.8	--
Total cloud cover (%)	79.6 ± 13.5	-3.3	-2.0
Boundary layer cloud cover (%)	44.9 ± 18.4	-6.9	-6.0
High cloud cover (%)	33.4 ± 11.9	5.3	2.6

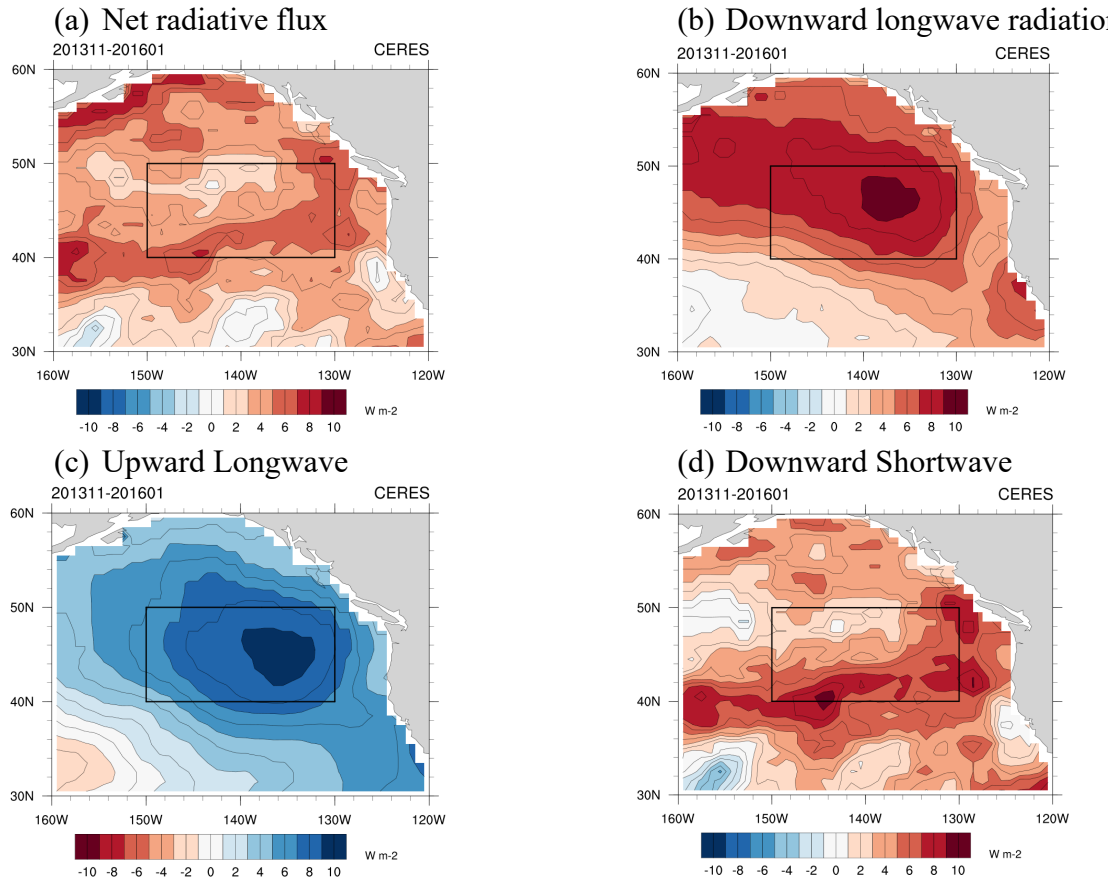

Figure B4. As in Figure 4.2 in manuscript, but using CERES-EBAF data (2001-2016) to compute MHW anomalies.

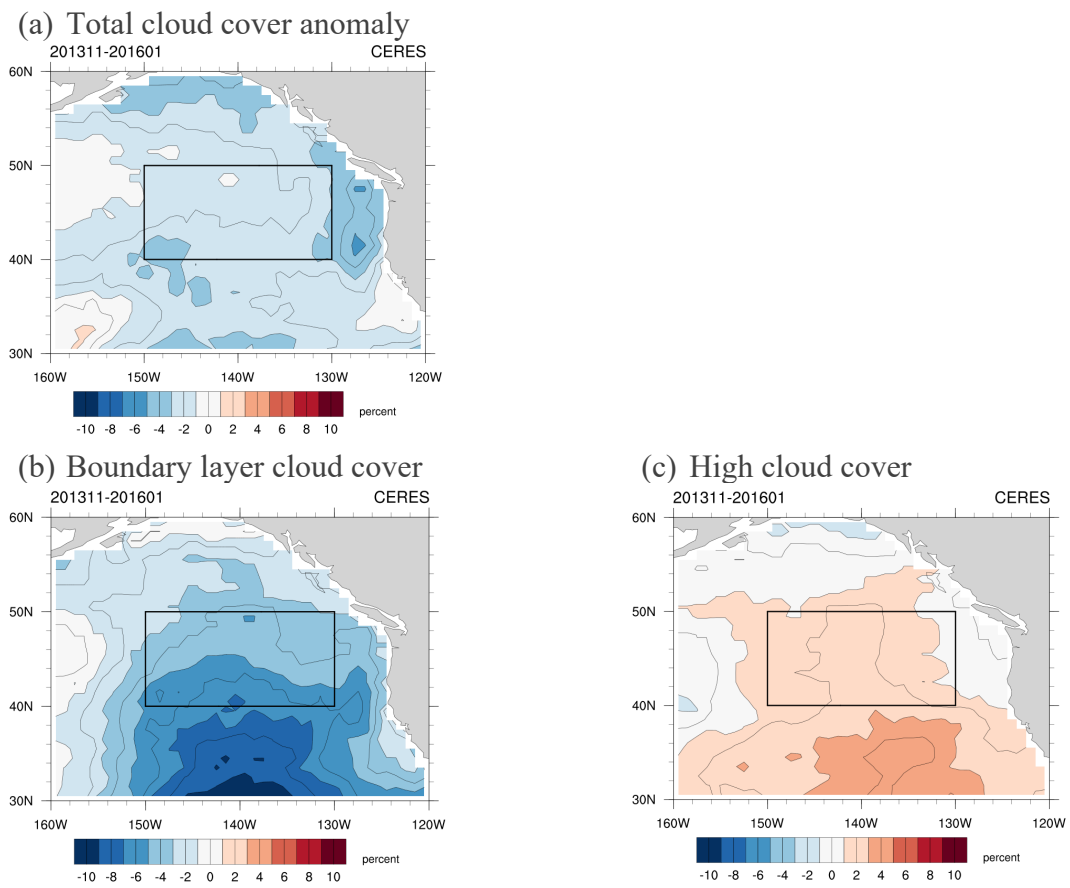

Figure B5. As in Figure 4.4 in manuscript, but using CERES-EBAF data (2001-2016) to compute MHW anomalies.

Appendix C
Supplementary information for Chapter 5

In order to ensure the results from Figure 5.1 are robust across a much longer time series, the analysis was repeated to compute the percentage change in forcing from the ocean surface to the atmosphere during MHWs. Figure C1 shows this percentage change, as computed with 148 years of SST data from 1870-2018. The general spatial patterns of forcing change are consistent between the shorter and longer datasets.

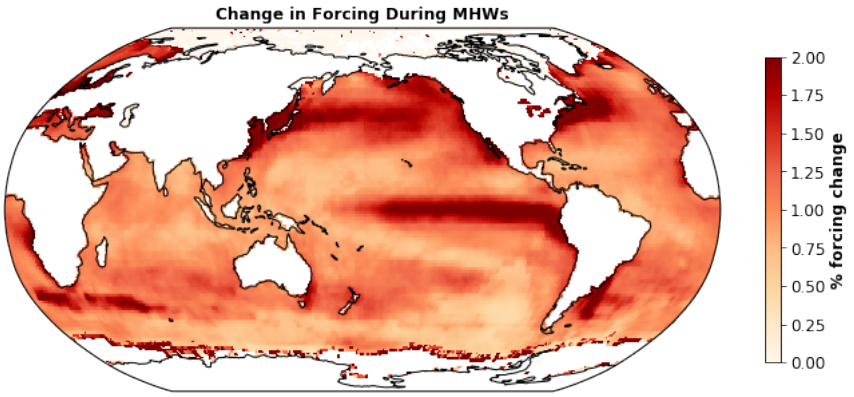

Figure C1. Forcing change using HadISST data from 1870-2018 (148 years) (compare to Figure 5.1)

In order to contextualize anomalies experienced during MHWs, Figures C2 and C3 present MHW-averaged magnitudes of all variables analyzed in the manuscript.

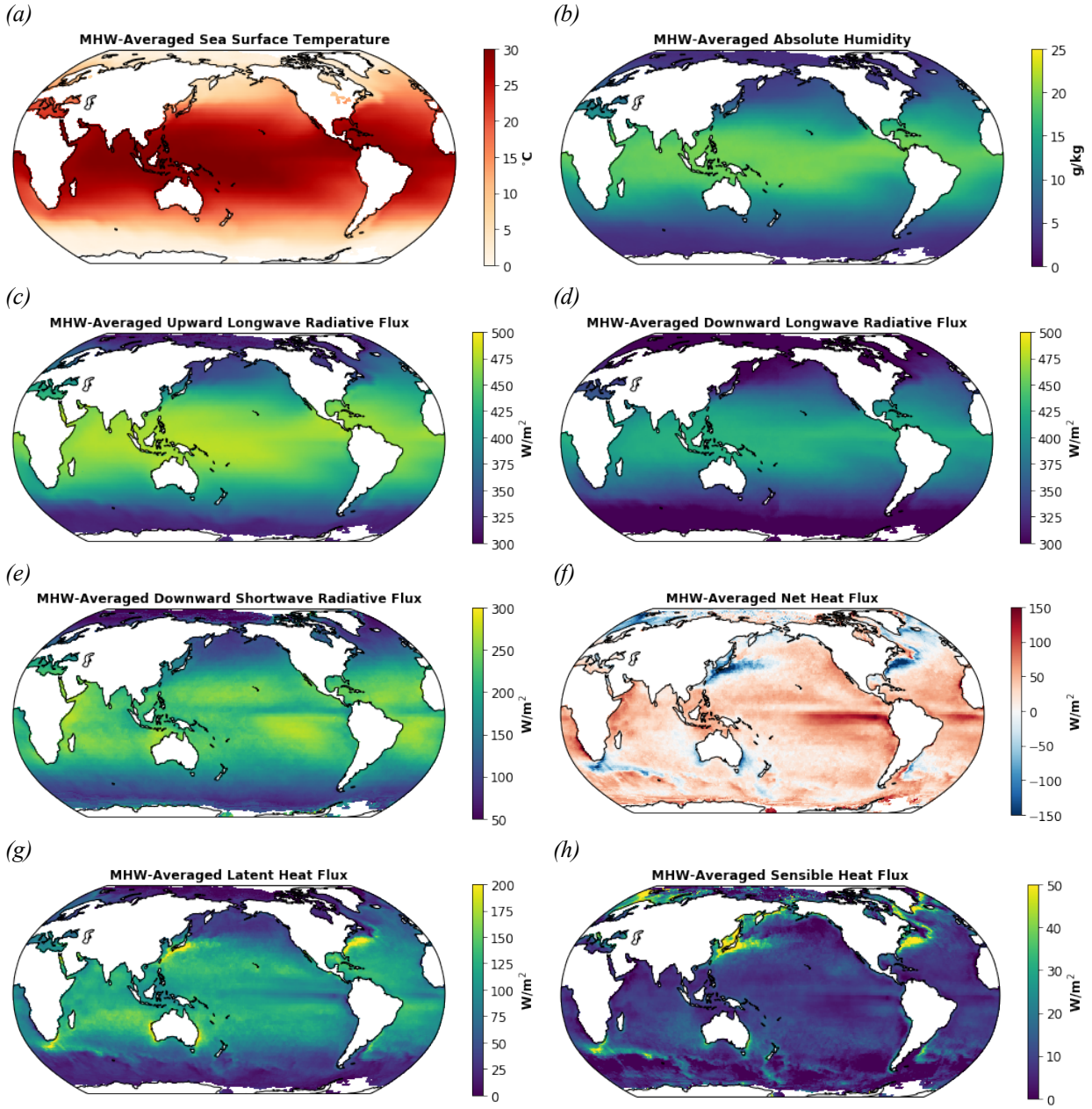

Figure C2. Magnitudes of atmospheric variables composited and averaged during MHW events: (a) SST (°C), (b) 2 m absolute humidity (g/kg), (c) upward longwave radiative flux at the surface (W/m^2) (positive is up), (d) downward longwave radiative flux at the surface (positive is down), (e) downward shortwave radiative flux at the surface (positive is down), (f) net heat flux (W/m^2), (g) latent heat flux (W/m^2), and (h) sensible heat flux (W/m^2) (positive is up).

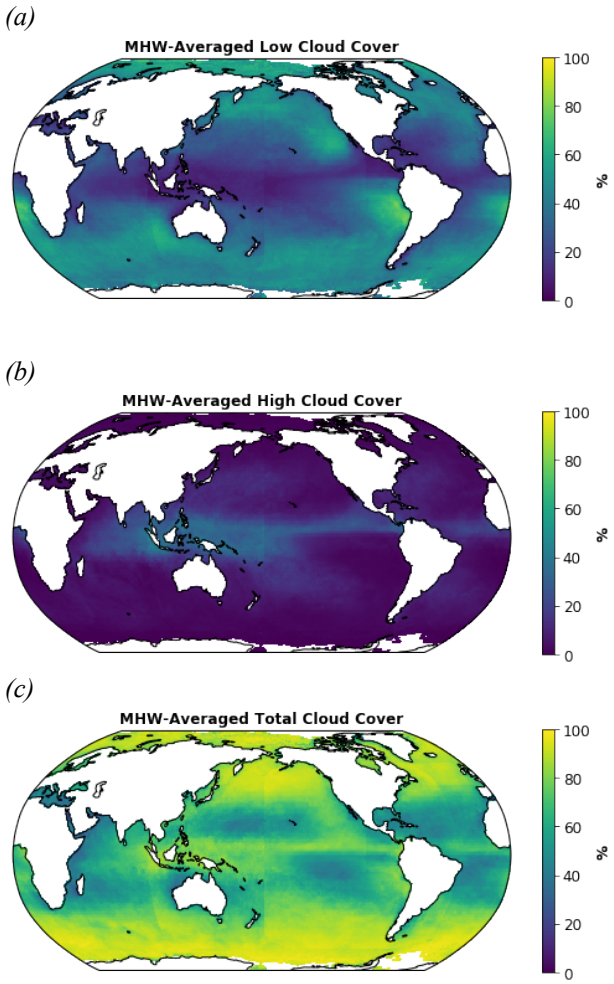

Figure C3. Magnitudes of cloud cover composited and averaged during MHW events: (a) low cloud cover (%), (b) non-low cloud cover (%), and (c) total cloud cover (%).

Appendix D
Supplementary information for Chapter 6

In Chapter 6.3.3, results show a statistical relationship between maximum MHW length and average net heat flux feedback in a given grid cell. There is a negative correlation between net heat flux feedback parameters and maximum MHW length that suggests areas with lower net heat flux feedback parameters experience more persistent MHWs. Table D1 shows the same statistics as in Table 6.1, but for statistics computed between maximum MHW length and average MHW net heat flux feedback.

Table D1. As in Table 6.1, but statistics are computed between maximum MHW length and average MHW net heat flux feedbacks (instead of annual average climatological feedbacks)

	n	Pearson correlation coefficient	p-value
All data	31718	-0.04	3e-12
Positive net heat flux feedback parameters	21073	-0.11	7e-58
Negative net heat flux feedback parameters	9795	0.07	2e-13

Figure D1 shows the same data as in Figure 6.12, but means are computed in each MHW length bin instead of medians. The relationship between means of net heat flux feedback parameters and length of MHW is essentially the same as that computed with medians.

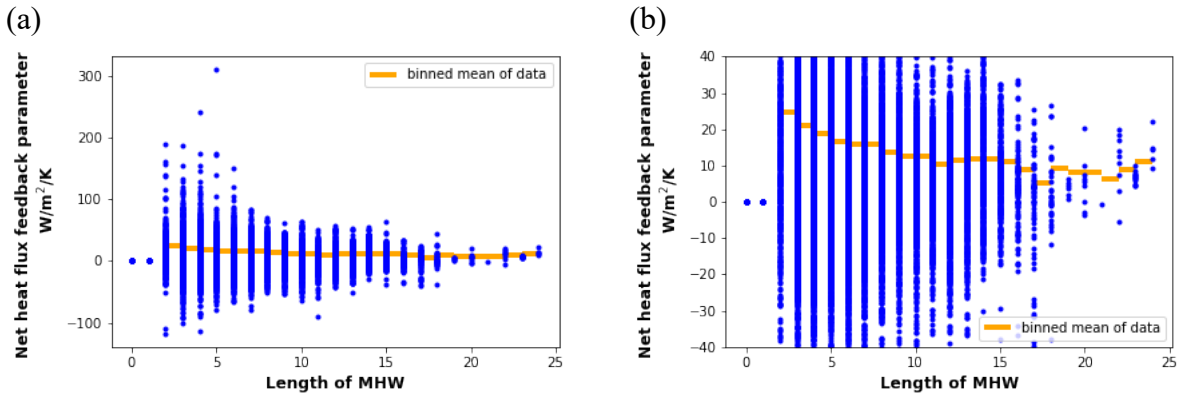

Figure D1. As in Figure 6.12, but each bin has computed means instead of computed medians.

VITA

Lauren Schmeisser earned a BS in Environmental Engineering and a MS in Civil Engineering from the University of Colorado at Boulder. Upon graduation, she accepted a Rotary International Ambassadorial Scholarship to the Universiteit van Amsterdam in the Netherlands, where she received a MSc in Earth Sciences with an emphasis in Climate Studies. While completing her MSc requirements, she finished her master's thesis research at the National Center for Atmospheric Research in Boulder, Colorado, and held an internship at the National Oceanic and Atmospheric Administration (NOAA) in Boulder, Colorado.

Before starting her PhD, Lauren worked as a professional research assistant at NOAA's Global Monitoring Division in the Aerosols Group, where she analyzed in situ measurements of aerosol optical properties. Lauren began her PhD at the University of Washington in September 2015 as an NSF IGERT fellow through the UW Program on Ocean Change. Through the IGERT fellowship, Lauren and her cohort collaborated on a project with the NGO Pacific Resources for Education and Learning (PREL) on climate change education on the island of Pohnpei in the Federated States of Micronesia. In 2019, Lauren was awarded the College of the Environment Dean's Medal- an honor recognizing academic accomplishments and outstanding leadership and service.

When she's not thinking about climate science, Lauren loves to teach yoga, cook vegetables, bike around town, be in the mountains, run half marathons, and hang out in the garden with her chickens and cat.